

The Pennsylvania State University
The Graduate School
Department of Civil and Environmental Engineering

Polyacrylamide-Treated Kaolin clay: A Fabric Study

A Thesis in
Civil Engineering
by
Sung ho Kim

© 2008 Sung ho Kim

Submitted in Partial Fulfillment
of the Requirements
for the Degree of

Master of Science

August 2008

The thesis of Sung ho Kim was reviewed and approved* by the following:

Angelica Maria Palomino
Assistant Professor of Civil Engineering
Thesis Advisor

Mian C. Wang
Professor of Civil Engineering

Shelley M. Stoffels
Associate Professor of Civil Engineering

Peggy A. Johnson
Professor of Civil Engineering
Head of the Department of Civil and Environmental Engineering

*Signatures are on file in the Graduate School

ABSTRACT

The field of surface-treated clays, especially polymer-treated clays, has been growing for the last a few decades, with a considerable number of studies conducted on the use of polymers as a clay-surface treatment. In spite of many studies on the behavior of clay-polymer systems at the level of particle-particle and particle-fluid interactions, fabric development over a wide range of solids content is poorly understood. The purpose of this study is to understand fabric development in a clay-polymer system, specifically kaolin-polyacrylamide systems over a wide range of solids content. Methodologies include sedimentation tests (low solids content), viscosity measurements (moderate solids content), and liquid limit measurements (high solids content), and are conducted to determine variation in fabric for kaolin-polyacrylamide systems at various concentrations, molecular weight and ionic types of polyacrylamide. Fabric development is verified using scanning electron microscopy (SEM). Fabric changes in sedimentation, viscosity, and liquid limit behavior in the presence of polyacrylamide corresponding to the change in the type of particle association are observed in SEM. Floc/aggregate size and density tend to increase with increasing polyacrylamide concentration, showing the formation of more larger, denser flocs. Final sediment height tends to decrease with an increase in polyacrylamide concentration, indicating denser particle associations (face-to-face) and verified with scanning electron microscopy. Viscosity tends to increase as polyacrylamide concentration increases, implying more flocculated/aggregated fabric formation. High molecular polyacrylamides tend to induce a higher liquid limit with increasing concentration, demonstrating the formation of open flocculated structure. It is observed that the most likely particle association in the presence of polyacrylamide is face-to-face association by polymer bridges, which in turn results in a dense fabric. The molecular weight and concentration of polyacrylamide determines the fabric formation over a wide range of solids content. The polymer charge type impacts on the resulting

fabric formation only at polymer concentration above the critical coagulation concentration. A relationship is found between polymer characteristics, solids contents, and micro-scale particle arrangement. This relationship is summarized in a series of fabric maps.

TABLE OF CONTENTS

| | |
|--|----|
| Chapter 1 INTRODUCTION..... | 1 |
| Hypothesis / Objective | 3 |
| Chapter 2 LITERATURE REVIEW..... | 4 |
| Nature of kaolin clay surface charge..... | 4 |
| Particle associations | 9 |
| Nature of kaolin-polyacrylamide interactions..... | 11 |
| Chapter 3 EXPERIMENTAL STUDY | 15 |
| Materials..... | 15 |
| Kaolin clay | 15 |
| Polyacrylamides | 18 |
| Selection of Polymer Concentration Tested | 19 |
| Sedimentation..... | 19 |
| Viscosity | 24 |
| Liquid Limit | 26 |
| Scanning Electron Microscopy Study | 28 |
| Chapter 4 RESULTS..... | 29 |
| Sedimentation..... | 29 |
| Observed settling behavior | 29 |
| Final sediment height | 35 |
| Size and density analysis | 36 |
| Viscosity | 37 |
| Liquid Limit | 41 |
| Chapter 5 DISCUSSION | 47 |
| Low solids content ($\phi = 0.02$) | 47 |
| Intermediate solids content ($\phi = 0.07$) | 54 |
| High solids content ($\phi > 0.4$)..... | 56 |
| Fabric maps | 57 |
| Chapter 6 CONCLUSIONS..... | 63 |
| Future Work | 65 |
| Mechanical properties of polyacrylamide-treated kaolin | 65 |
| Influence of PAM molecule conformation..... | 65 |
| Impact of preexisting exchangeable cations..... | 66 |

| | |
|--|----|
| Appendix A Charge calculation of kaolin clay particles and polyacrylamide molecules..... | 67 |
| Appendix B Sedimentation time series..... | 72 |
| Kaolin clay (pure)..... | 72 |
| Kaolin-Nonionic Polyacrylamide (N-PAM) | 73 |
| Kaolin-low molecular Nonionic Polyacrylamide (n-PAM) | 75 |
| Kaolin-Cationic Polyacrylamide (C-PAM)..... | 78 |
| Appendix C Settling Floc Size and Density Analysis..... | 81 |
| Appendix D Apparatus | 83 |
| REFERENCES | 86 |

LIST OF FIGURES

| | |
|--|----|
| Figure 2.1: Mineral composition of kaolinite (MMP, 2003) | 5 |
| Figure 2.2: Electrical potential (V_x) of double layer compiled from Israelachvili (1991), Stumm (1992), Santamarina et al. (2001), and Mitchell and Soga (2005). Plot from Santamarina et al. (2001) | 6 |
| Figure 2.3: Schematic of particle associations: (a) edge-to-face (EF), (b) face-to-face (FF), (c) edge-to-edge (EE), and (d) dispersed | 9 |
| Figure 2.4: Schematic of polymer bridging compiled from van Olphen (1977) and Theng (1979) | 13 |
| Figure 2.5: Schematic bonding mechanisms of kaolin-polyacrylamide composites at the molecular level: (a) nonionic PAM molecule, (b) cationic unit of cationic PAM, (c) charge neutralization | 14 |
| Figure 3.1: Particle size distribution curves for kaolin clay used for this study. Manufacturer and measured data | 17 |
| Figure 3.2: A schematic of (a) dispersed sedimentation and (b) flocculated/aggregated sedimentation | 23 |
| Figure 4.1: Plot of sedimentation boundary height with time for pure kaolin and kaolin-PAM nanocomposite (N-PAM). ■ and □ are for pure kaolin, ● and ○ are for 20 mg/L, ▲ and △ are for 80 mg/L, ◆ and ◇ are for 120 mg/L, + and x are for 240 mg/L, and and are for 500 mg/L. Open symbols and x denote supernatant-suspension boundary while closed symbols denote suspension-sediment boundary. After long time t , the two boundaries meet, except for the case of true dispersion. | 30 |
| Figure 4.2: Plot of sedimentation boundary height with time for pure kaolin and kaolin-PAM nanocomposite (n-PAM). ■ and □ are for pure kaolin, ● and ○ are for 20 mg/L, ▲ and △ are for 80 mg/L, ◆ and ◇ are for 120 mg/L, + and x are for 240 mg/L, and and are for 500 mg/L. Open symbols and x denote supernatant-suspension boundary while closed symbols denote suspension-sediment boundary. After long time t , the two boundaries meet, except for the case of true dispersion. | 31 |
| Figure 4.3: Plot of sedimentation boundary height with time for pure kaolin and kaolin-PAM nanocomposite (C-PAM). ■ and □ are for pure kaolin, ● and ○ are for 20 mg/L, ▲ and △ are for 80 mg/L, ◆ and ◇ are for 120 mg/L, + and x are for 240 mg/L, and and are for 500 mg/L. Open symbols and x denote supernatant-suspension boundary while closed symbols denote suspension-sediment boundary. After long time t , the two boundaries meet, except for the case of true dispersion. | 32 |
| Figure 4.4: Final sediment height measured after three weeks | 35 |

| | |
|---|----|
| Figure 4.5: Viscosity measurement for pure kaolin and kaolin-PAM (N-PAM) suspensions at rotational speeds of 1 to 100 rpm. Measurements taken with spindle S61 and S62. | 38 |
| Figure 4.6: Viscosity measurement for pure kaolin and kaolin-PAM (n-PAM) suspensions at rotational speeds of 1 to 100 rpm. Measurements taken with spindle S61 and S62. | 39 |
| Figure 4.7: Viscosity measurement for pure kaolin and kaolin-PAM (C-PAM) suspensions at rotational speeds of 1 to 100 rpm. Measurements taken with spindle S61 and S62. | 40 |
| Figure 4.8: Viscosity data for all suspensions at 100 rpm using Spindle S61 and S62. | 41 |
| Figure 4.9: Liquid limit lines for N-PAM-treated kaolin specimens at various PAM concentrations. ■ is for pure kaolin, ● is for 20 mg/L, ▲ is for 80 mg/L, ◆ is for 120 mg/L, + is for 240 mg/L, and * is for 500 mg/L. | 42 |
| Figure 4.10: Liquid limit lines for n-PAM-treated kaolin specimens at various PAM concentrations. ■ is for pure kaolin, ● is for 20 mg/L, ▲ is for 80 mg/L, ◆ is for 120 mg/L, + is for 240 mg/L, and * is for 500 mg/L. | 43 |
| Figure 4.11: Liquid limit lines for C-PAM-treated kaolin specimens at various PAM concentrations. ■ is for pure kaolin, ● is for 20 mg/L, ▲ is for 80 mg/L, ◆ is for 120 mg/L, + is for 240 mg/L, and * is for 500 mg/L. | 44 |
| Figure 4.12: Liquid limit for all mixtures of kaolin with various concentrations of PAMs. .. | 45 |
| Figure 4.13: Slopes of the fall cone liquid limit lines..... | 46 |
| Figure 5.1: SEM images, at $\phi = 0.02$, in the presence of n-PAM varying with concentrations: (a) 0 mg/L, (b) 20 mg/L, (c) 80 mg/L, (d) 120 mg/L, (e) 240 mg/L, and (f) 500 mg/L | 50 |
| Figure 5.2: Formation of EF flocs in the presence of excess cationic PAM molecules..... | 52 |
| Figure 5.3: SEM image of FF aggregates in EF flocs in the presence of 240 mg/L C-PAM..... | 53 |
| Figure 5.4: SEM images in the presence of 500 mg/L of (a) N-PAM and (b) C-PAM, at $\phi = 0.02$ | 53 |
| Figure 5.5: SEM images in the presence of (a) 500 mg/L n-PAM and (b) 500 mg/L N-PAM, at $\phi = 0.02$ | 54 |
| Figure 5.6: SEM images of (a) pure kaolin, (b) 500 mg/L N-PAM, (c) 500 mg/L n-PAM, and (d) 500 mg/L C-PAM, at $\phi = 0.07$ | 55 |

| | |
|---|----|
| Figure 5.7: EF and open EE associations in the presence of 500 mg/L N-PAM, at $\phi > 0.4$... | 57 |
| Figure 5.8: High molecular weight nonionic polyacrylamide-treated kaolin fabric map.  ,  ,  ,  , and  denotes FF aggregated, EF flocculated, EE flocculated, dispersed, and higher-order EF flocculated fabric, respectively. | 60 |
| Figure 5.9: Low molecular weight nonionic polyacrylamide-treated kaolin fabric map.  ,  ,  , and  denotes FF aggregated, EF flocculated, EE flocculated, and dispersed fabric, respectively. | 61 |
| Figure 5.10: High molecular weight cationic polyacrylamide-treated kaolin fabric map.  ,  ,  ,  , and  denotes FF aggregated, EF flocculated, EE flocculated, dispersed, and higher-order EF flocculated fabric, respectively. | 62 |
| Figure B.1: Sedimentation time series for pure kaolin. Blue dotted line denotes supernatant-suspension boundary and red solid line denotes suspension-sediment boundary. Mixed-Mode sedimentation | 72 |
| Figure B.2: Sedimentation time series for kaolin-PAM nanocomposite (20 mg-N-PAM/L). Blue dotted line denotes supernatant-suspension boundary and red solid line denotes suspension-sediment boundary. Mixed-Mode sedimentation | 73 |
| Figure B.3: Sedimentation time series for kaolin-PAM nanocomposite (80 mg-N-PAM/L). Blue dotted line denotes supernatant-suspension boundary and red solid line denotes suspension-sediment boundary. Mixed-Mode sedimentation (near to FF aggregation) | 73 |
| Figure B.4: Sedimentation time series for kaolin-PAM nanocomposite (120 mg-N-PAM/L). Blue dotted line denotes supernatant-suspension boundary and red solid line denotes suspension-sediment boundary. Mixed-Mode sedimentation (near to FF aggregation) | 74 |
| Figure B.5: Sedimentation time series for kaolin-PAM nanocomposite (240 mg-N-PAM/L). Blue dotted line denotes supernatant-suspension boundary and red solid line denotes suspension-sediment boundary. Mixed-Mode sedimentation (near to FF aggregation) | 74 |
| Figure B.6: Sedimentation time series for kaolin-PAM nanocomposite (500 mg-N-PAM/L). Blue dotted line denotes supernatant-suspension boundary and red solid line denotes suspension-sediment boundary. Mixed-Mode sedimentation (near to FF aggregation) | 75 |
| Figure B.7: Sedimentation time series for kaolin-PAM nanocomposite (20 mg-n-PAM/L). Blue dotted line denotes supernatant-suspension boundary and red solid line denotes suspension-sediment boundary. Mixed-Mode sedimentation | 75 |
| Figure B.8: Sedimentation time series for kaolin-PAM nanocomposite (80 mg-n-PAM/L). Blue dotted line denotes supernatant-suspension boundary and red solid line denotes suspension-sediment boundary. Mixed-Mode sedimentation | 76 |

| | |
|---|----|
| Figure B.9 : Sedimentation time series for kaolin-PAM nanocomposite (120 mg-n-PAM/L). Blue dotted line denotes supernatant-suspension boundary and red solid line denotes suspension-sediment boundary. Mixed-Mode sedimentation..... | 76 |
| Figure B.10 : Sedimentation time series for kaolin-PAM nanocomposite (240 mg-n-PAM/L). Blue dotted line denotes supernatant-suspension boundary and red solid line denotes suspension-sediment boundary. Mixed-Mode sedimentation (near to FF aggregation) | 77 |
| Figure B.11 : Sedimentation time series for kaolin-PAM nanocomposite (500 mg-n-PAM/L). Blue dotted line denotes supernatant-suspension boundary and red solid line denotes suspension-sediment boundary. Mixed-Mode sedimentation (near to FF aggregation) | 77 |
| Figure B.12 : Sedimentation time series for kaolin-PAM nanocomposite (20 mg-C-PAM/L). Blue dotted line denotes supernatant-suspension boundary and red solid line denotes suspension-sediment boundary. Mixed-Mode sedimentation..... | 78 |
| Figure B.13 : Sedimentation time series for kaolin-PAM nanocomposite (80 mg-C-PAM/L). Blue dotted line denotes supernatant-suspension boundary and red solid line denotes suspension-sediment boundary. Mixed-Mode sedimentation..... | 78 |
| Figure B.14 : Sedimentation time series for kaolin-PAM nanocomposite (120 mg-C-PAM/L). Blue dotted line denotes supernatant-suspension boundary and red solid line denotes suspension-sediment boundary. FF aggregation..... | 79 |
| Figure B.15 : Sedimentation time series for kaolin-PAM nanocomposite (240 mg-C-PAM/L). Blue dotted line denotes supernatant-suspension boundary and red solid line denotes suspension-sediment boundary. Mixed-Mode sedimentation (near to FF aggregation) | 79 |
| Figure B.16 : Sedimentation time series for kaolin-PAM nanocomposite (500 mg-C-PAM/L). Blue dotted line denotes supernatant-suspension boundary and red solid line denotes suspension-sediment boundary. Mixed-Mode sedimentation (near to FF aggregation) | 80 |
| Figure D.1 : Apparatus for viscosity measurement: (a) Brookfield LVDV-1 Prime Viscometer, and (b) Spindles #S61, #S62, #S63, and #S64..... | 83 |
| Figure D.2 : Apparatus for liquid limit measurement: Humboldt penetrometer (model number: H-4236, Humboldt Mfg. Co., IL) | 84 |
| Figure D.3 : Apparatus for SEM study: (a) SEM S-3500N (Hitachi Inc.), (b) gold sputter, and (c) SEM sampler..... | 85 |

LIST OF TABLES

| | |
|---|----|
| Table 2.1 : Point of zero charge and isoelectric point reported for kaolinite..... | 8 |
| Table 3.1 : Chemical composition of kaolin clay used for this study..... | 16 |
| Table 3.2 : Properties of kaolin clay. Manufacturer and measured (*) data | 16 |
| Table 3.3 : Characteristics of polyacrylamides used in this study | 18 |
| Table 3.4 : Observed suspension settlement modes defined for this study..... | 22 |
| Table 3.5 : Test matrix for sedimentation tests. $\phi = 0.02$ | 23 |
| Table 3.6 : Test matrix for viscosity measurements. $\phi = 0.07$ | 26 |
| Table 3.7 : Test matrix for fall cone test. $\phi > 0.4$ | 27 |
| Table 4.1 : Observed sedimentation modes of kaolin-PAM suspensions..... | 29 |
| Table 4.2 : Initial and final pH and conductivity of sedimentation suspensions. | 34 |
| Table 4.3 : Floc size and density calculated from sedimentation tests. | 37 |
| Table 5.1 : Results summary for sedimentation, viscosity, and fall cone tests..... | 49 |
| Table 5.2 : The influence of PAM concentration..... | 58 |
| Table 5.3 : The influence of positively charged groups of PAM..... | 59 |

ACKNOWLEDGEMENTS

I really appreciate my thesis advisor, Dr. Angelica M. Palomino for her special care on this thesis and for providing funding for this study. Her advising transcends the realm of my understanding, so will be forever helpful in my academic career. I also wish to acknowledge my thesis committee: Dr. Mian C. Wang and Dr. Shelly M. Stoffels. I appreciate their useful suggestions and comments.

Chapter 1

INTRODUCTION

Clay is one of the most important and commonly used natural materials. Clay minerals are used in a wide range of applications including geo-environmental engineering and material science, because of their ability to form stable, inert, systems. A clay particle forms from stacking mineral layers made of successive nano-sized platy sheets. The arrangement of sheets characterizes different clay minerals and the particle arrangement, or fabric, determines the properties of the clay system.

Clay fabric formation varies with the surrounding pore fluid environment, e.g., pH and ionic concentration (Rand and Melton, 1977; van Olphen, 1977; Theng, 1979; Peng and Di, 1994; Pierre et al., 1995; Pierre and Ma, 1999; Mitchell and Soga, 2005; Nasser and James, 2006). In other words, variations in pore fluid chemistry significantly influence interparticle forces and in turn particle associations. Clay fabric manipulation at the particle level can thus be accomplished by manipulating the pore fluid conditions, and the macro-scale clay properties that depend on fabric may be altered. For example, residual shear strength increases with an increase in ionic concentration and valence (i.e., a thinner double layer) (Moore, 1991; Barbour and Yang, 1993), and real permittivity (Moore and Mitchell, 1974). A thinner double layer results in FF-dominating fabric, thus more friction force between particles. Undrained shear strength also increases with increasing flocculated fabric (edge-to-face and edge-to-edge association) (Sridharan and Prakash, 1999). At the same void ratio, flocculated fabric has greater one dimensional compressive strength and higher compressibility, resulting from interaction forces between particles, than dispersed fabric does (Mitchell, 1956). Permeability increases with increasing the presence of large pores resulted from edge-to-face and/or edge-to-edge flocculation.

Face-to-face-dominated fabric exhibits flow-direction-dependent permeability (a higher permeability in the direction of particle alignment than in the direction perpendicular to the alignment) (Mitchell, 1956). The compressive yield stress for the edge-to-face fabric structure is greater than that for the face-to-face structure (Nasser and James, 2006).

In nature, the properties of clay-mineral soil systems must be determined for each location because numerous factors have influenced the soil layer formation. Inherently, not all soils have desirable engineering properties. Thus, physical and/or chemical processes are often used to obtain stability of clay soils in practice. Polymers may be a good alternative to achieve stability (van Olphen, 1977; Barvenik, 1994; Green et al., 2000). Polymers can be used as a treatment for the purpose of pore fluid environment manipulation. It is also expected that cationic or anionic charged polymers have a greater ability to flocculate and/or coagulate clay particles because clay particles can be charged negatively or positively (Theng, 1979). For example, kaolinite has negative charges on the face site and positive charges on the edge site, under moderate pH and low ionic conditions.

Over the last few decades, the use of polymers as an additive to enhance the performance of clay minerals has been studied in a large variety of technical areas such as soil conditioning (Nadler et al., 1996; Zhang and Miller, 1996), oil recovery (Stutzmann and Siffert, 1977; Pefferkorn, 1999), water treatment (Letterman and Pero, 1990), irrigation control (Sojka et al., 1998), infiltration (Ben-Hur and Keren, 1997; Green et al., 2000), soil erosion control (Zhang et al., 1998; Yu et al., 2003), and other industrial applications. Composites of clay-aqueous polymers (e.g., polyacrylamides, polyethyleneoxide, and polyvinylalcohol) have been designed for contaminant barriers (Daniels and Inyang, 2004; Inyang and Bae, 2005), waste containment (Inagaki et al., 1999; Daniels et al., 2003), elastomer reinforcement (Vu et al., 2001; Sadhu and Bhowmick, 2004; Zhu and Wool, 2006), plastics reinforcement (Vaia et al., 2001; Ahmadi et al., 2005; Yudin et al., 2005), coating and pigment agents (Zeng et al., 2005; Sun and Deng, 2006),

ceramics (Wei, 2005; Bakumov et al., 2007), packaging materials, and medicine and healthcare (Zeng et al., 2005; Torchilin, 2006).

Polymer adsorption on a clay particle surface alters the surface properties of the particle, such as surface charge, and hence interparticle forces between the particles. Polymer characteristics at the solid-liquid interface play an important role. The interaction with clay particles can be complex due to electrostatic force, chemical bonding, and other forces operating simultaneously. Understanding the interplay and relative significance of each of these phenomena is critical to the interpretation of a given polymer's affect on a clay system.

Polyacrylamide (PAM) is one of the most commonly used polymers in industrial applications because it is an inexpensive, highly effective agent for forming clay-polymer flocs. A nonionic polyacrylamide molecule strongly interacts with the surface of kaolin, via polymer bridging, reducing the overall negative charge through alteration of the electrical double layer repulsive force (Fleer et al., 1972; Carasso et al., 1997; Besra et al., 2002). A cationic polyacrylamide molecule binds to negatively charged mineral surfaces and in turn induces particle aggregation or dispersion. When cationic polyacrylamide molecules are adsorbed on clay particle surface, the surface charges become compensated and so the particles are subjected to van der Waal attraction. This phenomenon is maximized at the critical coagulation concentration of the system (Theng, 1979). The change in mineral surface charge due to cationic polymer adsorption has been observed as a change in zeta potential (Tekin et al., 2005).

Hypothesis / Objective

As mentioned, considerable number of studies on modifying pore fluid environment, mostly pH and ionic concentration, have been conducted for a purpose of manipulating clay fabric. However, pH and ionic concentration are easily subjected to alteration in nature. An

engineered clay soil system with resistant characteristics to such alteration is needed. The use of polyacrylamide as treatment may form such engineered kaolin clay systems due to its irreversible adsorption onto clay particle surface. If polyacrylamide is a viable tool for creating engineered kaolin clay systems, types of particle association, the mechanisms that determine those particle associations, and the influence of polyacrylamide characteristics such as molecular weight and ionic type will be investigated.

In spite of studies on the behavior of clay-polymer systems at the level of particle-particle and particle-fluid interactions, few studies focus on fabric development over a wide range of solids content and strain conditions. The purpose of this study is to understand fabric development in kaolin-polyacrylamide systems, investigating the impact of polyacrylamide on the behavior of kaolin clay over a wide range of solids contents and strain conditions. It is expected that the use of polyacrylamide results in flocculated systems. If the micro-scale single particle arrangement is related to applied polymer characteristics and solids content of the system, then a formulated fabric map in the presence of the polymer will be developed. Sedimentation tests (low solids content), viscosity measurements (moderate solids content), and liquid limit measurements (high solids content) will be conducted to determine variation in fabric for kaolin-polyacrylamide systems at various concentrations, molecular weight and ionic types of polyacrylamide. The resulting fabric at various solids contents will be verified using scanning electron microscopy (SEM) and the influence of the micro-scale manipulation on the macro-scale behaviors will be discussed with the results of sedimentation tests, viscosity measurements, and liquid limit measurements.

Chapter 2

LITERATURE REVIEW

An overview of the nature of clay particles, polymers, and their combinations is given in this chapter. Topics addressed in this section include: the nature of kaolin clay surface charge, clay particle associations, and the nature of kaolin-polyacrylamide interactions. Systematic studies found in the literature carried out on clay charge formation, particle association, and interaction of clays and polymers are summarized.

Nature of kaolin clay surface charge

Kaolinite is a well-known and well-studied clay mineral. Its surface characteristics are fairly well understood and allow for a more precise interpretation of sedimentation and rheological behavior in terms of particle interaction. Kaolinite has the general formula, $\text{Al}_2\text{O}_3 \cdot 2\text{SiO}_2 \cdot 2\text{H}_2\text{O}$ and has a layered structure composed of one silica sheet and one gibbsite sheet. Hence, the mineral layer has two different basal faces as shown in Figure 2.1. One basal face exhibits an inert tetrahedral siloxane structure (SiO_4). The other basal face consists of an octahedral gibbsite structure ($\text{Al}(\text{OH})_6$) terminating in OH^- . The layer edges terminate in both OH^- and O^{2-} groups. The silica and gibbsite sheets are strongly held together by shared oxygen atoms - covalent bonds - forming a layer. Hydrogen bonds, also a strong bond type, hold layers together, so very little swelling occurs (van Olphen, 1977; Israelachvili, 1991; Mitchell, 1993; Santamarina et al., 2001; Ebnesajjad, 2006).

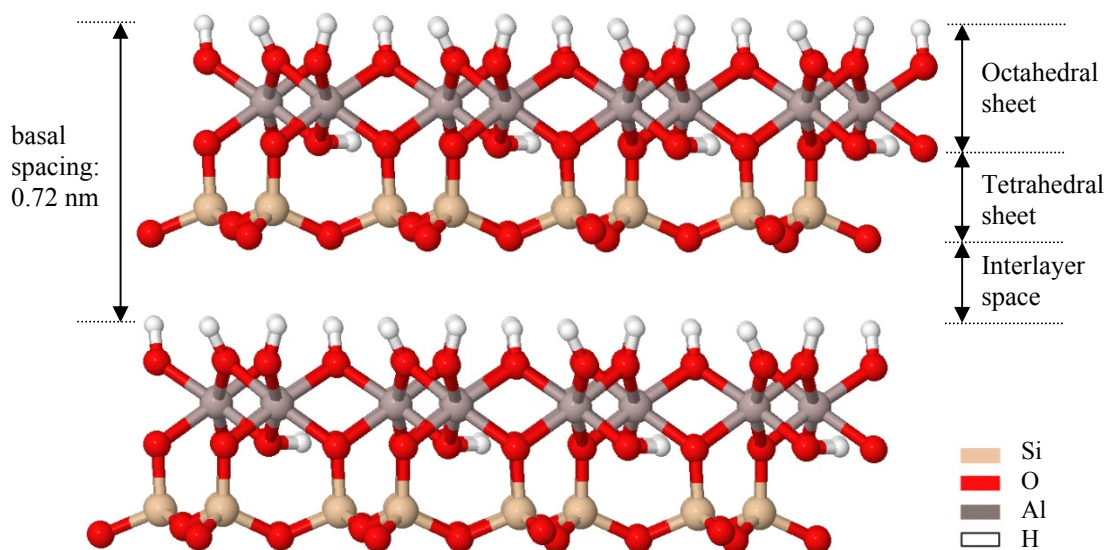


Figure 2.1: Mineral composition of kaolinite (MMP, 2003)

Kaolin clay particles have a net charge, in polar fluid, caused by a non-ideal chemical composition or defective structure containing isomorphous substitution, broken bonds, crystal defects, structural disorder, and protonation or deprotonation (Grim, 1968; Sposito, 1989; Brady et al., 1996). For kaolin, isomorphous substitution accounts for only a small percentage of the overall net charge. Isomorphous substitution of a single Si^{4+} by Al^{3+} or Fe^{3+} in every 400 Si^{4+} induces a very small permanent negative charge (less than 5% of overall charges) (van Olphen, 1977; Ma and Eggleton, 1999). While both basal surfaces are theoretically electrically neutral in infinite, most of the excess charge of kaolin particles occurs at the edge termination sites. At the particle edge, the silica tetrahedral and alumina octahedral edges are disrupted (broken bonds) exposing aluminol (Al-OH) and silanol (Si-OH) groups. This is the main mechanism of charge formation on kaolinite particles even though the edge area only contributes approximately 10% of the whole surface area (Wierer and Dobias, 1988; Tekin et al., 2005). In addition to broken bonds, protonation or deprotonation of the hydroxyl groups results in charge formation, and the

type of charge (i.e., positive, negative, or neutral) depends mainly on the pore fluid environment such as pH and ionic concentration (van Olphen, 1977; Sposito, 1984; Stumm, 1992).

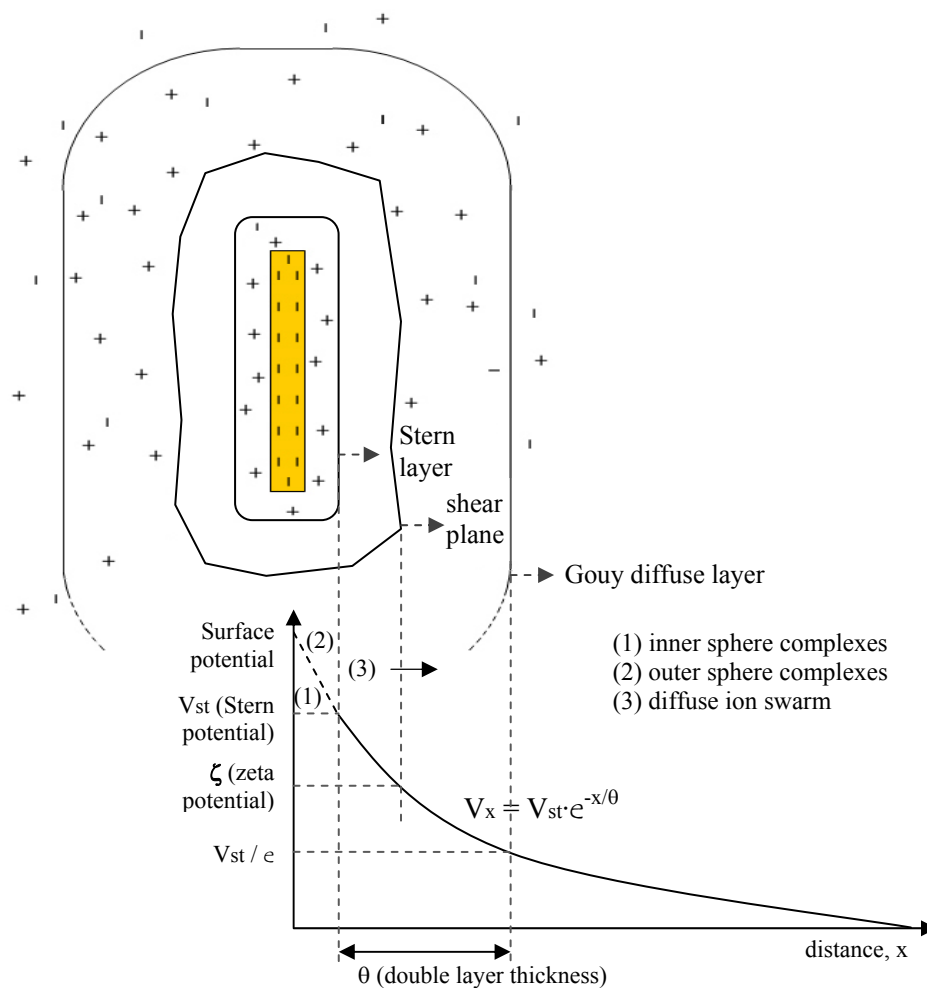


Figure 2.2: Electrical potential (V_x) of double layer compiled from Israelachvili (1991), Stumm (1992), Santamarina et al. (2001), and Mitchell and Soga (2005). Plot from Santamarina et al. (2001)

When a dry kaolinite particle is hydrated by water molecules, precipitated salts bound to the particle surface are also hydrated, exposing counterions that have an opposite charge to the surface. The hydrated counterions are attracted to the surface through Coulombian attraction, diffusing away from the surface due to water polarity and thermal agitation. The diffusion range is limited by the attraction force between the particle surface and the hydrated counterion, and the

electrical potential of the particle. The counterion concentration decreases to the bulk fluid concentration as a function of distance from the surface. The electrical double layer consists of the Stern layer and the Gouy diffuse layer as shown in Figure 2.2. The outer boundary of the Gouy diffuse layer is not well-defined (van Olphen, 1977; Stumm, 1992). The thickness of the double layer depends on temperature, bulk fluid concentration, ionic valence, and permittivity of pore fluid. In addition, an equal and opposite charge at the mineral surface influences the double layer thickness. Random movements of hydrated counterions in and out of the double layer induces a change in the thickness as a function of thermal agitation and the availability of counterions (van Olphen, 1977; Hunter, 1993; Santamarina et al., 2001).

Protonation or deprotonation of the mineral surface is accomplished with potential determining ions such as H^+ and OH^- . Other ions can form inner and outer sphere complexes through adsorption. Cation adsorption is especially significant because it alters the surface charge on O^{2-} termination sites, depending on the concentration, valence, and size of the ions. A silica tetrahedral basal face has one O^{2-} termination site every 4.8 \AA^2 (Santamarina et al., 2001). The total net surface charge (σ_p) is defined as (Sposito, 1989)

$$\sigma_p = \sigma_0 + \sigma_H + \sigma_{IS} + \sigma_{OS} \quad \text{Equation 2.1}$$

where σ_0 is permanent structural charge resulting from isomorphic substitution or broken bonds in particles, σ_H is net proton charge due to protonation or deprotonation, σ_{IS} is inner sphere complex charge, and σ_{OS} is outer sphere complex charge (Sposito, 1989; Stumm, 1992; Santamarina et al., 2001). Point of zero charge (PZC) is defined as pH value where total net surface charge (σ_p) is zero (Stern potential is zero). The isoelectric point (IEP) is reached when the electrophoretic mobility of a particle in an electric field is zero (zeta potential is zero). Due to the diffuse nature of the ion swarm, the PZC is typically not equal to the IEP (Sposito, 1998). The difference between PZC and IEP implies the amount of diffuse ions entrapped within the shear plane of the electric double layer. Both PZC and IEP of a clay particle depend on the availability of OH^-

termination sites along the particle surface, fluid pH, and the dominating counterion valence and concentration in the fluid (Stumm, 1992; Santamarina et al., 2001). PZC and IEP values reported for kaolinite are shown in Table 2.1.

Table 2.1: Point of zero charge and isoelectric point reported for kaolinite.

| | Value (pH) | | Electrolyte and concentration (mol/L) | Reference |
|-------|----------------------------|----------------------|---|-----------------------------|
| | Particle/face | Edge | | |
| IEP | 5.8 | 4.9 | NaCl, 10^{-4} NaCl, 10^{-3} NaCl, 10^{-2} to 10^{-4} cationic polyacrylamide, 225 mg/L, $\phi = 0.0015$ | (Flegmann et al., 1969) |
| | 7.3±0.2 | | | (Rand and Melton, 1977) |
| | 5.25 | | | (Siffert and Kim, 1992) |
| | 5, 4.25 | 7.2 | | (Braggs et al., 1994) |
| | 2 | | | (Schroth and Sposito, 1997) |
| | 3.9 | | | (Dobias et al., 1999) |
| | <3 | | | (Santamarina et al., 2001) |
| 7.9 | (Santamarina et al., 2001) | | | |
| | | (Tekin et al., 2005) | | |
| PZC | 7 | | | (Flegmann et al., 1969) |
| | 4.2 | | | (Stumm, 1992) |
| PZNPC | 7~8 | 7.5, 7.3 | | (Wieland and Stumm, 1992) |
| | 3 | 5 | | (Zhou and Gunter, 1992) |
| | 4.66, 4.5 | | | (Braggs et al., 1994) |
| PZNC | 4 | | | (Schroth and Sposito, 1997) |
| | 4.8, <4 | | | (Zhou and Gunter, 1992) |
| | | | | (Schroth and Sposito, 1997) |

IEP (isoelectric point): ζ potential = 0; PZC (point of zero charge): $\sigma_p = 0$; PZNPC (point of zero net proton charge): $\sigma_H = 0$; PZNC (point of zero net charge): $\sigma_0 + \sigma_H = 0$

The structural differences between basal surfaces and between face and edge lead to the coexistence of negatively charged faces and positively charged edges (Carty, 2001). The IEP of silica is 2.0~3.5 and the IEP of alumina is 8.5~10.4 based on pure mineral colloidal behavior. Thus it can be inferred that a silica basal face is negatively charged at pH above 3.5 and an alumina basal face is positively charged at pH below 8.5. At the edges, IEP values may be more sensitive because exposed silanol (Si-OH) and aluminol (Al-OH) groups are very reactive to protonation/deprotonation and complexation (Wierer and Dobias, 1988). The pore fluid pH determines the magnitude of edge and face charge because the major charge source of the

alumina basal face and the edges is protonation/deprotonation which is significantly pH-dependent.

Particle associations

Clay particles consist of stacks of mineral layers. A particle has two exposed faces and two exposed edge sites. Interactions between face and edge sites from two different particles can result in many different particle arrangements. These arrangements, or associations, are categorized into several types as shown in Figure 2.3. Interparticle forces strongly influence micro-scale fabric development under low confinement conditions, and in turn, the macro-scale properties of the soil, e.g. shear strength, compressive strength, compressibility, and permeability.

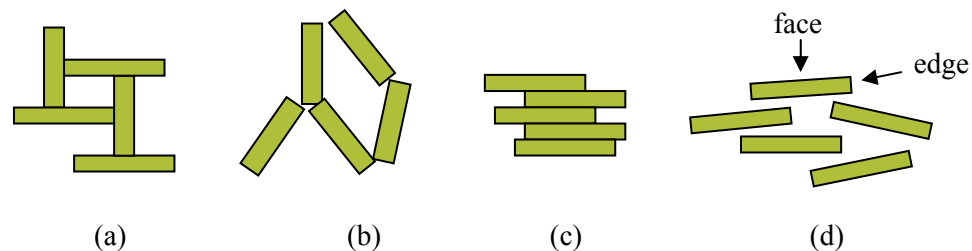


Figure 2.3: Schematic of particle associations: (a) edge-to-face (EF), (b) face-to-face (FF), (c) edge-to-edge (EE), and (d) dispersed

For clay particles, there are four major particle association types: edge-to-face (EF), face-to-face (FF), edge-to-edge (EE), and dispersed as shown in Figure 2.3. The association type depends on the governing interparticle forces (van Olphen, 1977). Edge-to-face (EF) flocculation is promoted by Coulombian attraction between a negative face and a positive edge. Van der Waals attraction and double layer repulsion, known together as DLVO forces after Derjaguin, Landau, Verwey, and Overbeek, between the same charged faces cause face-to-face (FF) aggregation or dispersed behavior. Dispersed behavior arises when particles do not interact with

one another to form associations. Particles remain dispersed when their double layers are large - high repulsive forces - or when all excess charges on the particle are compensated rendering the particle electrically neutral. FF aggregation occurs when van der Waals attraction prevails between particles. Slight repulsive forces between particle faces and van der Waals attraction between particle edges induce edge-to-edge (EE) associations. When particles are linked through EE and EF associations, larger sediment volumes develop with a higher void ratio (lower density) than soil fabrics consisting mostly of FF associations (Mitchell, 1956; Rand and Melton, 1977; van Olphen, 1977).

Pore fluid pH and ionic concentration affects the type and number of particle associations that develop in a particle suspension. At pH below the isoelectric point (IEP) of the edge site (for kaolinite, <7.2) and low ionic concentration, EF dominates due to Coulombian attraction between negatively charged faces and positively charged edges. FF aggregation is due to low double layer repulsion forces and prevails at high ionic concentration (for kaolinite, $>0.1\sim 0.15$ NaCl mol/L). EE is favored at pH = edge IEP (edge IEP at $\text{pH}\approx 7.2$, face or particle IEP at $\text{pH}\approx 4$) and low ionic concentration. The edge and face are both negatively charged, at high pH and low ionic concentration, and clay particles are dispersed due to increased double layer thickness (i.e., high repulsive force) (Santamarina et al., 2001; Palomino and Santamarina, 2005).

Noncovalent interactions are a major interparticle force between polymer molecules and between polymer molecules and clay mineral surfaces. Four types of noncovalent interactions are typically considered: van der Waals; electrostatic (e.g., Coulombian attraction between two oppositely charged molecules, and repulsion between like-charged molecules); polar (or Lewis acid-base); and Brownian motion interaction (Israelachvili, 1991; Van Oss, 2006). van der Waals force is a universal attractive interaction existing between neutral atoms, molecules, or particles. The magnitude between individual atoms is very low but it becomes more significant as particles increase in size.

Molecules, as well as particles, may develop a net negative or positive charge in a polar fluid. Electrostatic interactions between the molecules or between the mineral and molecule can be attractive or repulsive, depending on the dominating charges on both the mineral surface and the polymer molecule. Electrostatic forces are considered long-range forces acting at distance greater than a few nanometers. Within a short range - less than a few nanometers - polar interactions, including ion-dipole and dipole-dipole interactions, become the governing interaction. Polar interaction forces can be up to two orders of magnitude stronger than the long-range interaction forces, depending on the fluid medium properties and the particle surface properties, such as hydrophobicity, degree of crystallization, roughness, and rigidity. Polar interaction forces can be attractive (i.e., hydrophobic interaction), repulsive (i.e., hydration pressure), or fluctuating. Brownian motion takes place between suspended particles in liquid media and the forces are always repulsive (Van Oss, 2006).

Manipulation of interparticle forces can be used to control particle associations, and thereby fabric. Interparticle forces can be altered through changes in pore fluid chemistry. Thus, polymer treatment may be a viable method for design of macro-scale properties in addition to bulk fluid pH and ionic concentration.

Nature of kaolin-polyacrylamide interactions

Polymers are classified into two groups: aqueous and non-aqueous polymers. Aqueous are hydrophilic polymers while non-aqueous are hydrophobic. Non-aqueous polymers are not typically used in engineering practice due to the lack of affinity between hydrophilic clay mineral surfaces and hydrophobic polymers (Whittingham and Jacobson, 1982; Galimberti et al., 2007). Therefore, aqueous polymers are preferred in engineering practice.

Polyacrylamide (PAM), an aqueous polymer, is an important commercial water-soluble polymer discovered in the 1970s (Bikales, 1973). Polyacrylamides are commonly used in industry because they are cost-effective and can be produced in any ionic form. PAM is a homopolymer synthesized by the polymerization of acrylamide (Barvenik, 1994) and can be made in cationic, anionic and nonionic forms. The molecular weight can be manipulated ranging from a few thousand g/mol to 20×10^6 g/mol. It can also be formulated with copolymers such as quaternized ammonium chloride to provide a specific net charge (van Olphen, 1977; Theng, 1979). PAM characteristics depend on both charge type and molecular weight.

PAM has been observed to adsorb onto clay particles and external surfaces of soil aggregates (Stutzmann and Siffert, 1977). Interactions between clay particles and polymer molecules result from: polymer bridging, charge neutralization or compensation, complex formation between clay particle surfaces and polymer molecules, or from a combination of these mechanisms (van Olphen, 1977; Pefferkorn et al., 1987; Lee et al., 1991; Laird, 1997; Dobias et al., 1999; Mpofu et al., 2003; Deng et al., 2006). Polymer bridging plays a major role in the presence of nonionic polymers (Theng, 1982; Laird, 1997; Hogg, 1999; Deng et al., 2006), while charge neutralization plays a major role in the presence of cationic polymers. A polymer molecule can be adsorbed onto clay particles simultaneously bridging more than one particle as shown in Figure 2.4. The carbonyl (C=O) oxygen of PAM bonds to the aluminol group (Al-OH) on the edge site through hydrogen bonding. Hydrophobic bonding occurs between the hydrophobic backbone (CH₂-CH) of PAM and the hydrophobic basal face (i.e., uncharged sites on the siloxane face). Exchangeable cations on the clay surface are bridged to the carbonyl oxygen of PAM through ion-dipole interaction. Water molecules can bridge the exchangeable cation together with the carbonyl oxygen through hydrogen bonding, between the water molecule and the carbonyl group, and ion-dipole interaction between the water molecule and the exchangeable cation. Polymer bridging can be modified by the molecular weight of polymer,

conformation (i.e., coiled or extended) of polymer molecules, and preexisting exchangeable cations on the clay particle surface. The conformation of polymer molecules in aqueous systems is pH-dependent. At pH = 6, both cationic and nonionic polyacrylamide molecules are neither fully extended nor fully coiled, that is, intermediate conformation (Besra et al., 2004). The importance of the exchangeable cations in terms of ion-dipole interaction increases in the order: Na^+ , K^+ < Ca^{2+} , Mg^{2+} < Al^{3+} < Cu^{2+} , Ni^{2+} (Deng et al., 2006). In this study, Na^+ is the only exchangeable cation.

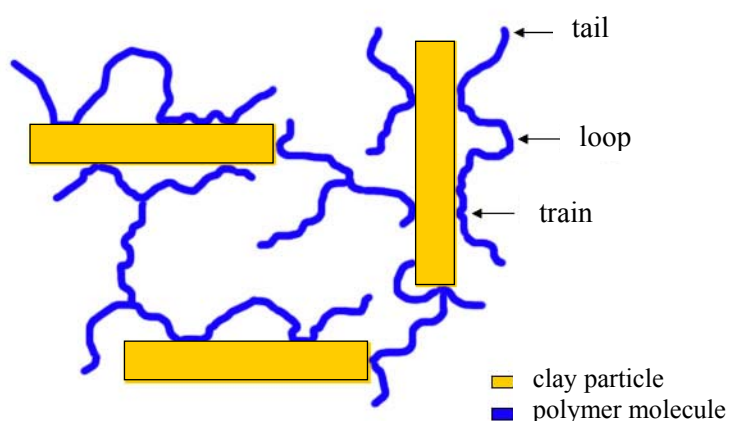


Figure 2.4: Schematic of polymer bridging compiled from van Olphen (1977) and Theng (1979)

Coulombian attraction is the dominating bonding mechanism between the clay surface and cationic PAM molecules (van Olphen, 1977; Theng, 1979; Laird, 1997; Mpofu et al., 2003). The positively charged trimethyl ammonium groups of cationic PAM are attracted to the negatively charged sites along clay particle surface. At the critical coagulation concentration (CCC) of PAM, all charges on the mineral surface are compensated. Once the CCC is exceeded, aggregation occurs through van der Waals attraction. The charged groups of cationic PAM may also adsorb onto more than one particle, and so may also contribute to polymer bridging. Cationic PAM molecules may also form an adsorption complex when a concentration of PAM

greater than the critical coagulation concentration is used. The hydrophobic backbones ($\text{CH}_2\text{-CH}$) of the excess cationic PAM molecules link together through van der Waals attraction. Schematic bonding mechanisms of kaolin-polyacrylamide composites at the molecular level are shown in Figure 2.5.

The polymer adsorption can also induce a dispersed system. Osmotic interaction is a secondary interaction caused by Brownian motion and/or van der Waals attraction, polar interaction, and electrostatic interaction forces and can lead to dispersion, especially at low solids content and at low molecular weight of polymer (Van Oss, 2006).

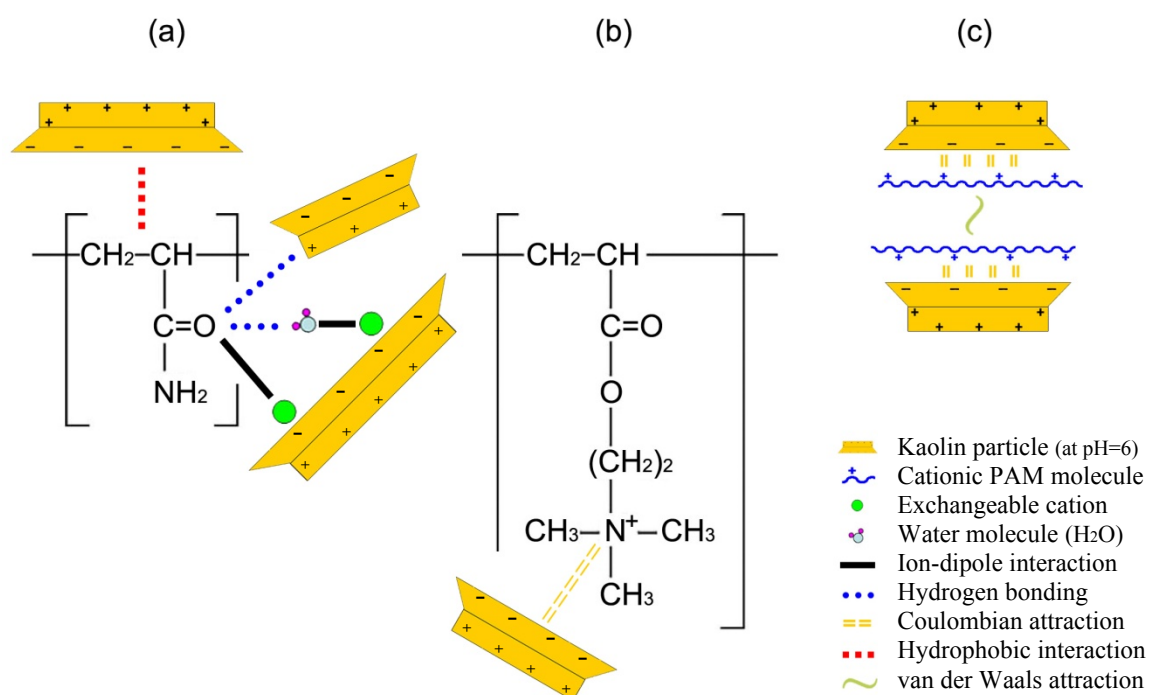


Figure 2.5: Schematic bonding mechanisms of kaolin-polyacrylamide composites at the molecular level: (a) nonionic PAM molecule, (b) cationic unit of cationic PAM, (c) charge neutralization.

Chapter 3

EXPERIMENTAL STUDY

The purpose of this study is to understand fabric development in kaolin-polyacrylamide systems by investigating the impact of polyacrylamide on the behavior of kaolin clay over a wide range of solids contents and strain conditions. Particle association types are inferred from macro-scale tests including sedimentation tests, viscosity measurements, and liquid limit measurements. Observed trends related to fabric properties indirectly provide dominating particle association types and therefore governing interparticle forces. A direct method, scanning electron microscopy (SEM), is used to verify the fabric development with the results from indirect measurements.

In this chapter, characteristics of materials used for this study are investigated. Methodologies of sedimentation tests, viscosity measurements, liquid limit measurements, and an SEM study to determine variation in fabric are described.

Materials

Kaolin clay

Kaolinite is a well-known, well-studied clay mineral, which makes it ideal for inclusion in this study. Kaolin particle surface characteristics are fairly well understood so that the effects of polymer addition can be more easily evaluated. Hence, a more precise interpretation of sedimentation and rheological behavior in terms of particle interaction is achievable.

The clay used in this study is an untreated kaolin clay from Wilkinson Kaolin Associates LLC (Gordon, Georgia). The kaolin is designated by the manufacturer as SA1 and segregated by size using air floatation. Its chemical composition is nearly the same as theoretical kaolinite indicating high purity, as shown in Table 3.1. Selected properties of the clay are given in Table 3.2 and grain size distributions obtained from the manufacturer and measured are shown in Figure 3.1.

Table 3.1: Chemical composition of kaolin clay used for this study.

| component | % component | |
|--------------------------------|-------------|---|
| | Kaolin clay | Theoretical kaolinite (Murray, 1991) |
| SiO ₂ | 45.6 | 46.3 |
| Al ₂ O ₃ | 38.4 | 39.8 |
| Fe ₂ O ₃ | 0.4 | |
| TiO ₂ | 1.5 | |
| CaO | 0.06 | |
| MgO | Trace | |
| K ₂ O | 0.18 | |
| Na ₂ O | Trace | |
| LOI | 13.82 | 13.9 |

Table 3.2: Properties of kaolin clay. Manufacturer and measured (*) data

| Property | Value |
|--|--------------------------|
| Median particle diameter, D ₅₀ (μm) | 1.1 |
| Specific gravity | 2.6 |
| Specific surface ^a (m ² /g) | 40.37* |
| pH (at solids content of 2% and 7%) | 7.5*, 6.7* |
| Isoelectric point (pH) | 2.3* |
| Charge density (C/m ²) | 1.6 x 10 ⁻² * |
| Viscosity (7% solids at pH=6, mPa·s ^b) | 8.88* |

^a methylene blue European spot method (Santamarina et al., 2002)

^b Brookfield #S00 Spindle at 100 rpm

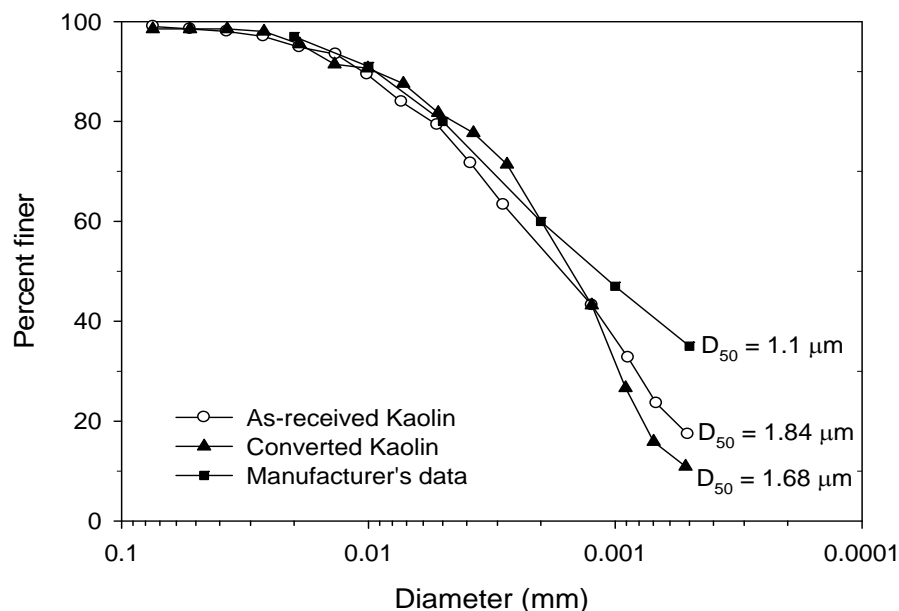


Figure 3.1: Particle size distribution curves for kaolin clay used for this study. Manufacturer and measured data.

The clay is washed with a high concentration of NaCl solution to replace mineral surface charge-compensating ions with Na^+ ions, converting the clay to monoionic form. This conversion method is modified after van Olphen (1977). First, dry clay is vigorously mixed with a 2M NaCl solution at a proportion of approximately 3ml solution per gram kaolin. The clay mixture hydrates for 48 hours, after which the supernatant is replaced with a 1M NaCl solution, mixed well again and left to hydrate for another 24 hours. The supernatant is decanted and replaced again with 1M NaCl solution, mixed, and allowed to hydrate for 24 hours. The conversion process has a total equilibrium time of 96 hours. After the final salt wash, the excess salt is removed by replacing the supernatant fluid with deionized water until the supernatant conductivity measures less than $100 \mu\text{S}/\text{cm}$. The converted clay slurry is oven-dried and ground using a pestle and mortar.

Polyacrylamides

Clay particle interactions are modified using three types of polyacrylamides: cationic containing 20% cationic quaternary ammonium salt groups, nonionic, and low molecular weight nonionic (Cytec Industries Inc., West Paterson, NJ). Select characteristics of the polymers are given in Table 3.3.

The influence of charge type is explored with a cationic polyacrylamide (C-PAM) and a nonionic polyacrylamide (N-PAM). The influence of polymer molecular weight is explored with a high molecular weight nonionic polyacrylamide (N-PAM) and a low molecular weight nonionic polyacrylamide (n-PAM). Polyacrylamides concentration is varied from 0 mg/L to 500 mg/L to observe a change in behavior. The range of concentration has been selected from charge calculation (see Appendix A).

Table 3.3: Characteristics of polyacrylamides used in this study

| Type | Trade Name | Structure | Fraction of charged units | Molecular weight (g/mol) ^a |
|---------------------------------|------------|---|-----------------------------|---------------------------------------|
| Nonionic | N300 | $\left[\begin{array}{c} \text{CH}_2-\text{CH} \\ \\ \text{C}=\text{O} \\ \\ \text{NH}_2 \end{array} \right]$ | None | $\sim 6 \times 10^6$ |
| Nonionic (low molecular weight) | N300LMW | | None | $\sim 8 \times 10^4$ |
| Cationic | C494 | $\left[\begin{array}{c} \text{CH}_2-\text{CH} \\ \\ \text{C}=\text{O} \\ \\ \text{NH}_2 \end{array} \right]_x \left[\begin{array}{c} \text{CH}_2-\text{CH} \\ \\ \text{C}=\text{O} \\ \\ \text{O} \\ \\ (\text{CH}_2)_2 \\ \\ \text{CH}_3-\text{N}^+-\text{CH}_3 \\ \\ \text{CH}_3 \end{array} \right]_y \text{Cl}^-$ | $\frac{y}{(x+y)} \cong 0.2$ | $\sim 4 \times 10^6$ |

a : Measured using viscometry method (Brandrup and Immergut, 1989; Ravve, 2000)

Selection of Polymer Concentration Tested

Charges in the electric double layer must balance excess charges on the kaolin particle surface. In the presence of cationic PAM molecules, inorganic cations in the ion cloud are displaced with cationic groups of the PAM (Theng, 1979; Laird, 1997). When all inorganic cations are replaced, the particle becomes electrically neutral. At this point, the dosage of cationic PAM is a fitted concentration for charge neutralization. This concentration can be calculated based on the charge density of the polymer and the particle. The charge calculations are attached in Appendix A.

According to the charge calculation, 1 gram of kaolin has 3.98×10^{18} charges. The same number of cationic groups will neutralize all the kaolin surface charges. 3.16 mg of the cationic PAM, which contains 3.98×10^{18} positively charged groups, theoretically induces charge neutralization in the system. For sedimentation test at solids content of 0.02, which has minimal hindered effects caused by particle collisions, a concentration of 164 mg/L is the fitted concentration (critical coagulation concentration) for achieving charge neutralization. In order to investigate the effect on the number of polymer charge groups, three concentrations (20, 80, 120 mg/L) below 164 mg/L and two excess concentrations (240, 500 mg/L) are selected.

Under the same PAM concentration range, the influence of molecular weight, different ionic group, and different solids contents are investigated.

Sedimentation

The relative state of dispersion of a low solids content slurry is inferred from observing settling behavior and relative final sediment volume. Observed sedimentation behavior implies various modes of particle association types as defined in Table 3.4: EF flocculated, FF aggregated,

and dispersed. Mixed-mode sedimentation is defined when the settling behavior exhibits characteristics of both flocculated and dispersed. Modes are defined after Palomino (2004). Particle associations are defined herein as flocculated for EF and EE associations, aggregated for FF associations, and dispersed for particles with minimal interaction. The final clay fabric is determined by pore fluid environment and polymer characteristics. In this study, pore fluid environment remains constant: pH=6 and zero ionic concentration prior to the addition of PAMs. Particle associations are subjected to alteration with the addition of PAMs at various concentrations, molecular weight, and ionic types.

Settling behavior and relative final sediment volume are easily observable parameters useful in inferring fabric and, at the micro-scale, particle associations. For example, suspension-sediment boundary for dispersed sedimentation moves upward as sediment builds while that for flocculated sedimentation moves downward as flocs or aggregates form. Dispersed sedimentation has cloudy supernatant while flocculated sedimentation displays clear supernatant (Pierre et al., 1995; Palomino and Santamarina, 2005). A schematic of dispersed and flocculated sedimentation is shown in Figure 3.2. In reference to final sediment height, dispersed settling has the most compact sediment, while flocculated and aggregated settling include flocs or aggregates formation which results in more open, voluminous fabric.

Particle association can also be inferred in terms of floc size and density calculated from sedimentation test. The induction period is defined as the slope of the initial phase of the sediment height-time curve. A flocculated system settles rapidly and has a short induction time. The correlation between settling rate for suspension-sediment interface and volume of the final sediment provides an indication of floc density and size formed when flocculation or aggregation occurs, and when the particles remain dispersed in the system (Richardson and Zaki, 1954; Godard and Richardson, 1969; Bhatti et al., 1978; Font et al., 1999). Floc density (ρ_f) and size (D) are calculated as

$$\rho_f = \frac{\rho_s + (k-1) \cdot \rho_L}{k} \quad \text{Equation 3.1}$$

$$D = \left(\frac{18\mu \cdot \mu_u}{g(\rho_f - \rho_L)} \right)^{0.5} \quad \text{Equation 3.2}$$

where ρ_s is the solid density, ρ_L is the liquid density, and μ is the liquid viscosity (0.01 poise for water at 20°C), k and μ_u are parameter obtained from the relationship between settling rate and solids content in terms of volume:

$$V_s^{1/n} = -k \cdot \mu_u^{1/n} + \mu_u^{1/n} \quad \text{Equation 3.3}$$

where V_s is settling rate ($-dh/dt$), n is the nature of the particles as a function of the flow regime (4.65 for rigid particles). Because of the buoyancy effect, i.e. resistance force to settling increases with increasing the volume of floc, both floc size and density are considered together with the settling behavior (Kaya et al., 2006).

Sedimentation suspensions are prepared with a final solids content (ϕ) of 0.02. Various concentrations of PAMs prepared with the suspension are shown in Table 3.5. The solids content is defined as the proportion of solids volume with respect to the total suspension volume. The solids content of 0.02 is selected to minimize particle collisions and support initial free fabric formation (Irani and Callis, 1963).

Table 3.4: Observed suspension settlement modes defined for this study

| Sedimentation Characteristics | Mode | | | |
|----------------------------------|---|--|---|--|
| | Dispersed Sedimentation | EF Flocculation Sedimentation | FF aggregation Sedimentation | Mixed-Mode Sedimentation |
| Particle Interaction | Minimal; Any aggregates formed remain dispersed | Strong; flocs readily form | Strong; aggregates readily form | Minimal → Floc/Agg. Formation |
| Suspension Appearance | Milky with increasing density from top to bottom | Uniform density | Uniform density | Top to bottom increasing density → uniform |
| Supernatant Appearance | Cloud of suspended fine particles | Clear | Clear | Cloudy → Clear |
| Supernatant-Suspension Interface | None | Well-defined, moves downward as flocs settle | Well-defined, moves downward as aggregates settle | None → Well-defined |
| Suspension-Sediment Interface | Well-defined, moves upward as sediment builds | None | None | Well-defined → None |
| Settlement Rate | Very slow | Rapid, constant | Very rapid, constant | Slow → Rapid |
| Sediment Formation | Particles settle into lowest possible position and according to size, largest first | Flocs settle in random pile | Aggregates settle according to size | Particles settle according to size → Formed flocs/aggregates settle uniformly |
| Sediment Volume | Compact; strongly resists redispersion | Voluminous; easily redispersed | Compact to voluminous | Layer of compact sediment below layer of voluminous sediment |

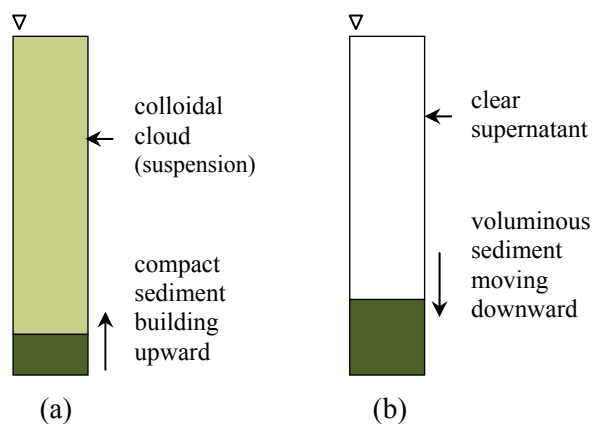


Figure 3.2: A schematic of (a) dispersed sedimentation and (b) flocculated/aggregated sedimentation

Table 3.5: Test matrix for sedimentation tests. $\phi = 0.02$

| Polymer type | Cationic Polyacrylamide (C-PAM) | Nonionic Polyacrylamide (N-PAM) | Low molecular nonionic Polyacrylamide (n-PAM) |
|----------------------|---------------------------------|---------------------------------|---|
| Concentration (mg/L) | 0 | 0 | 0 |
| | 20 | 20 | 20 |
| | 80 | 80 | 80 |
| | 120 | 120 | 120 |
| | 240 | 240 | 240 |
| | 500 | 500 | 500 |

The total volume of each suspension is 100 ml. 5.2g of kaolin is placed in 200-ml beaker and mixed with deionized water. The beaker is placed on a Corning magnetic stirrer and hydrated for 24 hours before pH control. The suspension pH value is adjusted by adding either 0.2 M hydrochloric acid (HCl) or 0.2 M sodium hydroxide (NaOH) until the target pH=6 is reached. The beaker is placed on the stirrer for another 24 hours mixing with various concentrations of PAMs before the sedimentation test. During hydration and mixing with PAM, the suspensions are covered to prevent evaporation. The suspension is transferred to a 28 mm-

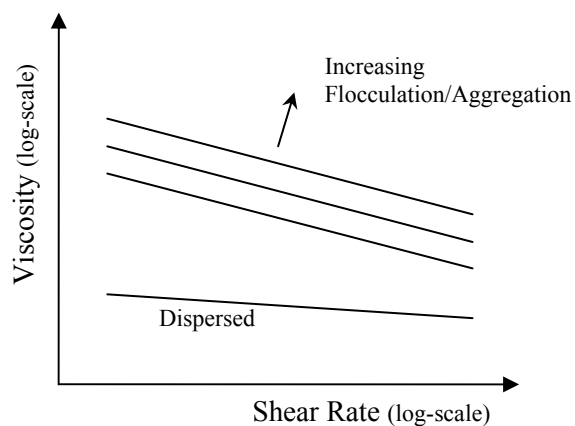
inner diameter graduated glass cylinder. Air that may be entrapped in the pores is removed with a low vacuum ($u \approx -0.01$ Pa, Duo Seal vacuum pump from Welch Scientific Company, IL) until no bubbles are seen. The vacuum is removed and the cylinder is capped with a rubber stopper or laboratory film. The solids are resuspended by repeatedly inverting the cylinder for one minute.

The settling behavior, suspension height, and sediment height are monitored with time. The heights are recorded for at least three weeks starting at $t = 1$ minute: time intervals are 1, 2, 4, 8, 15, 30, 60 minutes, 2, 3, 6, 18 hours, 1 day, 2 days, 4 days, 1 week, 2 weeks, and 3 weeks. The supernatant pH and conductivity of each suspension are measured using the Accumet XL50 pH & conductivity meter (Fisher Scientific) after the last suspension and sediment heights are recorded.

Viscosity

Viscosity of a fluid is a measure of its resistance to deform under shear stress and is an indication of molecular interaction forces. Viscosity increases with increasing amount of energy required to overcome the shear deformation resistance. In slurries, suspended particles promote higher viscosities than that of the pure fluid phase because particles induce fluctuations in the stream lines even under laminar conditions. The concentration of the suspended solids, the size and shape of the suspended particles, and the interaction forces between the particles influence the rheological properties of dispersed systems (Mpfu et al., 2003). In other words, viscosity measurements for particulate systems give an indication of stability or flocculation of the suspension. At moderate solids content, flocculated kaolinite suspensions have a much higher viscosity than that of well dispersed kaolinite suspensions because of the greater energy required to overcome the shear deformation resistance, that is, the flocculated suspensions have a higher shear strength than the dispersed ones. Rheological behavior of clay suspensions are typically between shear-thinning and near-Newtonian behavior. Shear-thinning indicates that the number

of interparticle bonds in a flocculated suspension decreases with increasing shear rate. Thus, the shear-thinning rheological behavior of clay suspensions can be regarded as mechanical deflocculation (Rand and Melton, 1977; Hunter, 2001).



All the mixtures prepared for this study have a solids content of 0.07. Various concentrations of PAMs prepared with the suspension are shown in Table 3.6. The temperature is monitored throughout and remains fairly constant at $21.5^{\circ}\text{C} \pm 2^{\circ}\text{C}$. For each tests, the appropriate solids mass (91 g kaolin) for forming a suspension with a solids content (ϕ) of 0.07 is placed in a 600-ml beaker. The total volume of the suspension is 500 ml. The beaker is placed on a Corning magnetic stirrer and hydrated with deionized water for 24 hours before pH control. The suspension pH value is adjusted by adding either 0.2 M hydrochloric acid (HCl) or 0.2 M sodium hydroxide (NaOH) until the target pH (pH=6 in this study) is reached. The beaker is placed on the stirrer for another 24 hours mixing with various concentrations and ionic types of PAMs prior to measurement. During hydration and mixing with PAMs, the suspensions are covered to prevent evaporation.

Table 3.6: Test matrix for viscosity measurements. $\phi = 0.07$

| Polymer type | Cationic Polyacrylamide (C-PAM) | Nonionic Polyacrylamide (N-PAM) | Low molecular nonionic Polyacrylamide (n-PAM) |
|----------------------|---------------------------------|---------------------------------|---|
| Concentration (mg/L) | 0 | 0 | 0 |
| | 20 | 20 | 20 |
| | 80 | 80 | 80 |
| | 120 | 120 | 120 |
| | 240 | 240 | 240 |
| | 500 | 500 | 500 |

Viscosity is measured using a Brookfield LVDV-1 Prime Viscometer fitted with spindles #00, 61, or 62, depending on the suspension viscosity and spindle measurement range. Spindle #00 has the largest diameter and is therefore used to measure fluids with very low viscosity (1 ~ 600 mPa·s). The spindle rotational speed is varied between 1 rpm and 100 rpm, and the viscosity reading as well as torque % and degree of settlement are recorded at 30-second intervals for each rotational speed setting. Between readings, the suspensions are mixed for 20 seconds to counteract particle settlement. The final pore fluid pH is determined by centrifuging a small sample (10 ml) and measuring the supernatant.

Liquid Limit

Soil fabric can be estimated by liquid limit because the shear strength of clay at its liquid limit is dependent on the soil fabric (Wroth and Wood, 1978; Mitchell, 1993). The liquid limit is the water content of a soil at the boundary between the plastic and liquid behavioral states. Soils at the liquid limit have a shear strength ranging from 2.4 kN/m² to 1.3 kN/m² over the range of liquid limit ranging from 30% to 200% (Wroth and Wood, 1978). A higher liquid limit implies

that flocculated fabrics dominate the system. A flocculated fabric resists shear more than an aggregated and a dispersed fabric, as indicated by a lower liquid limit (Mitchell, 1993). Manipulating pore-fluid chemistry by variation of polymer type and concentration will alter the soil shear strength exhibiting variation of the liquid limit. The sensitivity to pore fluid changes is indicated by the slope of the measured penetration depth-water content lines. As the slope increases, the soil shear strength reduces rapidly for a given increase in water content.

The fall cone test is conducted with the Humboldt penetrometer (model number: H-4236, Humboldt Mfg. Co., IL) to determine the liquid limit of high specific surface soils following the British Standard BS1377-1 (British Standard, 1990). According to the British Standard, liquid limit is defined as the water content at which 80g stainless steel cone with a 30° angle penetrates a remolded soil specimen 20 mm from the soil surface. Various concentrations of PAMs mixed with kaolin clay pastes are shown in Table 3.7.

Table 3.7: Test matrix for fall cone test. $\phi > 0.4$

| Polymer type | Cationic Polyacrylamide (C-PAM) | Nonionic Polyacrylamide (N-PAM) | Low molecular nonionic Polyacrylamide (n-PAM) |
|----------------------|---------------------------------|---------------------------------|---|
| Concentration (mg/L) | 0 | 0 | 0 |
| | 20 | 20 | 20 |
| | 80 | 80 | 80 |
| | 120 | 120 | 120 |
| | 240 | 240 | 240 |
| | 500 | 500 | 500 |

Scanning Electron Microscopy Study

Scanning electron microscopy is a direct method to observe soil fabric (Mitchell and Soga, 2005). SEM provides direct images of the particle systems, thus allowing for fabric development verification. In the SEM study of soil fabric, sample preparation is critical. A freeze-drying technique is adopted to preserve the soil fabric by bypassing the effects of capillary forces. Surface coating with a conductive material, gold, is used to increase the electrical conductivity of the otherwise poorly conductive clay mineral sample surface.

A small amount (less than 5ml) of the suspensions for each test case is placed in a 15-ml glass test tube. The suspension in the tube is rapidly frozen by placing into liquid nitrogen. The sample is then freeze-dried with the dry-ice benchtop freeze dry chamber 75227 (Labconco Co., MO). A very small amount of freeze-dried sample is gently placed onto a SEM sampler. A gold coating, one to three monolayers, is applied using a sputter-coating technique. Gold-coated specimens of kaolin-PAM composites are observed in SEM S-3500N (Hitachi Inc.).

Chapter 4

RESULTS

Sedimentation

Observed settling behavior

Table 4.1 shows observed sedimentation modes defined according to Table 3.4. Settling behaviors for both supernatant-suspension and suspension-sediment boundaries are plotted in Figures 4.1 through 4.3. The initial pH and conductivities for suspensions, measured prior to the PAM addition (i.e., controlled pH), and the final pH and conductivities for supernatants measured after three weeks are given in Table 4.2. Pictures of sedimentation time series are attached in Appendix B.

Table 4.1: Observed sedimentation modes of kaolin-PAM suspensions.

| Polymer type | PAM concentration (mg/L) | | | | | |
|--------------|--------------------------|------------|--|--|--|--|
| | 0 | 20 | 80 | 120 | 240 | 500 |
| N-PAM | Mixed-Mode | Mixed-Mode | Mixed-Mode (near to FF aggregation) |
| n-PAM | | Mixed-Mode | Mixed-Mode | Mixed-Mode | Mixed-Mode (near to FF aggregation) | Mixed-Mode (near to FF aggregation) |
| C-PAM | | Mixed-Mode | Mixed-Mode | FF Aggregation | Mixed-Mode (near to FF aggregation) | Mixed-Mode (near to FF aggregation) |

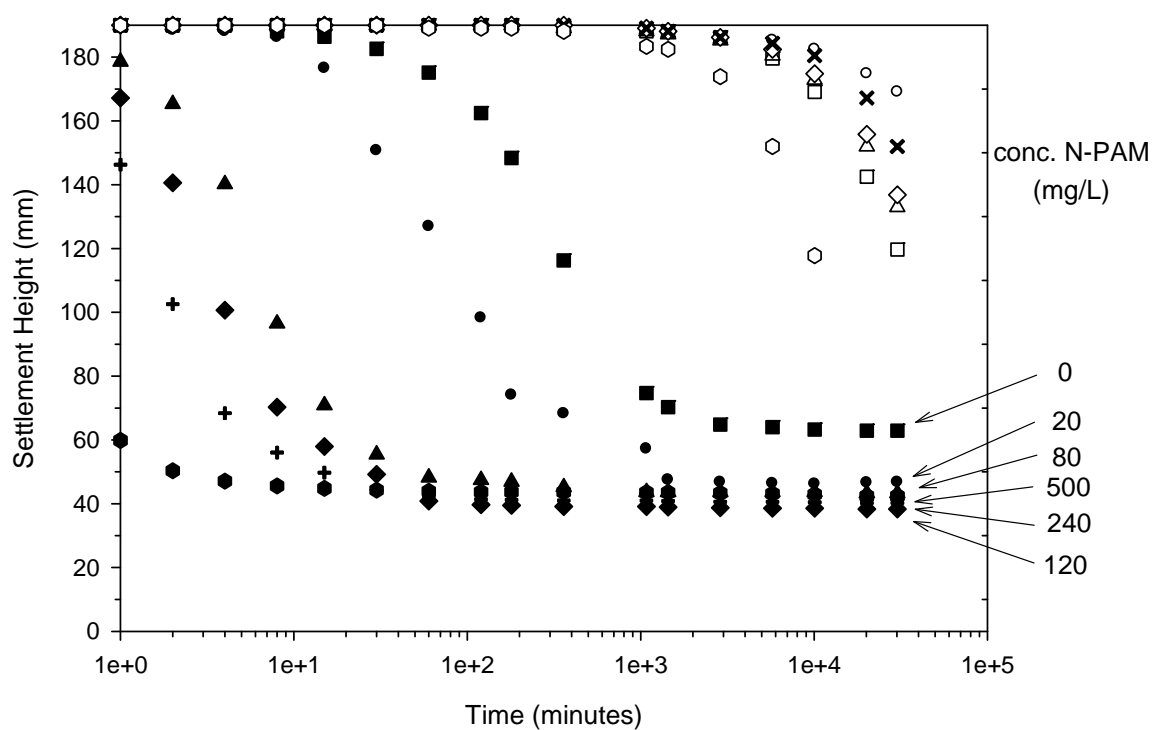


Figure 4.1: Plot of sedimentation boundary height with time for pure kaolin and kaolin-PAM nanocomposite (N-PAM). ■ and □ are for pure kaolin, ● and ○ are for 20 mg/L, ▲ and △ are for 80 mg/L, ◆ and ◇ are for 120 mg/L, + and x are for 240 mg/L, and ● and ○ are for 500 mg/L. Open symbols and x denote supernatant-suspension boundary while closed symbols denote suspension-sediment boundary. After long time t, the two boundaries meet, except for the case of true dispersion.

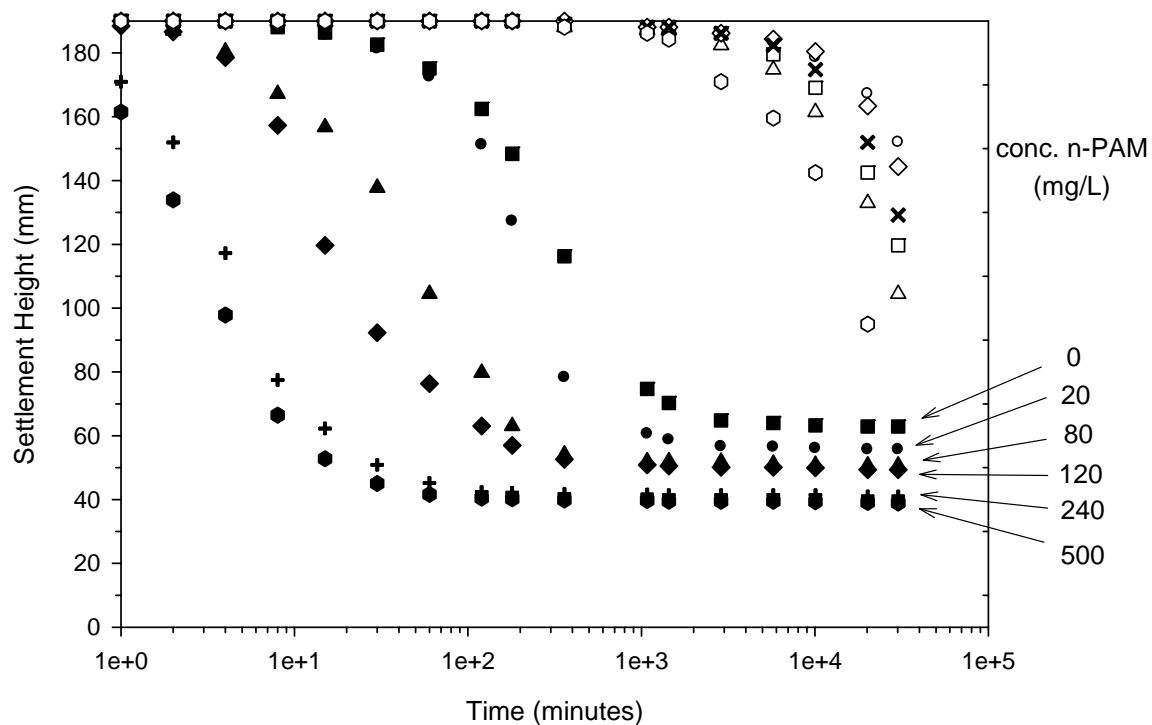


Figure 4.2: Plot of sedimentation boundary height with time for pure kaolin and kaolin-PAM nanocomposite (n-PAM). ■ and □ are for pure kaolin, ● and ○ are for 20 mg/L, ▲ and △ are for 80 mg/L, ◆ and ◇ are for 120 mg/L, + and x are for 240 mg/L, and ● and ○ are for 500 mg/L. Open symbols and x denote supernatant-suspension boundary while closed symbols denote suspension-sediment boundary. After long time t , the two boundaries meet, except for the case of true dispersion.

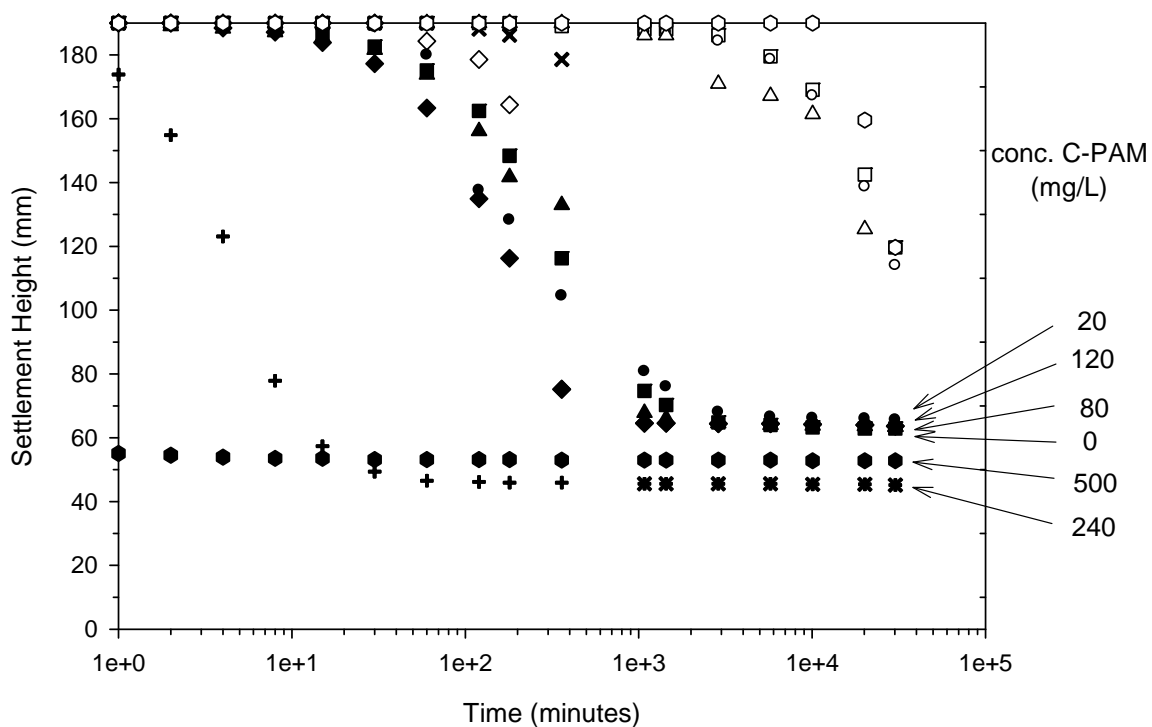


Figure 4.3: Plot of sedimentation boundary height with time for pure kaolin and kaolin-PAM nanocomposite (C-PAM). ■ and □ are for pure kaolin, ● and ○ are for 20 mg/L, ▲ and △ are for 80 mg/L, ◆ and ◇ are for 120 mg/L, + and x are for 240 mg/L, and ● and ○ are for 500 mg/L. Open symbols and x denote supernatant-suspension boundary while closed symbols denote suspension-sediment boundary. After long time t , the two boundaries meet, except for the case of true dispersion.

Salient trends include that all suspensions, except 120 mg/L C-PAM, are characterized as mixed-mode and tend to become FF aggregated with increasing PAM concentration. At C-PAM concentration of 120 mg/L, the suspension displays apparent FF aggregation sedimentation. The density of colloidal clouds is inversely proportional to the final conductivity (See Table 4.2), ranging from 39 to 179 $\mu\text{S}/\text{cm}$. The cloud density decreases as the final conductivity increases. It is observed that the molecular weight of PAM influences the settling behavior of suspension-sediment boundary while the difference in ionic type does not. The suspension-sediment boundary settles more rapidly in the presence of high molecular PAM (N-PAM and C-PAM). The supernatant-suspension boundary for nonionic PAM (N-PAM and n-PAM)-treated kaolin suspension settles slightly more rapidly with increasing PAM concentration, while that for C-PAM-treated suspension does not have any tendencies.

Table 4.2: Initial and final pH and conductivity of sedimentation suspensions.

| Polymer type | Concentration (mg/L) | Initial | | Final (t = 3 weeks) | | Difference | |
|--------------|----------------------|---------|-----------------------------------|---------------------|-----------------------------------|------------|-----------------------------------|
| | | pH | Conductivity ($\mu\text{S/cm}$) | pH | Conductivity ($\mu\text{S/cm}$) | pH | Conductivity ($\mu\text{S/cm}$) |
| Pure kaolin | 0 | 6.15 | 29.32 | 6.07 | 39 | -0.08 | 9.68 |
| N-PAM | 20 | 6.01 | 26.02 | 6.3 | 43 | 0.29 | 16.98 |
| | 80 | 6 | 38.52 | 6.28 | 52.34 | 0.28 | 13.82 |
| | 120 | 6.06 | 29.75 | 6.13 | 57.21 | 0.07 | 27.46 |
| | 240 | 6 | 29.18 | 6.12 | 55.2 | 0.12 | 26.02 |
| | 500 | 5.96 | 29.63 | 6 | 67.7 | 0.04 | 38.07 |
| n-PAM | 20 | 6.08 | 47.37 | 6.07 | 61.18 | -0.01 | 13.81 |
| | 80 | 6 | 69.88 | 6.2 | 75.81 | 0.2 | 5.93 |
| | 120 | 6.01 | 42.78 | 6.48 | 56.02 | 0.47 | 13.24 |
| | 240 | 6.05 | 25.51 | 6.37 | 46.9 | 0.32 | 21.39 |
| | 500 | 5.94 | 26.17 | 6.37 | 60.27 | 0.43 | 34.1 |
| C-PAM | 20 | 6.04 | 76.8 | 6.24 | 93.8 | 0.2 | 17 |
| | 80 | 6.02 | 44 | 6.02 | 90.65 | 0 | 46.65 |
| | 120 | 6.02 | 71.56 | 6.48 | 115.1 | 0.46 | 43.54 |
| | 240 | 6.01 | 77.84 | 6.16 | 140.5 | 0.15 | 62.66 |
| | 500 | 6.01 | 72.03 | 5.71 | 178.6 | -0.3 | 106.57 |

Final sediment height

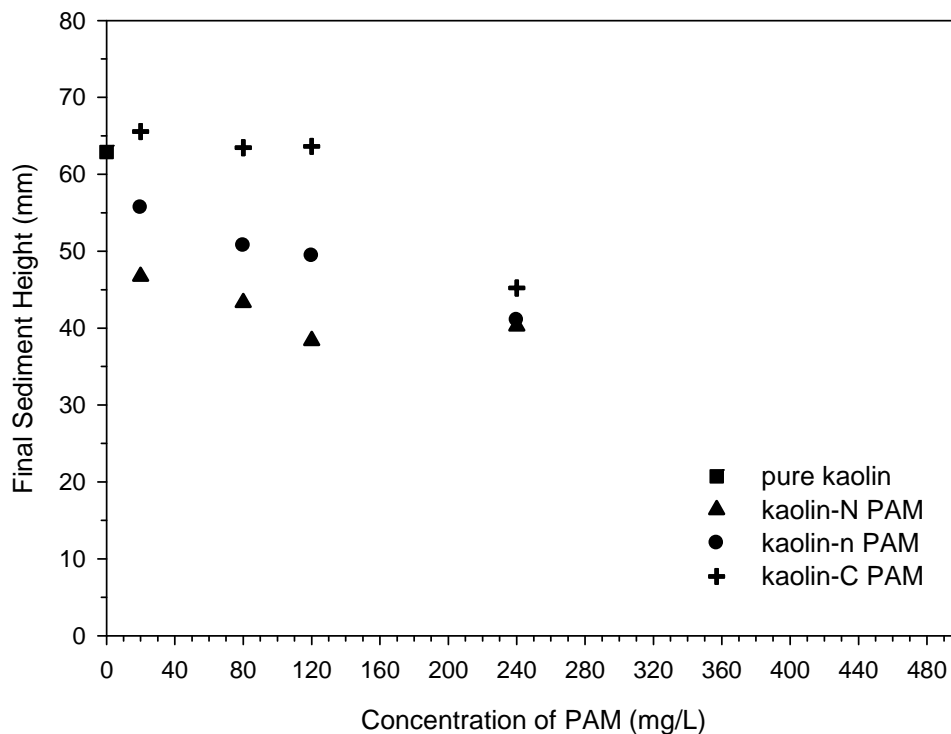


Figure 4.4: Final sediment height measured after three weeks.

Figure 4.4 summarizes the final sediment heights for each suspension. At concentrations less than 120 mg/L, the final sediment height decreases with increasing PAM concentration. The n-PAM results in a more open sediment than N-PAM at lower concentrations while little change is observed for n-PAM and N-PAM at higher concentrations. C-PAM induces a more voluminous sediment at 500 mg/L. In the presence of C-PAM, nearly the same final sediment heights are observed until the C-PAM concentration of 120 mg/L, at which the height significantly decreases. At C-PAM concentrations above 240 mg/L, the final sediment height again increases implying the formation of EF flocs by FF aggregates. It is observed that

molecular weight influences final sediment height at low PAM concentration ranging from 20 to 120 mg/L, i.e. the final sediment height decreases with increasing molecular weight. In the experimental range of PAM concentration, nonionic PAM (both N-PAM and n-PAM) is observed to form denser structures than cationic PAM does. For all three polymers tested, the final sediment heights have similar values at concentration of 240 mg/L. Furthermore, the fabric has been densified in the C-PAM and n-PAM cases, indicating a higher ratio of FF aggregates.

Size and density analysis

Table 4.3 shows floc diameter and density calculated by using Equations 3.1 and 3.2. With increasing nonionic PAMs concentration, floc diameter and floc density increase until the sediment height reaches a minimum, i.e. FF aggregation-dominated. In the presence of C-PAM, floc diameter tends to increase with increasing PAM concentration. At PAM concentration of 240 mg/L, the lowest final sediment height is observed, while the calculated floc density is at a maximum.

Table 4.3: Floc size and density calculated from sedimentation tests.

| Polymer type | PAM concentration (mg/L) | Induction rate (mm/min) | Floc density (g/cm ³) | Floc diameter (μm) | Final Sediment Height (mm) |
|--------------|--------------------------|-------------------------|-----------------------------------|--------------------|----------------------------|
| Pure kaolin | 0 | 0.24 | 1.118 | 4.0 | 62.89 |
| N-PAM | 20 | 0.48 | 1.153 | 7.1 | 46.74 |
| | 80 | 11.4 | 1.154 | 26.6 | 43.32 |
| | 120 | 22.8 | 1.178 | 29.0 | 38.38 |
| | 240 | 43.7 | 1.164 | 52.2 | 40.28 |
| | 500 | 130.2 | 1.143 | 634.7 | 42.37 |
| n-PAM | 20 | 0.29 | 1.138 | 4.6 | 55.67 |
| | 80 | 1.5 | 1.142 | 10.5 | 50.73 |
| | 120 | 1.7 | 1.139 | 16.8 | 49.40 |
| | 240 | 19 | 1.166 | 28.8 | 41.04 |
| | 500 | 28.5 | 1.173 | 32.8 | 38.95 |
| C-PAM | 20 | 0.04 | 1.110 | 7.1 | 65.55 |
| | 80 | 0.31 | 1.137 | 3.4 | 63.46 |
| | 120 | 0.41 | 1.125 | 6.3 | 63.65 |
| | 240 | 16.1 | 1.155 | 34.2 | 45.22 |
| | 500 | 134.9 | 1.115 | 9621 | 52.82 |

Viscosity

Viscosity data for all suspensions measured with increasing shear rate are plotted in Figures 4.5 through 4.7. All PAM-treated suspensions exhibit a typical shear-thinning behavior, i.e. viscosity decreases as rotational speed increases. Shear-thinning behavior is observed in suspensions with flocs or aggregates. The greater the suspension viscosity, the more flocculated the suspension is relative to the other test cases.

The viscosity data under the maximum shear rate, at 100 rpm, are shown in Figure 4.8. Viscosity data at 100 rpm are used as the comparison viscosity at maximum shear rate. Viscosity

increases with increasing PAM concentration. In the presence of C-PAM, the suspensions increase in viscosity until C-PAM concentration of 240 mg/L, and is constant thereafter. At PAM concentration above 240 mg/L, N-PAM-treated suspension shows the greatest viscosity. The ionic group of C-PAM has a greater effect on viscosity than the molecular weight does at PAM concentration from 20 to 240 mg/L. However, the molecular weight of PAM becomes a significant factor at PAM concentration above 240 mg/L.

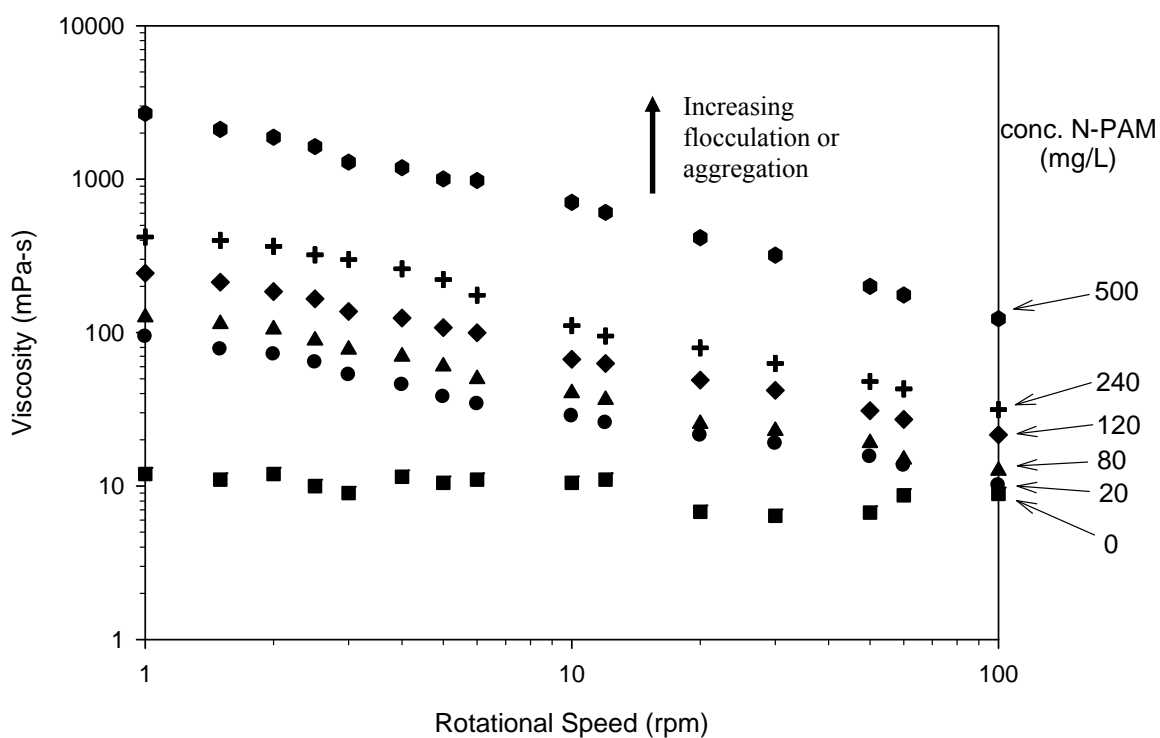


Figure 4.5: Viscosity measurement for pure kaolin and kaolin-PAM (N-PAM) suspensions at rotational speeds of 1 to 100 rpm. Measurements taken with spindle S61 and S62.

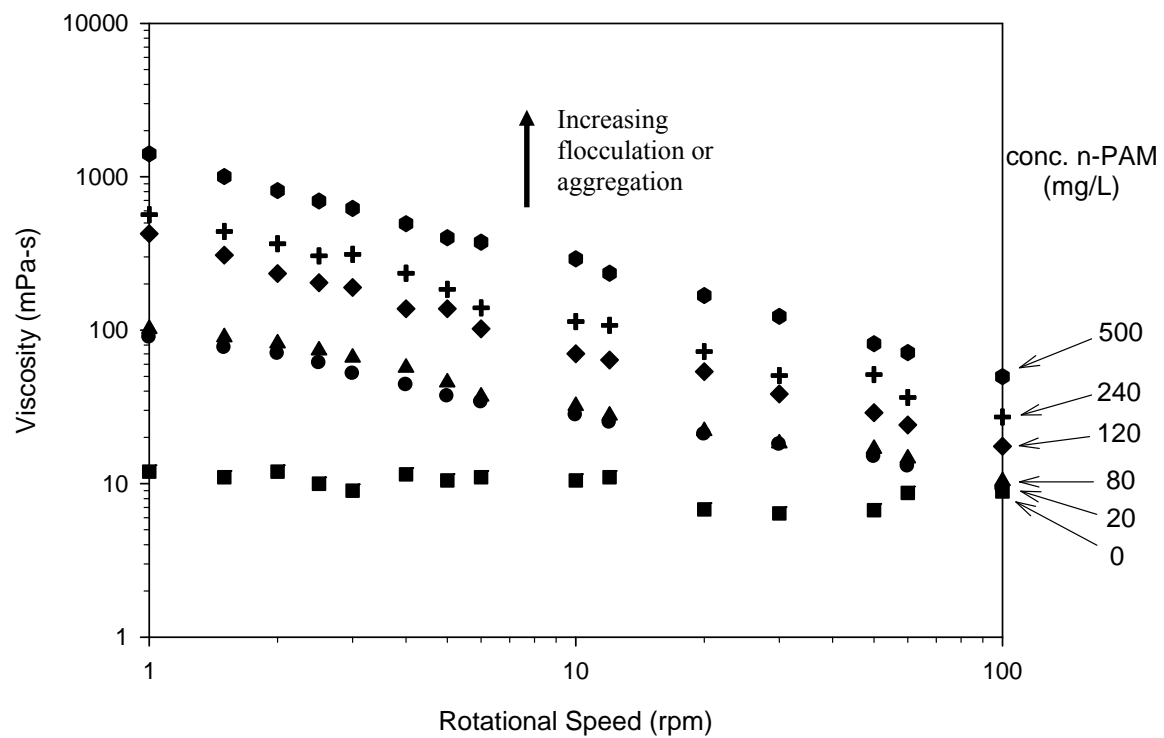


Figure 4.6: Viscosity measurement for pure kaolin and kaolin-PAM (n-PAM) suspensions at rotational speeds of 1 to 100 rpm. Measurements taken with spindle S61 and S62.

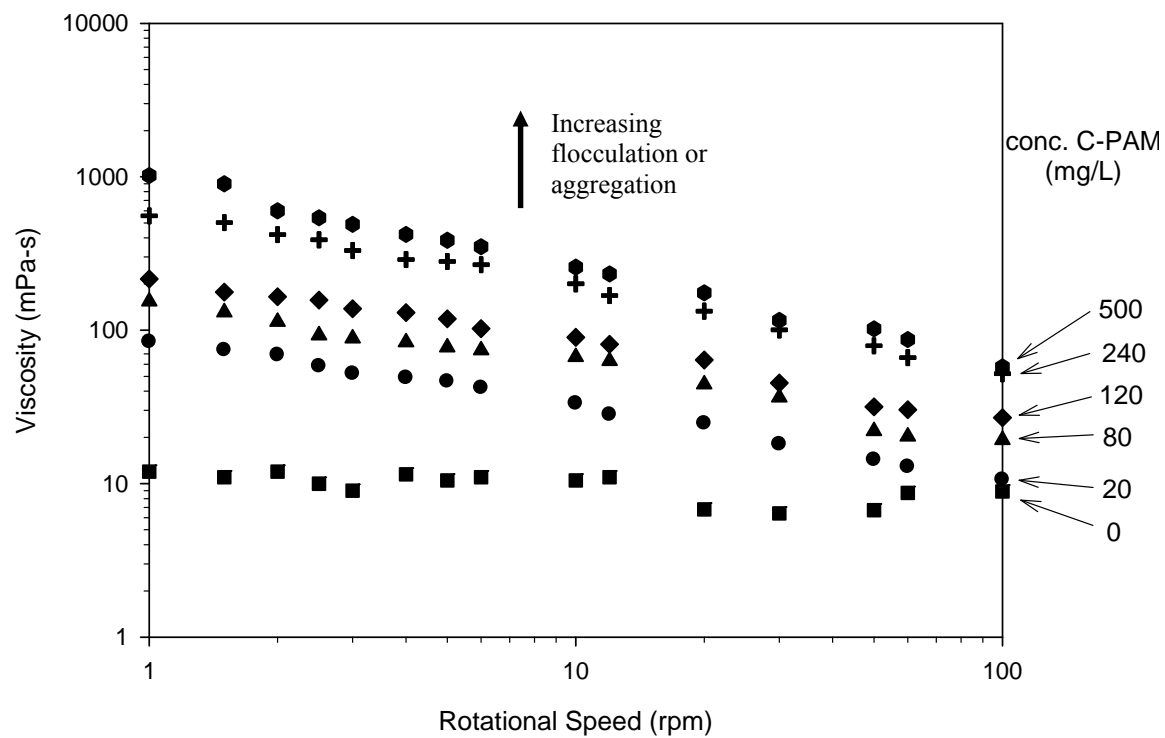


Figure 4.7: Viscosity measurement for pure kaolin and kaolin-PAM (C-PAM) suspensions at rotational speeds of 1 to 100 rpm. Measurements taken with spindle S61 and S62.

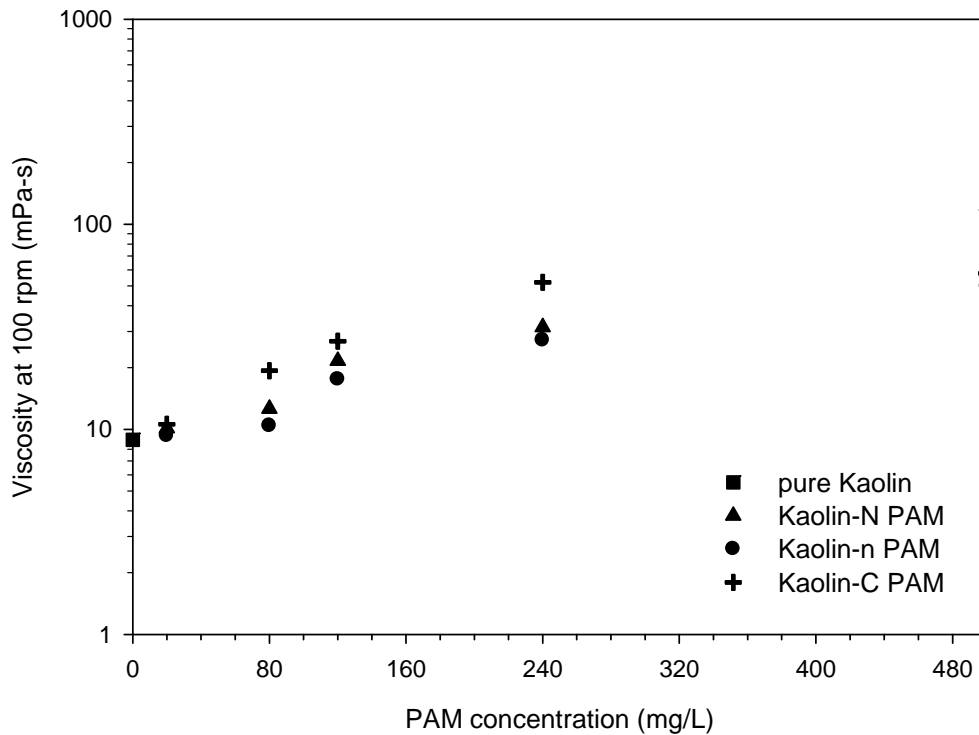


Figure 4.8: Viscosity data for all suspensions at 100 rpm using Spindle S61 and S62.

Liquid Limit

Liquid limits for each soil paste measured according to fall cone test are shown in Figures 4.9 through 4.11 and the liquid limits are plotted in Figure 4.12. Liquid limit increases with an increase in PAM concentration. Only slight differences between C-PAM and N-PAM are observed, while n-PAM-treated specimens have a lower liquid limit trend across the tested concentration. Liquid limit line slopes are shown in Figure 4.13. A higher slope appears with a high molecular weight PAM, i.e. N-PAM and C-PAM, at intermediate PAM concentration. At 20 and 500 mg/L of PAM concentration, all liquid limit trend lines have nearly the same slope indicating fairly insensitive behavior to water content in the presence of polymer.

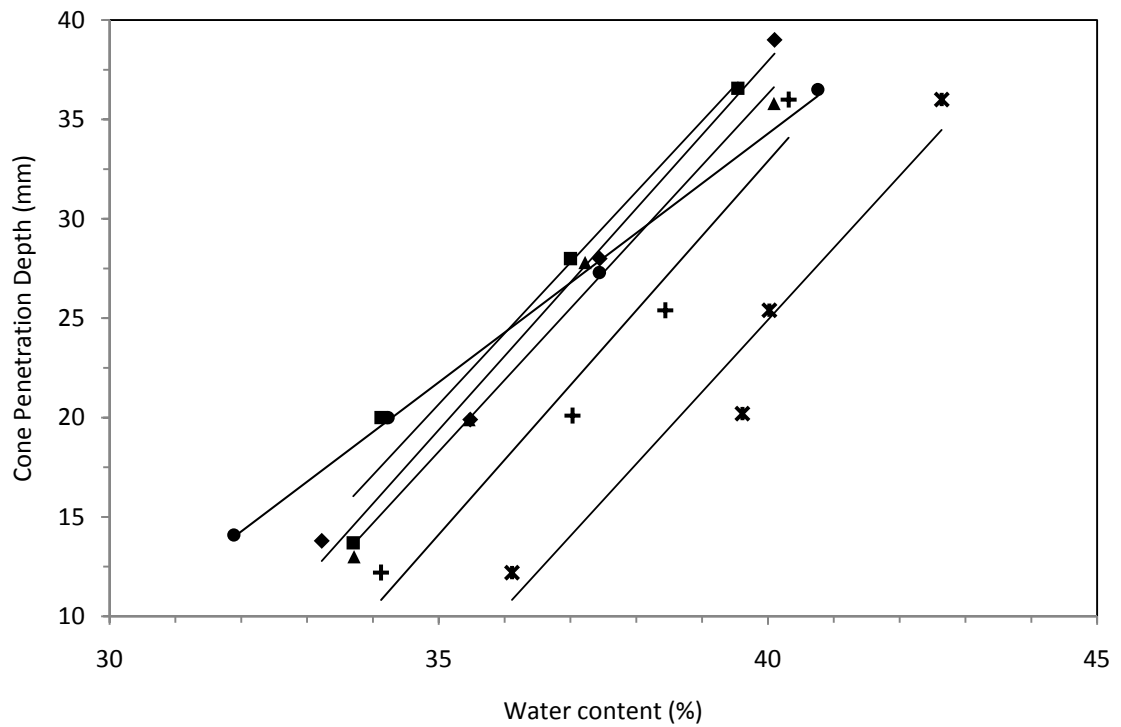


Figure 4.9: Liquid limit lines for N-PAM-treated kaolin specimens at various PAM concentrations. ■ is for pure kaolin, ● is for 20 mg/L, ▲ is for 80 mg/L, ◆ is for 120 mg/L, + is for 240 mg/L, and * is for 500 mg/L.

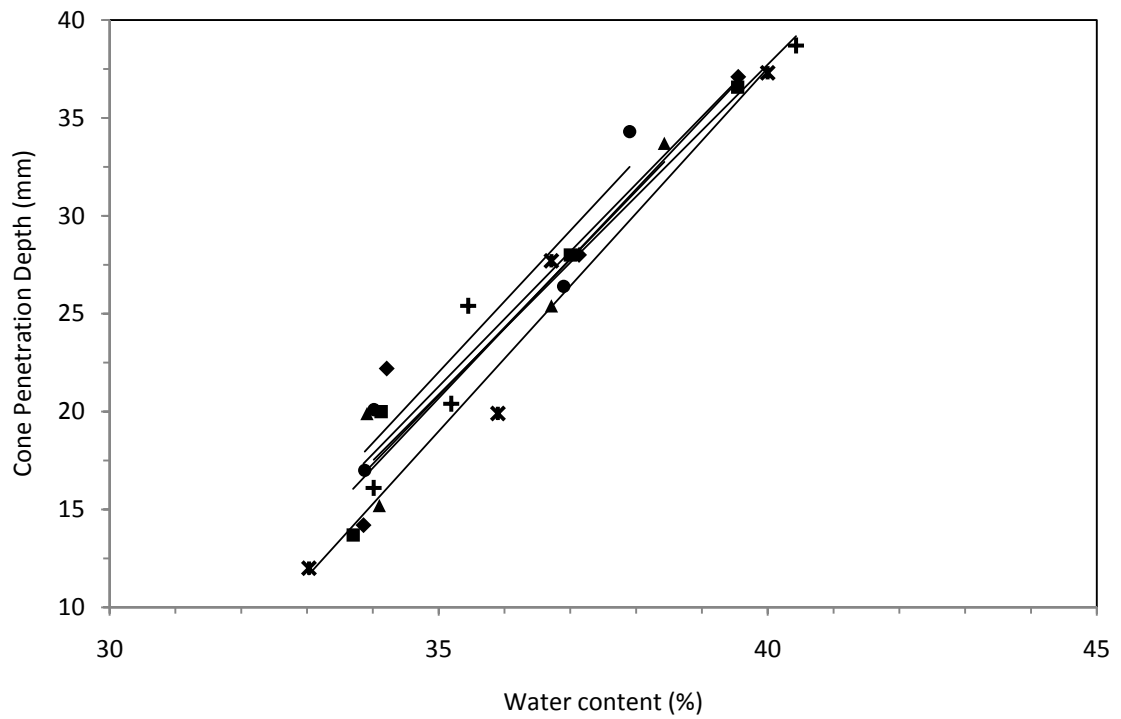


Figure 4.10: Liquid limit lines for n-PAM-treated kaolin specimens at various PAM concentrations. ■ is for pure kaolin, ● is for 20 mg/L, ▲ is for 80 mg/L, ◆ is for 120 mg/L, + is for 240 mg/L, and * is for 500 mg/L.

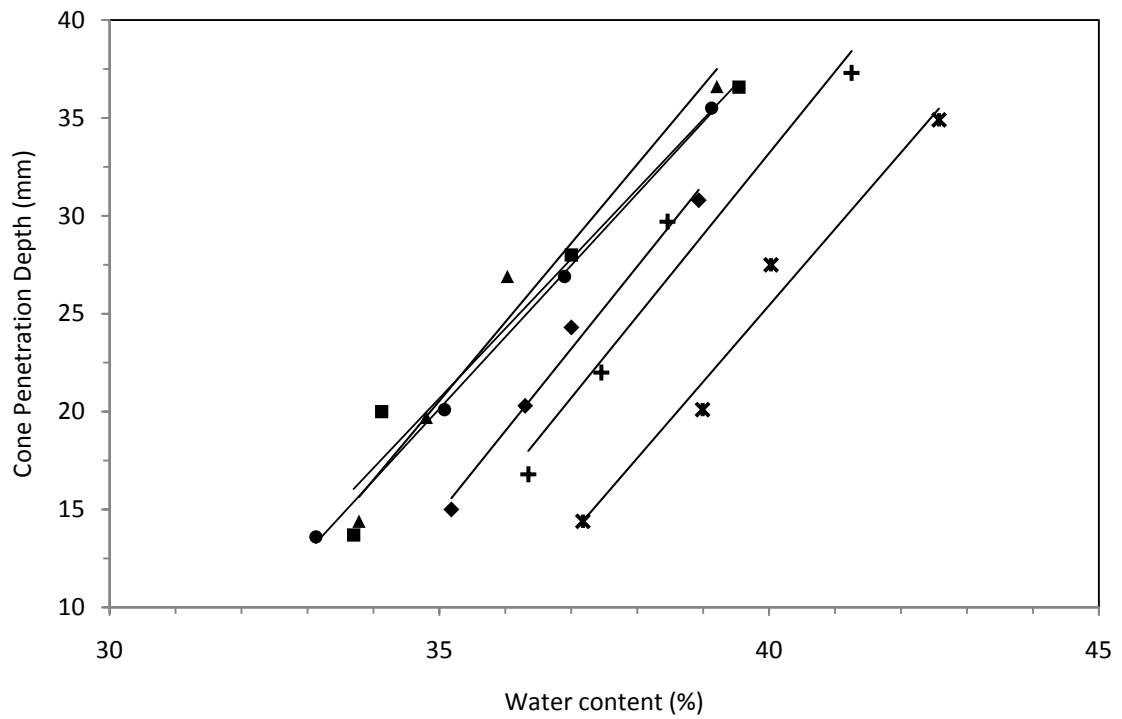


Figure 4.11: Liquid limit lines for C-PAM-treated kaolin specimens at various PAM concentrations. ■ is for pure kaolin, ● is for 20 mg/L, ▲ is for 80 mg/L, ◆ is for 120 mg/L, + is for 240 mg/L, and * is for 500 mg/L.

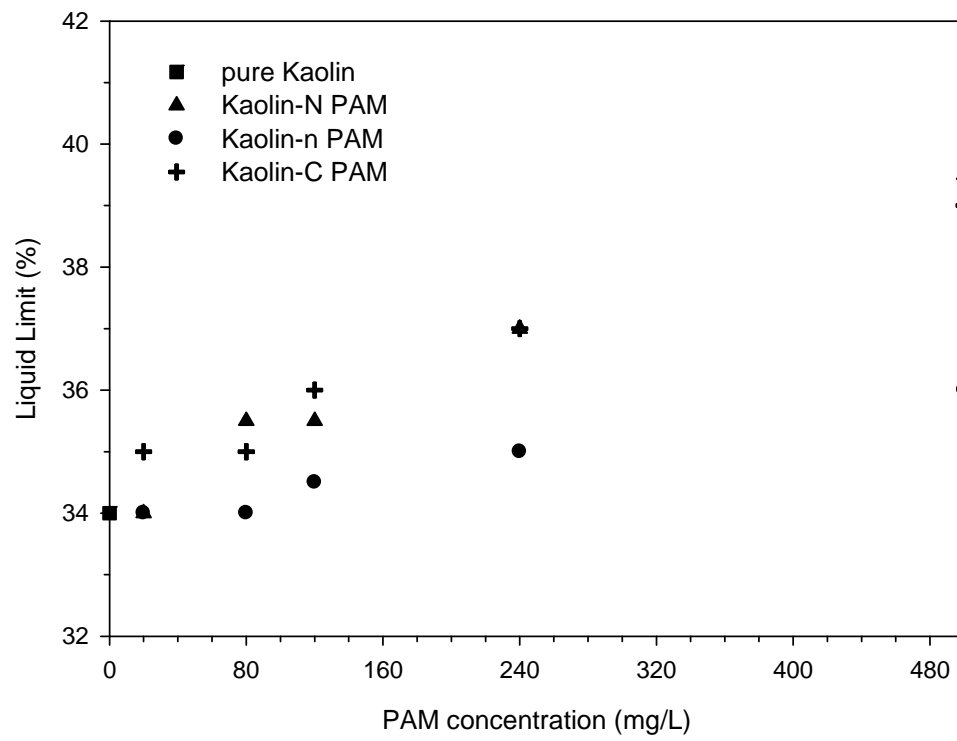


Figure 4.12: Liquid limit for all mixtures of kaolin with various concentrations of PAMs.

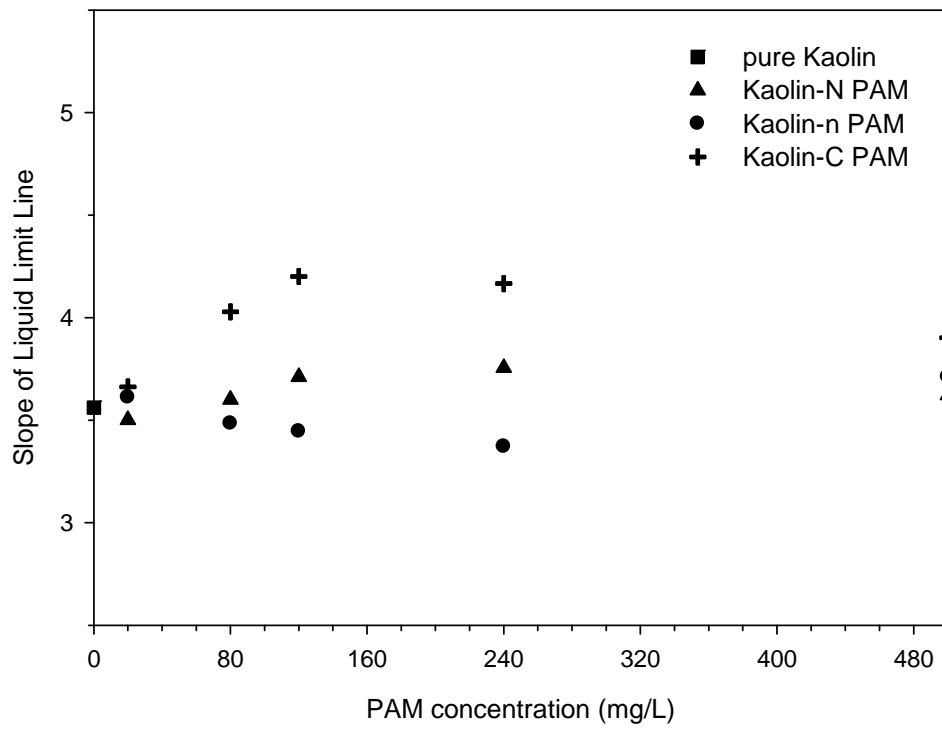


Figure 4.13: Slopes of the fall cone liquid limit lines

Chapter 5

DISCUSSION

In this chapter, kaolin-PAM interactions, over a range of solids content, PAM concentration, and ionic type and molecular weight of PAM, according to all major test results presented in Table 5.1 are discussed and compared with SEM images.

Low solids content ($\phi = 0.02$)

Under constant pore fluid pH and low ionic concentration, particle interactions are governed by polymer characteristics and dosage of the polymer. Particle collisions, that may induce hindered settling are minimized at low solids content, approximately $\phi < 0.02$ (Irani and Callis, 1963). Thus, low solids content allows observation of free fabric formation of kaolin particles with polymer molecules.

The number of flocs/aggregates increases with increasing PAM concentration and molecular weight in the tested low solids content suspensions. All polymer-treated suspensions, except cationic PAM of 120 mg/L, have mixed-mode sedimentation behavior, which includes both dispersed characteristics and flocculated/aggregated characteristics. The ratio of flocculated/aggregated particles to dispersed particles, for a given polymer type, increases with increasing PAM concentration. Both cationic and nonionic PAM molecules can be adsorbed onto both face and edge sites of kaolin particles. However, the most likely particle association is FF due to a much larger proportion of face area compared to edge area on the kaolin particle. Bridging between particles occurs when polymer molecules link two or more particles together. Thus, it is more likely that the polymer molecules bind to the face of at least one particle and

bridge with another particle via face adsorption. As shown in Figure **5.1**, more FF associations are observed as PAM concentration increases.

Table 5.1: Results summary for sedimentation, viscosity, and fall cone tests

| Polymer Type | Concentration (mg/L) | Sedimentation ($\phi = 0.02$) | | | | Viscosity ($\phi = 0.07$) | Liquid limit ($\phi > 0.4$) | |
|--------------|----------------------|---------------------------------|----------------------------|-----------------------------------|---------------------------------|------------------------------|-------------------------------|------------------|
| | | Observed Mode | Final Sediment Height (mm) | Floc Density (g/cm ³) | Floc Diameter (μm) | Viscosity at 100 rpm (mPa·s) | Liquid Limit | LL slope (mm/w%) |
| Pure kaolin | 0 | Mixed | 62.89 | 1.118 | 4.0 | 8.88 | 34 | 3.5613 |
| N-PAM | 20 | Mixed | 46.74 | 1.153 | 7.1 | 10.1 | 34 | 3.5012 |
| | 80 | Mixed* | 43.32 | 1.154 | 26.6 | 12.6 | 35.5 | 3.6002 |
| | 120 | Mixed* | 38.38 | 1.178 | 29.0 | 21.6 | 35.5 | 3.7114 |
| | 240 | Mixed* | 40.28 | 1.164 | 52.2 | 31.5 | 37 | 3.7551 |
| | 500 | Mixed* | 42.37 | 1.143 | 634.7 | 123 | 39.5 | 3.6222 |
| n-PAM | 20 | Mixed | 55.67 | 1.138 | 4.6 | 9.3 | 34 | 3.6112 |
| | 80 | Mixed | 50.73 | 1.142 | 10.5 | 10.4 | 34 | 3.4833 |
| | 120 | Mixed | 49.4 | 1.139 | 16.8 | 17.5 | 34.5 | 3.4455 |
| | 240 | Mixed* | 41.04 | 1.166 | 28.8 | 27.2 | 35 | 3.3712 |
| | 500 | Mixed* | 38.95 | 1.173 | 32.8 | 49.8 | 36 | 3.7106 |
| C-PAM | 20 | Mixed | 65.55 | 1.110 | 7.1 | 10.6 | 35 | 3.6622 |
| | 80 | Mixed | 63.46 | 1.137 | 3.4 | 19.3 | 35 | 4.0278 |
| | 120 | Aggregation | 63.65 | 1.125 | 6.3 | 26.9 | 36 | 4.2004 |
| | 240 | Mixed* | 45.22 | 1.155 | 34.2 | 52.1 | 37 | 4.1663 |
| | 500 | Mixed* | 52.82 | 1.115 | 9621 | 57.6 | 39 | 3.9020 |

*: near to FF aggregation

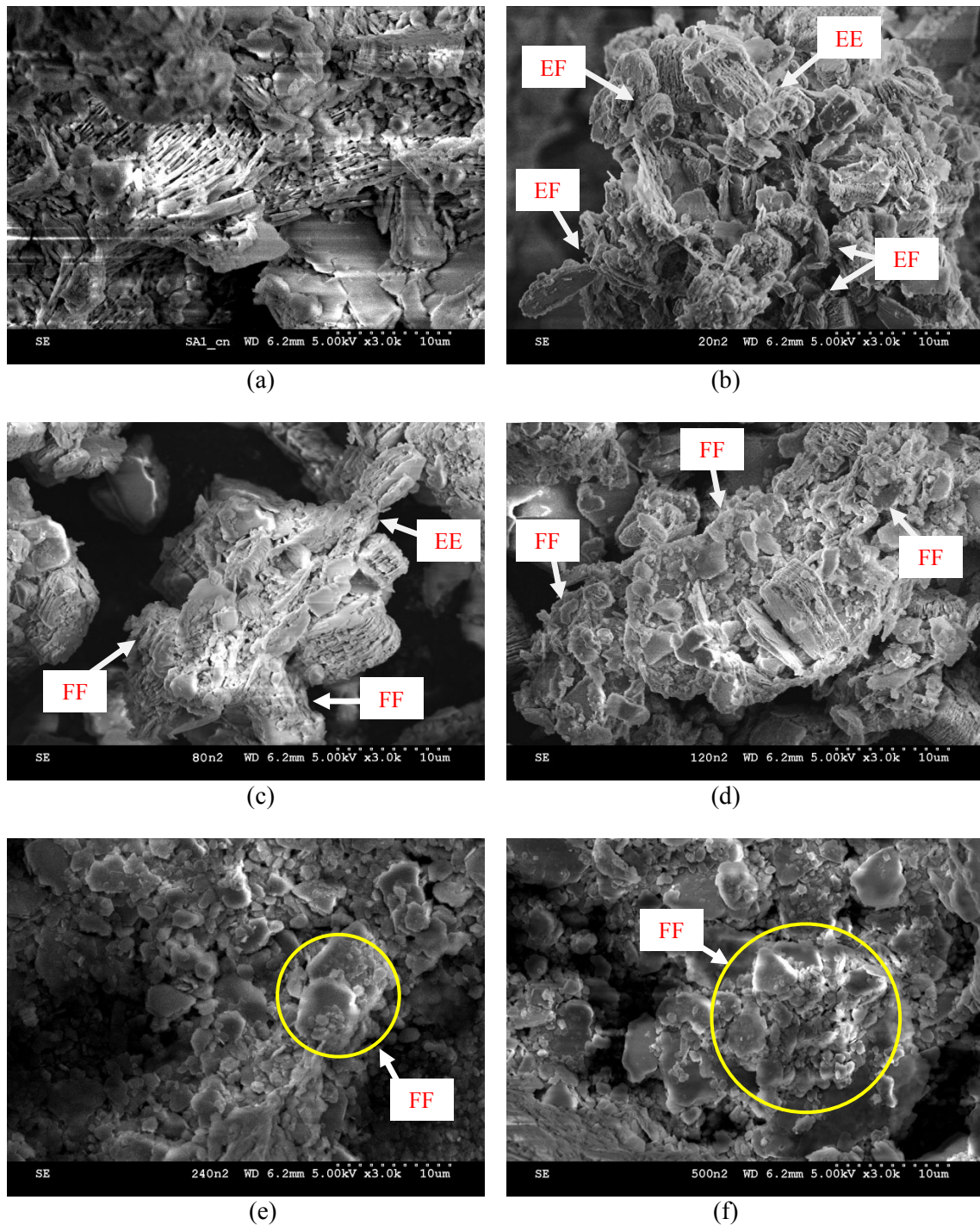


Figure 5.1: SEM images, at $\phi = 0.02$, in the presence of n-PAM varying with concentrations: (a) 0 mg/L, (b) 20 mg/L, (c) 80 mg/L, (d) 120 mg/L, (e) 240 mg/L, and (f) 500 mg/L

The final sediment height (Figure 4.4) and induction rate (Table 4.3) also indicate an increase in FF aggregation with increasing PAM concentration. The induction rate increases with increasing PAM concentration, indicating flocculated/aggregated fabric formation. The final sediment height decreases with increasing PAM concentration up to 120 mg/L for high molecular weight nonionic PAM, 240 mg/L for low molecular weight nonionic PAM, and 240 mg/L for high molecular weight cationic PAM. Hence, these concentrations are apparent optimum concentrations for the densest sediment at solids content of 0.02, indicating the highest ratio of FF aggregates. At PAM concentration above 240 mg/L, the final sediment height of cationic PAM again increases with increase in PAM concentration while that of nonionic PAM stays nearly constant. This may be explained according to the charge calculation of kaolin particle and cationic PAM molecule (See Appendix A). 5.2g of kaolin used for a suspension with solids content of 0.02, which has 2.07×10^{19} of surface charge, interacts with the same number of cationic groups of cationic PAM at a concentration of 164 mg/L (CCC) to neutralize all the particles surface charge. Therefore, charge neutralization is achieved between 120 and 240 mg/L of cationic PAM concentration.

Once charge neutralization is reached, in case of 240 mg/L cationic PAM-treated suspensions, long-range van der Waals forces and short-range ion-dipole interactions dominate the system resulting in FF aggregate formation. At concentrations above the critical coagulation concentration, hydrogen bonding between the molecule and mineral surface, which mainly occurs at edge sites, becomes the dominating bonding mechanism due to the lack of available exchangeable cations at the face sites. Aggregates link together with excess cationic PAM molecules through polymer bridging and hydrogen bonds forming higher-order EF or EE flocs as schematically shown in Figure 5.2. Such association development is likely because the kaolin particle surface charge is compensated and hydrogen bonds can dominate instead of stronger ion-dipole interaction (Israelachvili, 1991; Ebnesajjad, 2006). These higher-order EF flocs have a

greater volume than EF flocs formed by single particles. The stacking of these higher-order structures leads to an increase in final sediment height. This type of higher-order floc is seen in a scanning electron micrograph (Figure 5.3). A more open structure (EF and EE) formed in the presence of cationic PAM is seen in Figure 5.4. FF aggregation formation is also interpreted through the floc size and density analysis (Table 4.3). The floc density of cationic PAM-treated suspension abruptly increases at PAM concentration above 120 mg/L. This phenomenon is considered with the lowest sediment height at PAM concentration of 240 mg/L.

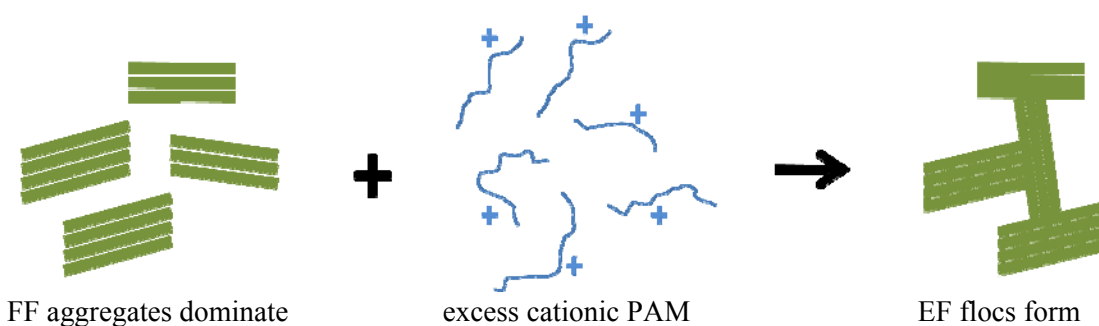


Figure 5.2: Formation of EF flocs in the presence of excess cationic PAM molecules

The higher molecular weight nonionic PAM has more monomer units per molecule than the low molecular weight nonionic PAM. This leads to a more aggregated and compact sediment compared to the low molecular weight polymer case. With respect to the final sediment height, the ratio of FF/EE associations (dense structure) to EF associations (open structure) is higher for high molecular nonionic PAM than that for low molecular nonionic PAM. Higher molecular nonionic PAM forms larger denser flocs according to the floc size and density calculation. This is verified in Figure 5.5 where larger flocs, at the same magnification, are observed in the presence of high molecular weight nonionic PAM than low molecular weight nonionic PAM.

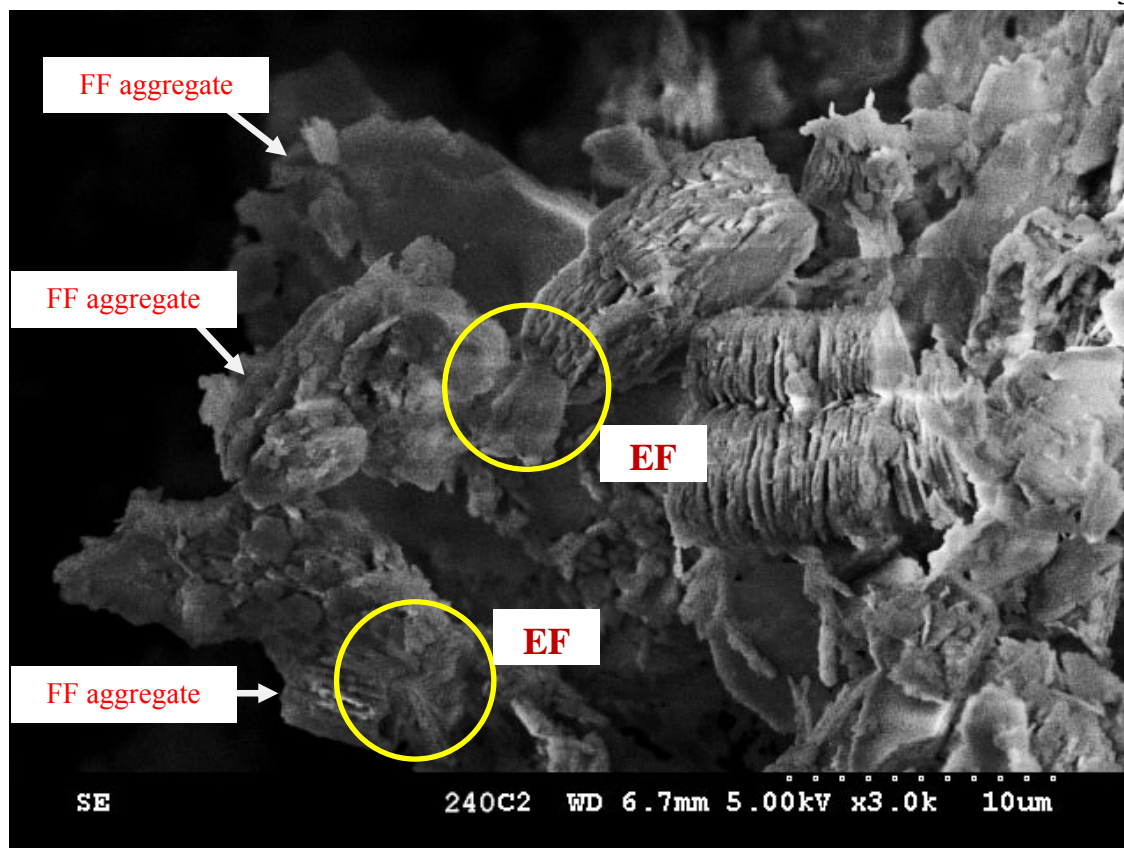


Figure 5.3: SEM image of FF aggregates in EF flocs in the presence of 240 mg/L C-PAM

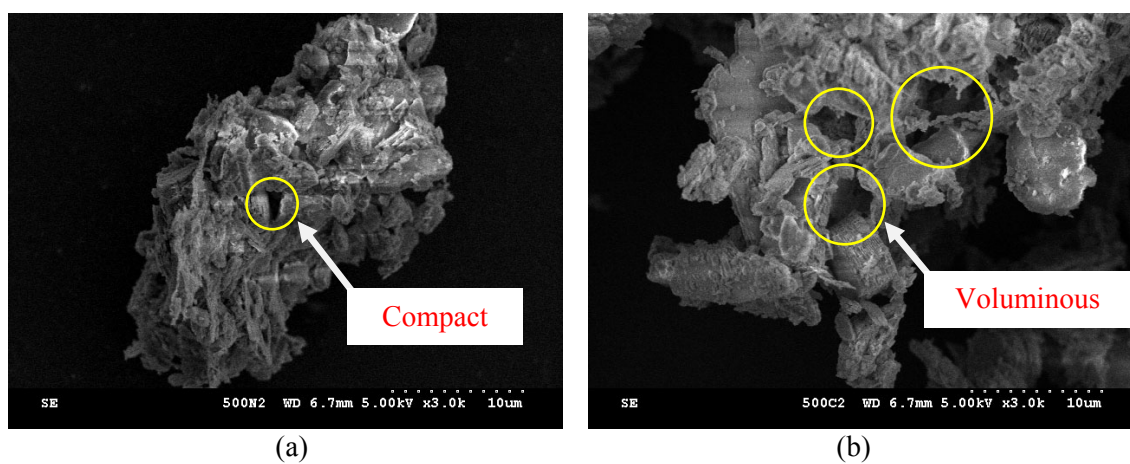


Figure 5.4: SEM images in the presence of 500 mg/L of (a) N-PAM and (b) C-PAM, at $\phi = 0.02$

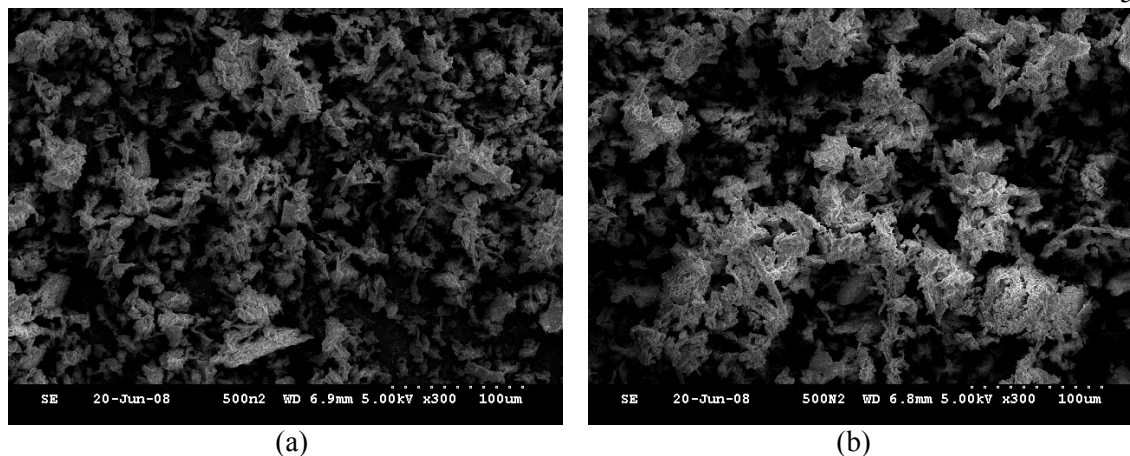


Figure 5.5: SEM images in the presence of (a) 500 mg/L n-PAM and (b) 500 mg/L N-PAM, at $\phi = 0.02$

Intermediate solids content ($\phi = 0.07$)

Intermediate solids content of 0.07 is low enough to maximize the effects of interparticle forces and high enough to be measurable within the viscometer range. Thus, consistent variations in viscosity behavior can be observed at this solids content.

At intermediate solids content ($\phi = 0.07$), the molecular weight of PAM greatly impacts viscosity while the ionic group of PAM shows minimal influence. Viscosity, and therefore flocculation/aggregation increases with all increasing PAM concentrations (Figures 4.5 through 4.7). As shown in Figures 5.6, higher viscosity results from larger flocs formed in the presence of increasing PAM concentrations. The same trend is seen in the case of low solids content (Figure 5.1 and 5.5). All PAM-treated suspensions show shear thinning behavior, while the pure kaolin case has dispersed characteristics.

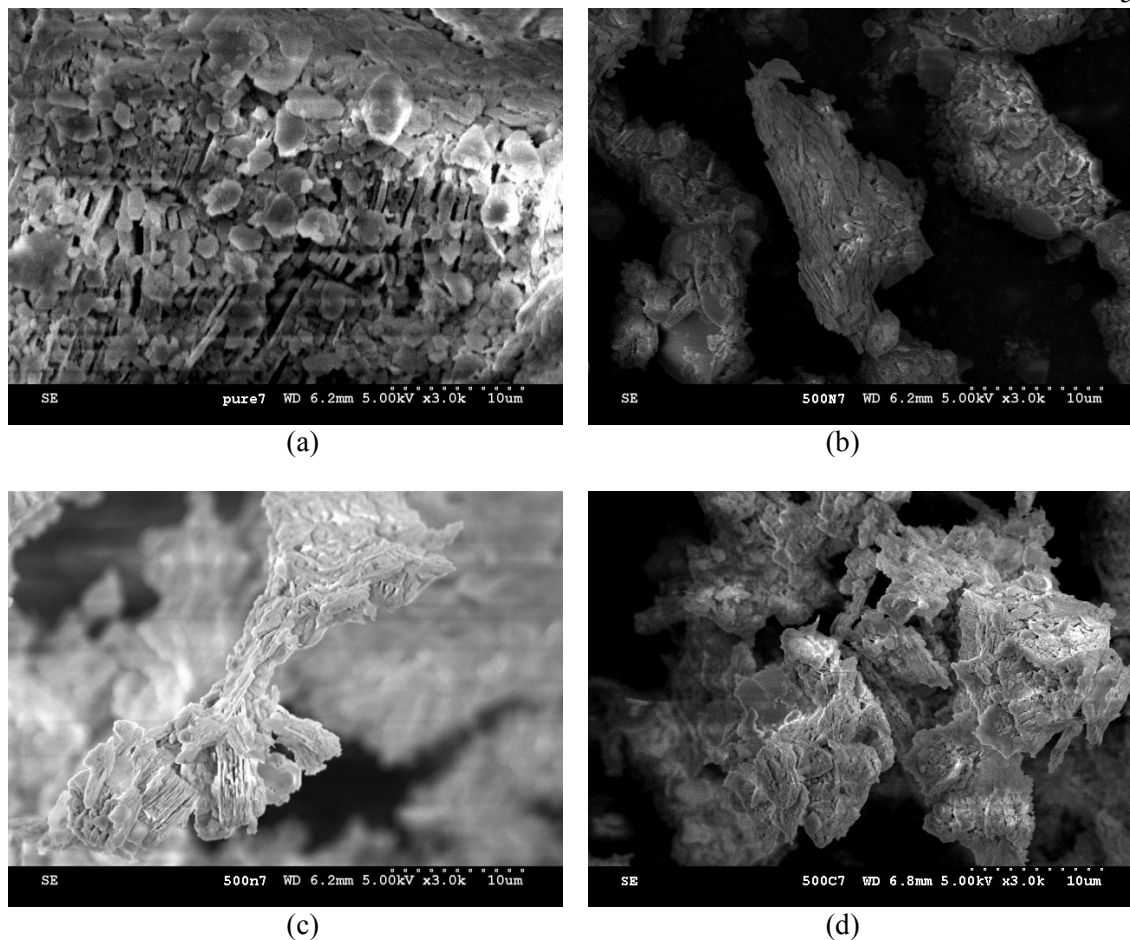


Figure 5.6: SEM images of (a) pure kaolin, (b) 500 mg/L N-PAM, (c) 500 mg/L n-PAM, and (d) 500 mg/L C-PAM, at $\phi = 0.07$

The affects of polymer ionic type are also compared. Although a fitted cationic PAM concentration (critical coagulation concentration) for achieving charge neutralization is theoretically 574 mg/L (not tested in this study), cationic PAM-treated kaolin suspensions have a higher viscosity than nonionic cases at PAM concentration below the CCC. This may be due to a higher bonding energy of ion-related bonds, such as Coulombian attraction and ion-dipole interaction, than that of non-ion-related bonds such as hydrogen bonds and hydrophobic bonds. A greater molecular interaction force results in an increase in flocculation, and thus a higher viscosity.

High solids content ($\phi > 0.4$)

For high molecular weight and solids content, an increase in PAM concentration results in an increase in liquid limit. Particles are linked together with polymer molecules, leading to flocs/aggregates. In a flocculated system, water becomes trapped within and between open flocs. A more flocculated, voluminous fabric can accommodate more water, thereby increasing the liquid limit. With increasing polymer concentration, a more open fabric is observed at the micro-scale (Figure 5.7). In addition to water trapped within the particle flocs and pores, PAM molecules are hydrophilic and so provide additional adsorption sites for water molecules. This phenomenon results in a higher liquid limit and is more likely at a higher polymer concentration for all tested types of PAM. The slope of fall cone liquid limit lines (an indicator of sensitivity to water content) does not vary significantly with PAM concentration for all types of PAM. The presence of PAM molecules helps prevent shear strength from abruptly decreasing when water content increases.

While the molecular weight of PAM is observed to influence the tested high solids content systems, the effect of ionic type is insignificant in the tested range of PAM concentrations. More polymer bridging occurs in the presence of higher molecular weight PAM regardless of charge type, since higher molecular weight polymer chains have even more groups with which to interact with particle surfaces. Due to the relatively very low number of charges on cationic PAM compared to that of the total surface area of the kaolin clay at high solids content, the impact of positively charged groups of PAM becomes less important at high solids content (>0.4). This is evidenced by only slight difference in liquid limit between N-PAM-treated kaolin mixtures and C-PAM-treated kaolin mixtures. This indicates that polymer bridging is a more effective bonding mechanism than electrostatic forces at very high solids content.

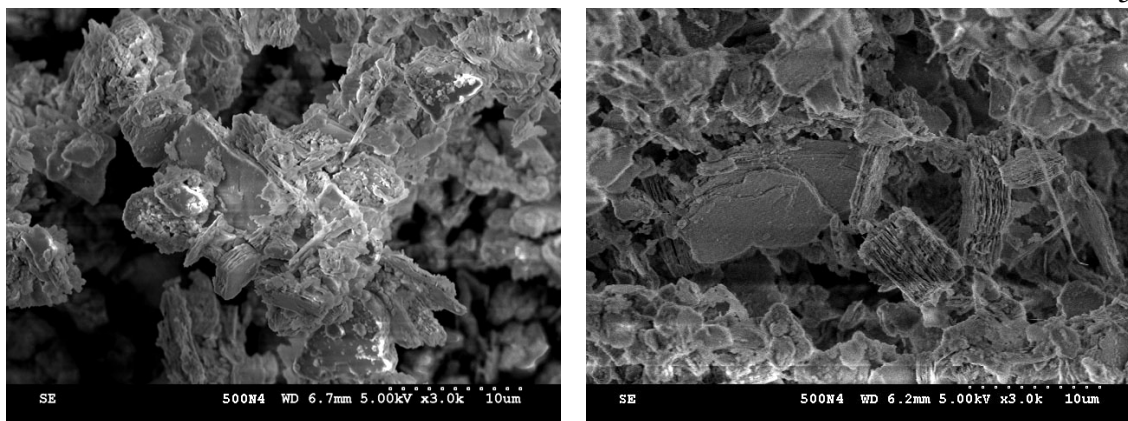


Figure 5.7: EF and open EE associations in the presence of 500 mg/L N-PAM, at $\phi > 0.4$

Fabric maps

Table 5.2 shows mass ratio of PAM (mg) to kaolin (g). FF aggregation appears at the mass ratio above 0.04 for the case of nonionic PAM. With increasing mass ratio, FF aggregation becomes the dominating fabric. The degree of aggregation depends on the molecular weight of PAM and solids content. In the presence of higher molecular weight PAM, FF becomes the dominating fabric at lower PAM concentration. More polymer molecules per unit mass for higher molecular weight PAM result in more polymer bridging. More polymer bridging results in a more flocculated/aggregated fabric. At higher solids content, FF becomes the dominating fabric at lower PAM concentration. With increasing solids content, a greater amount of mineral surface area per unit volume provides more accessible sites for polymer molecules leading to more polymer bridges between adjacent particles.

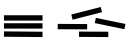
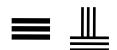
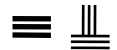
The number of charged groups relative to available sites at the mineral surface influences fabric formation for the case of cationic PAM. Hence, the degree of the influence varies with total mineral surface area (solids content). The relationship between the observed fabric and the ratio between the number of available kaolin particle surface charges to the total number of charged groups on the cationic PAM molecules at all solids contents and PAM concentrations

tested, is tabulated in Table 5.3. The number of FF aggregation is maximized when the charge ratio is 1 at low solids content. At the charge ratio greater than 1, excess cationic polyacrylamide molecules bind FF aggregates and form higher-order EF or EE flocs. At higher solids contents, FF aggregation appears at relatively lower charge ratio.

Table 5.2: The influence of PAM concentration

| PAM concentration (mg/L) | Solids content = 0.02 | Solids content = 0.07 | Solids content > 0.4 |
|--------------------------|------------------------------------|------------------------------------|------------------------------------|
| | Mass ratio of PAM to kaolin (mg/g) | Mass ratio of PAM to kaolin (mg/g) | Mass ratio of PAM to kaolin (mg/g) |
| 20 | 0.39 | 0.11 | 0.0067 |
| 80 | 1.54 | 0.44 | 0.027 |
| 120 | 2.31 | 0.66 | 0.04 |
| 240 | 4.62 | 1.32 | 0.08 |
| 500 | 9.62 | 2.75 | 0.167 |

Table 5.3: The influence of positively charged groups of PAM

| C-PAM concentration (mg/L) | Solids content = 0.02 | | Solids content = 0.07 | | Solids content > 0.4 | |
|----------------------------|---------------------------------|---|---------------------------------|---|---------------------------------|---|
| | Charge ratio of C-PAM to kaolin | Observed fabric | Charge ratio of C-PAM to kaolin | Observed fabric | Charge ratio of C-PAM to kaolin | Observed fabric |
| 20 | 0.122 |  | 0.035 |  | 0.002 |  |
| 80 | 0.487 |  | 0.139 |  | 0.008 |  |
| 120 | 0.731 |  | 0.209 |  | 0.013 |  |
| 240 | 1.461 |  | 0.417 |  | 0.025 |  |
| 500 | 3.044 |  | 0.87 |  | 0.053 |  |

The relationship between polymer concentration, solids content, and resulting association type(s) for all polymer types tested are summarized as fabric maps in Figures 5.8 through 5.10. Kaolin particles associate by linking through polyacrylamide molecules. An increase in polyacrylamide molecules, whether through molecular weight or higher concentration, leads to an increase in kaolin particle bridging. Subsequently, bridging leads to FF particle aggregation. High molecular weight nonionic polyacrylamide causes the most FF-aggregated fabric for all polymer concentrations. At concentrations greater than the CCC, cationic polyacrylamide tends to induce higher-order EF flocculation. As solids content increases, less ratio of FF aggregate is seen over all polymer concentrations. The molecular weight, which is a main factor to form polymer bridging, becomes the dominating factor with increasing solids content. At high solids content, the effect of ionic type of polymer becomes relatively insignificant compared to the influence of molecular weight.

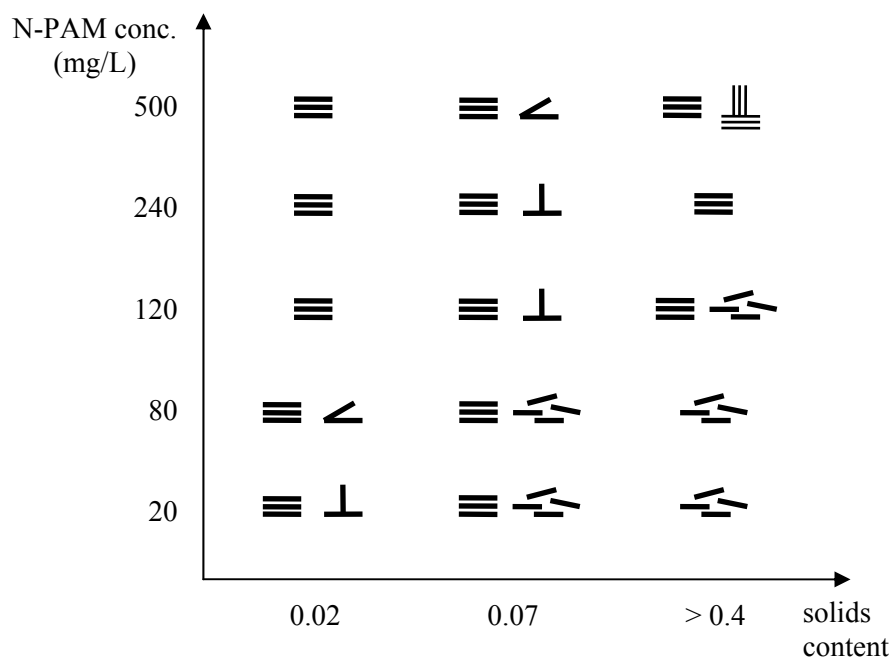


Figure 5.8: High molecular weight nonionic polyacrylamide-treated kaolin fabric map. ≡, ⊥, ∠, ∠, and ≡ denotes FF aggregated, EF flocculated, EE flocculated, dispersed, and higher-order EF flocculated fabric, respectively.

With regard to the molecular weight, for the cases of high molecular weight nonionic polyacrylamide (Figure 5.8) and low molecular weight nonionic polyacrylamide (Figure 5.9), higher molecular weight increases the degree of flocculation/aggregation at the same polymer concentration. The main particle association through nonionic polyacrylamide molecules is FF aggregation. This phenomenon is valid at all solids contents tested in this study.

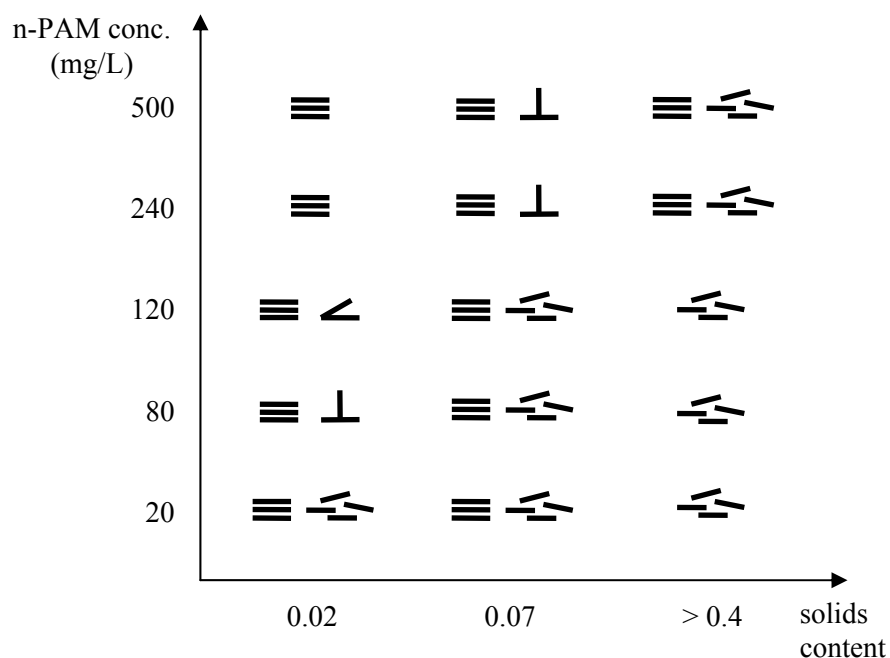


Figure 5.9: Low molecular weight nonionic polyacrylamide-treated kaolin fabric map. ≡, ⊥, ↙, and ↗ ↘ denotes FF aggregated, EF flocculated, EE flocculated, and dispersed fabric, respectively.

Regarding the effect of ionic type, for the case of high molecular weight nonionic polyacrylamide (Figure 5.8) and high molecular weight cationic polyacrylamide (Figure 5.10), the presence of cationic groups leads to higher-order flocs/aggregates at low solids content. However, this impact becomes insignificant as solids content increases.

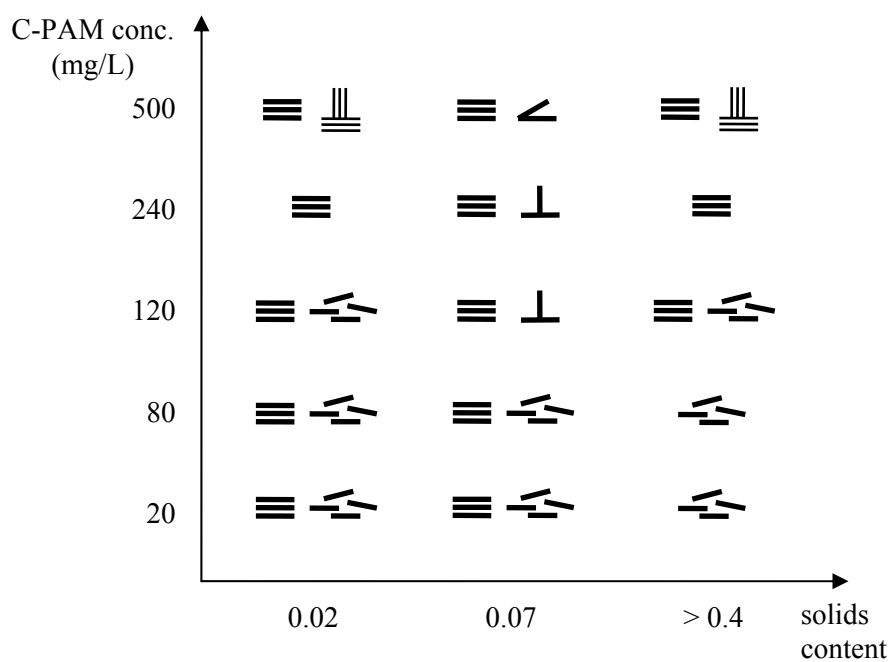


Figure 5.10: High molecular weight cationic polyacrylamide-treated kaolin fabric map. ≡, ⊥, ⌵, ≡, and ≡ denotes FF aggregated, EF flocculated, EE flocculated, dispersed, and higher-order EF flocculated fabric, respectively.

Chapter 6

CONCLUSIONS

Particle interactions, and in turn fabric, determine the behavior of clay system. Polymers with deliberately chosen characteristics, such as molecular weight and ionic type, can manipulate clay fabric. Once polyacrylamide molecules bind to kaolin clay particles, the adsorption strongly alters the clay particle surface characteristics, leading to altered particle associations and therefore fabric. Macro-scale tests, representing a wide range of solids contents, can be used to infer fabric resulting from various particle associations. Clay fabrics are verified with scanning electron microscopy.

The molecular weight of polyacrylamide has a greater impact on kaolin fabric formation than charge type. A higher molecular weight and polymer concentration result in a greater number of monomer units per single polymer chain, compared to a lower molecular weight and polymer concentration. With increasing number of monomer units in the system, more polymer bridges take place leading to a more flocculated system. This is evidenced by an increase in face-to-face (FF) aggregation with increasing nonionic polymer molecular weight (high molecular weight versus low molecular weight) and concentration at the same solids content. FF aggregation is the dominating particle association in the nonionic polyacrylamide-treated kaolin systems. More polymer bridges induce more FF aggregations which manifest as a denser final sediment.

Although to a lesser degree, the ionic type of polyacrylamide also influences kaolin fabric formation. At cationic polymer concentrations above the critical coagulation concentration (CCC), FF aggregates form higher-order edge-to-face (EF) floc structures by linking FF aggregates. The CCC is determined by the ratio between number of available mineral surface

charges and number of charged polymer monomer units. At the CCC, the cationic polyacrylamide-treated kaolin system has the densest final sediment height due to FF aggregation. The final sediment height increases at polymer concentrations above the CCC, corresponding to larger flocs and a more open fabric. This finding is consistent with the floc size and density analysis performed in this study. At low cationic polymer concentrations, significant differences in macro-scale behavior are observed while at high solids content nearly the same macro-scale behavior is observed as in the pure kaolin case.

It is observed that polyacrylamide contributes to higher liquid limits, compared to the pure kaolin case. The polymer molecules bind formed FF aggregates leading to higher-order of EF/EE flocs (open fabric), and in turn, higher liquid limit. In addition, polymer molecules provide additional adsorption sites for water molecules, also contributing to the higher liquid limit. As the number of monomer unit increases (with higher molecular weight and higher concentration), the number of adsorption sites also increase.

This study indicates that kaolin clay fabric can be successfully modified with the use of polyacrylamide. The influence of polyacrylamide on kaolin fabric, particle association type, and number of associations that develop depends on the molecular weight, concentration, and ion type of the polymer as function of the solids content of the system. Finally, fundamental fabric maps for the kaolin clay with different concentration, molecular weight and ionic type of polyacrylamides are developed taking into account sedimentation, viscosity, liquid limit behavior at solids contents: 0.02, 0.07, and above 0.4, respectively. The proposed fabric maps can be utilized for modifying the properties of clay-mineral soil systems, such as low water retention capacity, by using polyacrylamide. This polymer-clay combination may offer a new outlook for purpose of creating engineered soil systems.

Future Work

Mechanical properties of polyacrylamide-treated kaolin

It is expected that the addition of polymer induces an alteration in mechanical properties of the system. For example, the bonding between polymer molecules and clay particles may be stronger than that for pure clay systems. Hence, greater mechanical properties such as shear strength and compressive strength may be obtained. Polymer molecules are typically flexible while clay particles are relatively rigid, and so higher flexible strength may be expected for polymer-treated clay system.

Influence of PAM molecule conformation

Polyacrylamide molecules have different conformations varying with bulk fluid pH (Besra et al., 2004). Nonionic polyacrylamide molecules have highly coiled conformation at acidic pH (2.3) while highly expanded form at alkaline pH (10.95). On the other hand, cationic polyacrylamide molecules have open coiled conformation at acidic pH but highly dense coiled form at alkaline pH. These differences as a function of bulk fluid pH may strongly influence kaolin fabric formation. Under a condition that highly coiled conformation dominates, denser floc/aggregate may form and the permeability of the system may be low, while more open bigger floc/aggregate may be the governing fabric in systems dominated by highly expanded conformation. In addition, polyacrylamide molecules with expanded conformation are more likely to result in more number of polymer bridges, and in turn more flocculation/aggregation.

Impact of preexisting exchangeable cations

Ion-dipole interaction, which is the strongest bonding mechanism between polyacrylamide molecules and kaolin particles, is affected by exchangeable cations (Deng et al., 2006). Exchangeable cations with higher valence and heavier atomic mass are easier to induce ion-dipole interaction binding polyacrylamide molecules to kaolin particles. In the presence of an exchangeable cation with high valence and heavy atomic mass, stronger flocculation/aggregation may be expected resulting in greater mechanical properties as well.

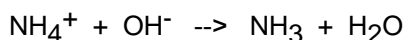
Appendix A

Charge calculation of kaolin clay particles and polyacrylamide molecules

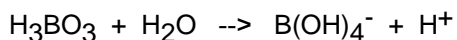
Kaolin surface charge density determined by ion exchange (Hunter, 1993)

Procedure

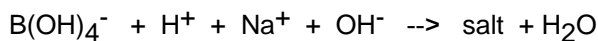
1. Kaolin clay (e.g., 20g) is saturated (vigorously mixed) with ammonium ion (1M NH₄Cl solution) at a proportion of approximately 5ml solution per gram kaolin
2. Allow it to stand overnight and then the excess is repeatedly washed with distilled/deionized water until conductivity is constant
3. (If the final conductivity is very low (close to that of distilled water), skip this process)
To convert the NH₄⁺ to ammonia (NH₃), the sample is treated (mixed well) with 1M NaOH solution at a proportion of approximately 5ml solution per gram kaolin



4. Take 10ml of the sample into a glass tube and centrifuge
5. Place the supernatant in a new container and the glass tube containing clay sediment is oven-dried to measure mass of kaolin clay used
6. Mix the supernatant with known volume of boric acid (H₃BO₃) solution at known concentration (e.g., 25ml of 0.0107M H₃BO₃)



7. Titrate using 0.0144M NaOH solution until pH is 7



8. Prepare the same volume of boric acid (e.g., 25ml of 0.0107M H₃BO₃) and titrate using 0.0144M NaOH solution until pH is 7

Calculation

Constants

Avogadro's number $N_{av} := 6.022 \frac{10^{23}}{\text{mol}}$

Elementary charge (electron charge) $e_0 := 1.60217610^{-19} \text{ coul}$

atomic weight

$aw_H := 1.00794 \text{ gm}$

$aw_B := 10.81 \text{ gm}$

$aw_N := 14.0067 \text{ gm}$

$aw_O := 15.9994 \text{ gm}$

$aw_{Na} := 22.9898 \text{ gm}$

$aw_{Cl} := 35.453 \text{ gm}$

Mass of kaolin clay (g) after oven dried

Surface area of kaolin clay (m^2/g)

$mass_{kaolin} := 0.8715 \text{ gm}$

$Sa_{kaolin} := 40.369 \frac{\text{m}^2}{\text{gm}}$

Boric acid (H_3BO_3) mixed with the supernatant

concentration $conc_{H_3BO_3} := 0.0107 \frac{\text{mol}}{\text{L}}$

volume $vol_{H_3BO_3} := 100 \text{ mL}$

Sodium hydroxide (NaOH) used for neutralization of solution of NH_4^+ and $\text{B}(\text{OH})_4^-$

concentration $conc_{NaOH} := 0.0144 \frac{\text{mol}}{\text{L}}$

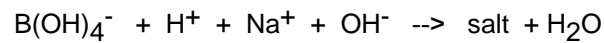
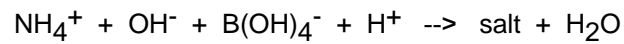
volume $vol_{NaOH} := 0.2 \text{ mL}$

Sodium hydroxide (NaOH) used for neutralization of pure boric acid solution with the same volume and concentration

$$\text{concentration} \quad \text{conc}_{\text{NaOH.c}} := 0.0144 \frac{\text{mol}}{\text{L}}$$

$$\text{volume} \quad \text{vol}_{\text{NaOH.c}} := 0.6 \text{mL}$$

Calculation of kaolin surface charge



$$\text{MW}_{\text{H}_3\text{BO}_3} := 3 \cdot \text{aw}_{\text{H}} + \text{aw}_{\text{B}} + 3 \cdot \text{aw}_{\text{O}} = 61.832 \text{ gm}$$

$$\text{MW}_{\text{BOH}_4} := \text{aw}_{\text{B}} + 4 \cdot (\text{aw}_{\text{O}} + \text{aw}_{\text{H}}) = 78.839 \text{ gm}$$

$$\text{MW}_{\text{NH}_4\text{Cl}} := \text{aw}_{\text{N}} + 4 \cdot \text{aw}_{\text{H}} + \text{aw}_{\text{Cl}} = 53.491 \text{ gm}$$

$$\text{MW}_{\text{NH}_4} := \text{aw}_{\text{N}} + 4 \cdot \text{aw}_{\text{H}} = 18.038 \text{ gm}$$

$$\text{MW}_{\text{NaOH}} := \text{aw}_{\text{Na}} + \text{aw}_{\text{O}} + \text{aw}_{\text{H}} = 39.997 \text{ gm}$$

mole of NaOH consumed for charge neutralization

$$\text{mol}_{\text{NaOH.n}} := \text{conc}_{\text{NaOH.c}} \cdot \text{vol}_{\text{NaOH.c}} - \text{conc}_{\text{NaOH}} \cdot \text{vol}_{\text{NaOH}} = 5.76 \times 10^{-6} \text{ mol}$$

Cation charge capacity (CEC)

$$\text{CEC}_{\text{kaolin}} := \frac{\text{mol}_{\text{NaOH.n}}}{\text{mass}_{\text{kaolin}}} = 6.609 \times 10^{-4} \cdot \frac{\text{mol}}{100 \text{ gm}}$$

Surface charge density

$$\sigma_{\text{kaolin}} := \text{CEC}_{\text{kaolin}} \cdot \frac{e_0 \cdot N_{\text{av}}}{S_{\text{a}_{\text{kaolin}}}} = 0.016 \frac{\text{coul}}{\text{m}^2}$$

Number of charges per g kaolin

$$N_{\text{c.g.kaolin}} := \sigma_{\text{kaolin}} \cdot \frac{S_{\text{a}_{\text{kaolin}}}}{e_0} = 3.98 \times 10^{18} \cdot \frac{1}{\text{gm}}$$

Number of charged units on cationic polyacrylamide (C-PAM)

$$\text{MW} := 4000000 \frac{\text{gm}}{\text{mole}}$$

Individual Atom Molecular Weights

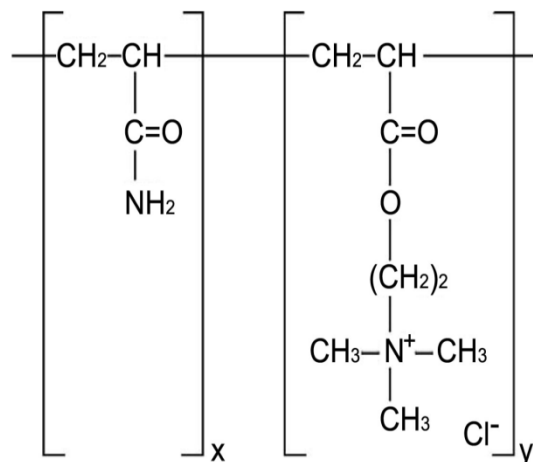
$$\text{H} := 1.007947 \frac{\text{gm}}{\text{mole}}$$

$$\text{C} := 12.01078 \frac{\text{gm}}{\text{mole}}$$

$$\text{N} := 14.007 \frac{\text{gm}}{\text{mole}}$$

$$\text{O} := 15.99943 \frac{\text{gm}}{\text{mole}}$$

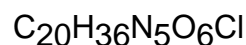
$$\text{Cl} := 35.453 \frac{\text{gm}}{\text{mole}}$$



$$(x=4, y=1)$$

(one monomer has one charged unit)

Molecular Formula



Approximate Number of Monomers per Molecule, n

$$n_{\text{monomer}} := \frac{\text{MW}}{4(3\text{C} + 5\text{H} + 1\text{N} + 1\text{O}) + (8\text{C} + 16\text{H} + 2\text{O} + 1\text{N} + 1\text{Cl})}$$

$$n_{\text{monomer}} = 8.368 \times 10^3$$

Approximate Number of PAM molecules per g PAM, N

Avogadro's number $N_{\text{av}} := 6.022 \frac{10^{23}}{\text{mol}}$

$$N_{\text{molecules}} := N_{\text{av}} \cdot \frac{1}{\text{MW}} \quad N_{\text{molecules}} = 1.506 \times 10^{17} \cdot \frac{1}{\text{gm}}$$

Approximate Number of Charged units per g PAM, N_c

$$N_{\text{c}} := N_{\text{molecules}} \cdot n_{\text{monomer}} \quad N_{\text{c}} = 1.26 \times 10^{21} \cdot \frac{1}{\text{gm}} \quad (\text{potential maximum})$$

Appendix B

Sedimentation time series

Kaolin clay (pure)

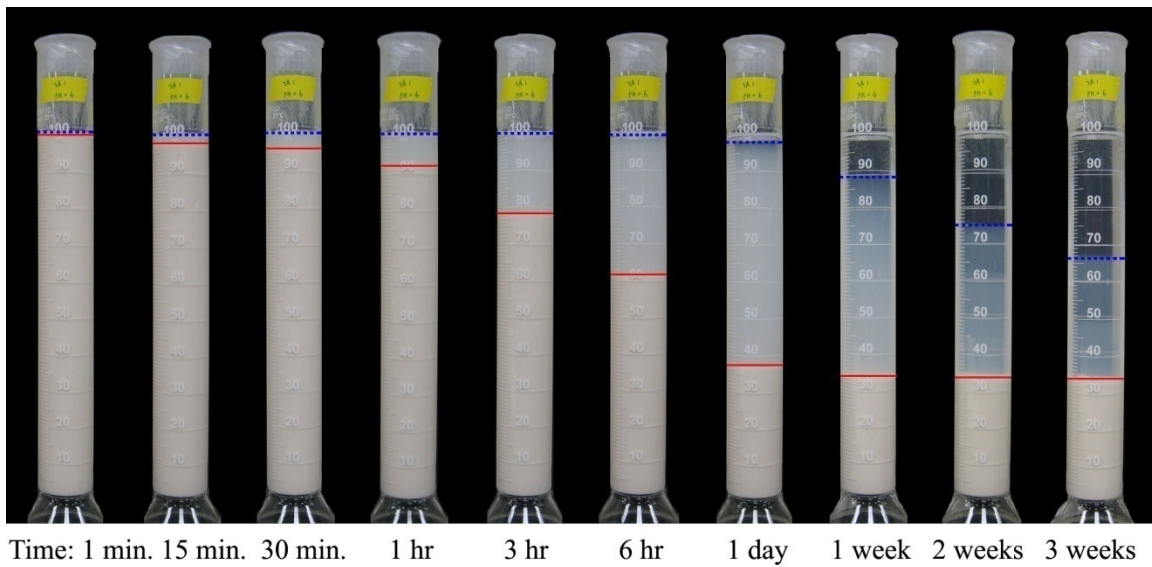


Figure **B.1**: Sedimentation time series for pure kaolin. Blue dotted line denotes supernatant-suspension boundary and red solid line denotes suspension-sediment boundary. Mixed-Mode sedimentation

Kaolin-Nonionic Polyacrylamide (N-PAM)

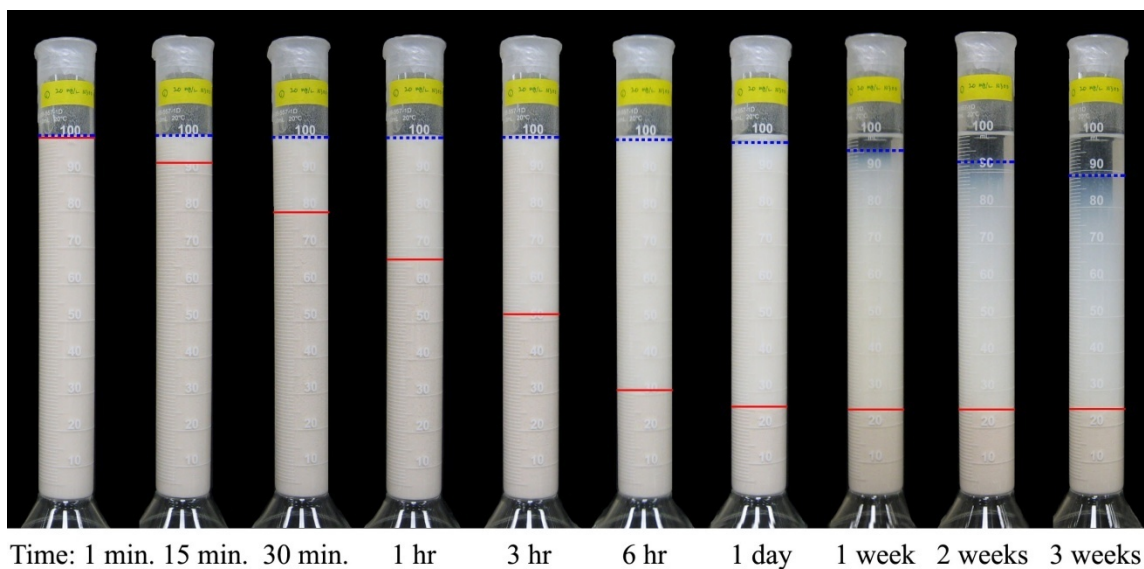


Figure **B.2**: Sedimentation time series for kaolin-PAM nanocomposite (20 mg-N-PAM/L). Blue dotted line denotes supernatant-suspension boundary and red solid line denotes suspension-sediment boundary. Mixed-Mode sedimentation

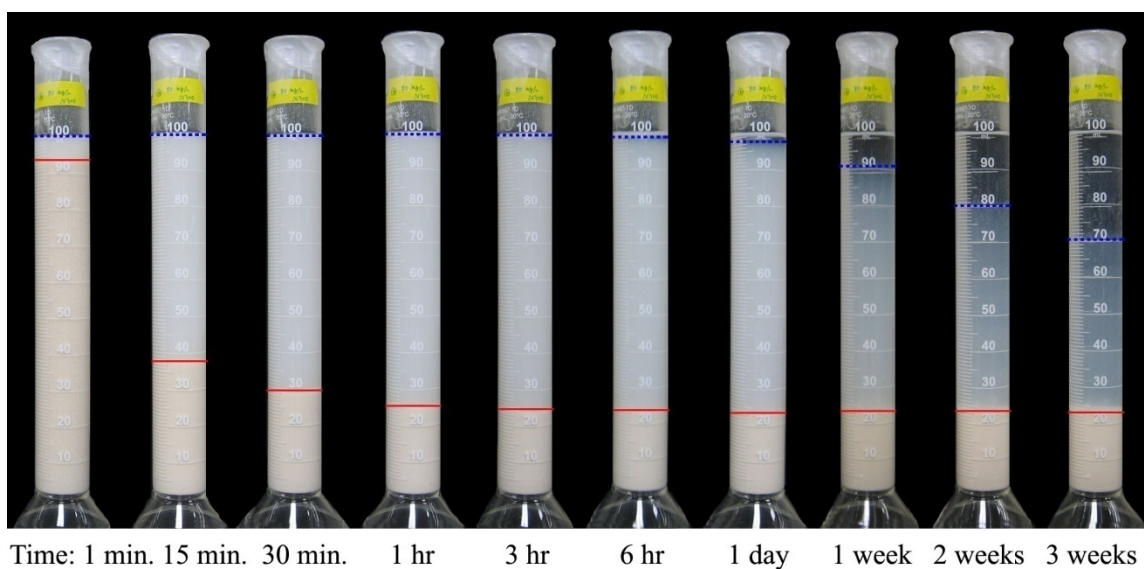


Figure **B.3**: Sedimentation time series for kaolin-PAM nanocomposite (80 mg-N-PAM/L). Blue dotted line denotes supernatant-suspension boundary and red solid line denotes suspension-sediment boundary. Mixed-Mode sedimentation (near to FF aggregation)



Time: 1 min. 15 min. 30 min. 1 hr 3 hr 6 hr 1 day 1 week 2 weeks 3 weeks

Figure **B.4**: Sedimentation time series for kaolin-PAM nanocomposite (120 mg·N-PAM/L). Blue dotted line denotes supernatant-suspension boundary and red solid line denotes suspension-sediment boundary. Mixed-Mode sedimentation (near to FF aggregation)



Time: 1 min. 15 min. 30 min. 1 hr 3 hr 6 hr 1 day 1 week 2 weeks 3 weeks

Figure **B.5**: Sedimentation time series for kaolin-PAM nanocomposite (240 mg·N-PAM/L). Blue dotted line denotes supernatant-suspension boundary and red solid line denotes suspension-sediment boundary. Mixed-Mode sedimentation (near to FF aggregation)

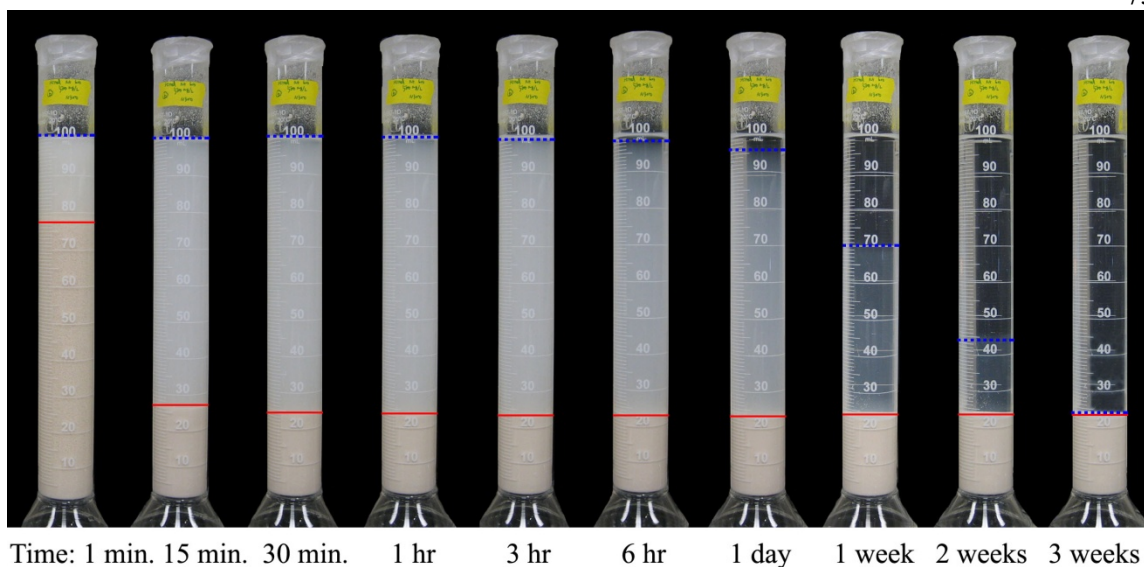


Figure **B.6**: Sedimentation time series for kaolin-PAM nanocomposite (500 mg-N-PAM/L). Blue dotted line denotes supernatant-suspension boundary and red solid line denotes suspension-sediment boundary. Mixed-Mode sedimentation (near to FF aggregation)

Kaolin-low molecular Nonionic Polyacrylamide (n-PAM)

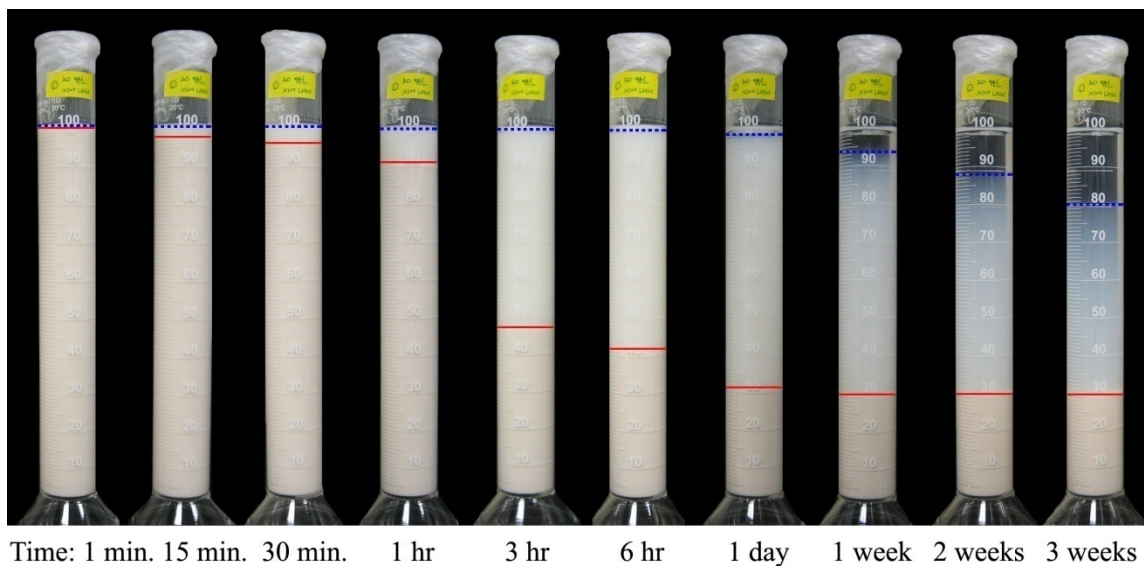


Figure **B.7**: Sedimentation time series for kaolin-PAM nanocomposite (20 mg-n-PAM/L). Blue dotted line denotes supernatant-suspension boundary and red solid line denotes suspension-sediment boundary. Mixed-Mode sedimentation

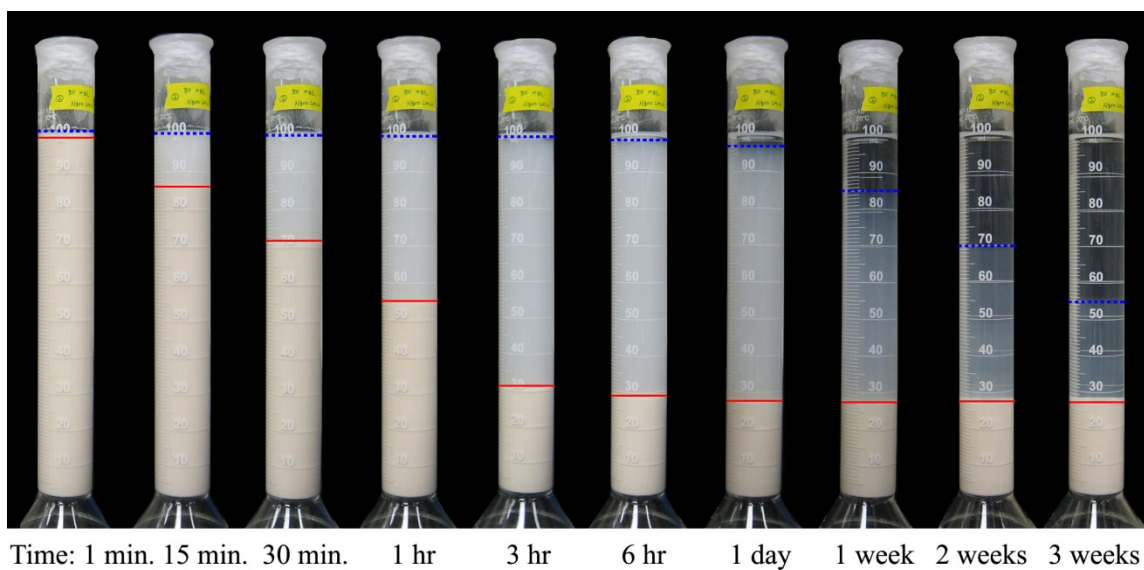


Figure **B.8**: Sedimentation time series for kaolin-PAM nanocomposite (80 mg-n-PAM/L). Blue dotted line denotes supernatant-suspension boundary and red solid line denotes suspension-sediment boundary. Mixed-Mode sedimentation

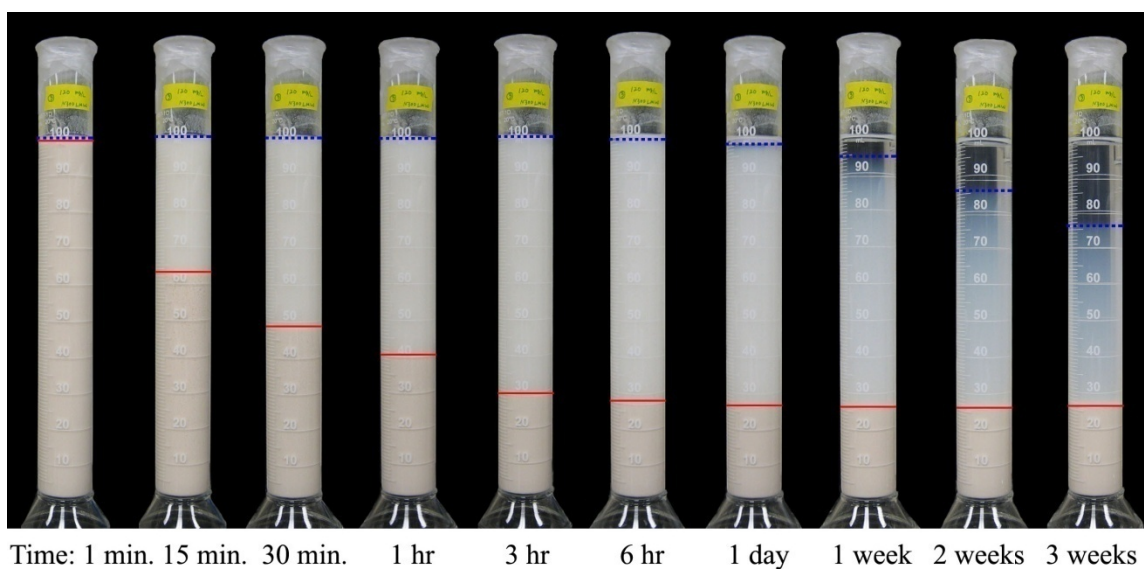
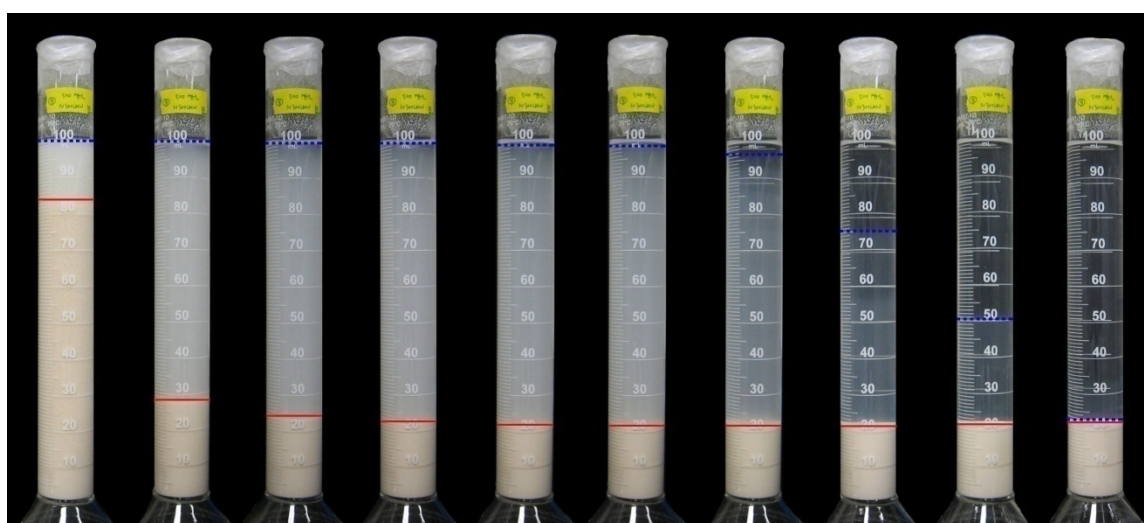


Figure **B.9**: Sedimentation time series for kaolin-PAM nanocomposite (120 mg-n-PAM/L). Blue dotted line denotes supernatant-suspension boundary and red solid line denotes suspension-sediment boundary. Mixed-Mode sedimentation



Time: 1 min. 15 min. 30 min. 1 hr 3 hr 6 hr 1 day 1 week 2 weeks 3 weeks

Figure **B.10**: Sedimentation time series for kaolin-PAM nanocomposite (240 mg-n-PAM/L). Blue dotted line denotes supernatant-suspension boundary and red solid line denotes suspension-sediment boundary. Mixed-Mode sedimentation (near to FF aggregation)



Time: 1 min. 15 min. 30 min. 1 hr 3 hr 6 hr 1 day 1 week 2 weeks 3 weeks

Figure **B.11**: Sedimentation time series for kaolin-PAM nanocomposite (500 mg-n-PAM/L). Blue dotted line denotes supernatant-suspension boundary and red solid line denotes suspension-sediment boundary. Mixed-Mode sedimentation (near to FF aggregation)

Kaolin-Cationic Polyacrylamide (C-PAM)

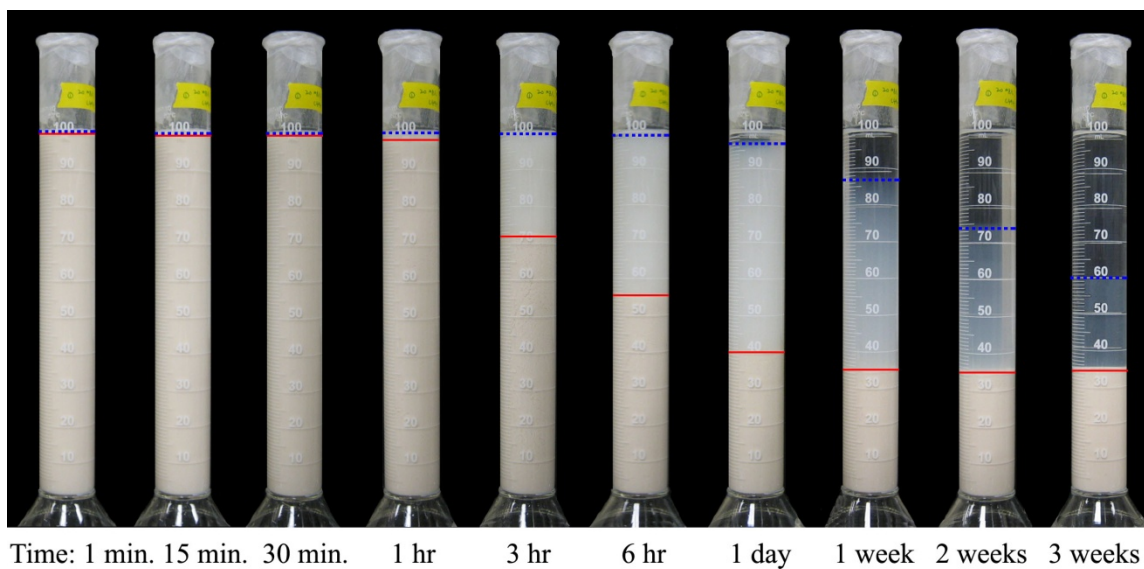


Figure **B.12**: Sedimentation time series for kaolin-PAM nanocomposite (20 mg-C-PAM/L). Blue dotted line denotes supernatant-suspension boundary and red solid line denotes suspension-sediment boundary. Mixed-Mode sedimentation

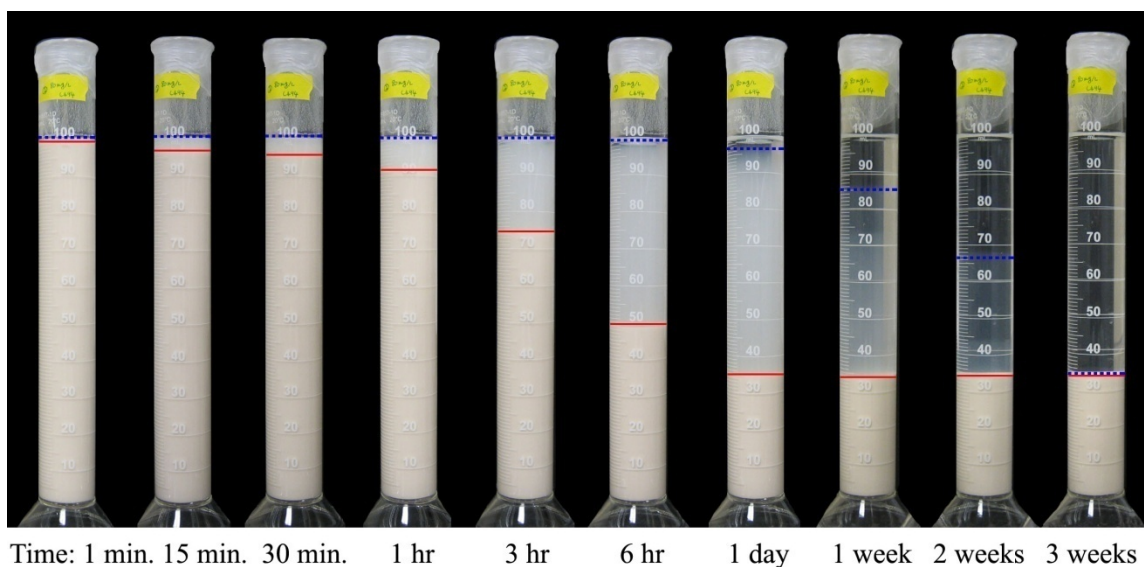


Figure **B.13**: Sedimentation time series for kaolin-PAM nanocomposite (80 mg-C-PAM/L). Blue dotted line denotes supernatant-suspension boundary and red solid line denotes suspension-sediment boundary. Mixed-Mode sedimentation



Time: 1 min. 15 min. 30 min. 1 hr 3 hr 6 hr 1 day 1 week 2 weeks 3 weeks

Figure **B.14**: Sedimentation time series for kaolin-PAM nanocomposite (120 mg·C-PAM/L). Blue dotted line denotes supernatant-suspension boundary and red solid line denotes suspension-sediment boundary. FF aggregation



Time: 1 min. 15 min. 30 min. 1 hr 3 hr 6 hr 1 day 1 week 2 weeks 3 weeks

Figure **B.15**: Sedimentation time series for kaolin-PAM nanocomposite (240 mg·C-PAM/L). Blue dotted line denotes supernatant-suspension boundary and red solid line denotes suspension-sediment boundary. Mixed-Mode sedimentation (near to FF aggregation)



Time: 1 min. 15 min. 30 min. 1 hr 3 hr 6 hr 1 day 1 week 2 weeks 3 weeks

Figure **B.16**: Sedimentation time series for kaolin-PAM nanocomposite (500 mg-C-PAM/L). Blue dotted line denotes supernatant-suspension boundary and red solid line denotes suspension-sediment boundary. Mixed-Mode sedimentation (near to FF aggregation)

Appendix C

Settling Floc Size and Density Analysis

Calculation for 20 mg/L N-PAM-treated kaolin suspension

(Richardson and Zaki, 1954; Godard and Richardson, 1969; Bhatta et al., 1978; Font et al., 1999)

$$\text{Solid density } \rho_s := 2.6 \frac{\text{gm}}{\text{cm}^3}$$

$$\text{Flow regime constant } n := 4.65$$

$$\text{Liquid density } \rho_l := 1 \frac{\text{gm}}{\text{cm}^3}$$

$$\text{Liquid viscosity } \mu := 0.001 \text{Pa}\cdot\text{s}$$

$$\text{Gravitational acceleration } g := 9.80665 \frac{\text{m}}{\text{s}^2}$$

$$\text{solids \% } \phi := \begin{pmatrix} 0.022 \\ 0.025 \\ 0.03 \\ 0.039 \\ 0.051 \\ 0.056 \\ 0.066 \\ 0.08 \\ 0.081 \end{pmatrix}$$

$$\text{settling rate } V_{s,1,n} := \begin{pmatrix} 1.109 \\ 1.021 \\ 0.89 \\ 0.838 \\ 0.64 \\ 0.425 \\ 0.427 \\ 0.33 \\ 0.17 \end{pmatrix}$$

$$a := \text{slope}(\phi, V_{s,1,n}) = -14.3$$

$$b := \text{intercept}(\phi, V_{s,1,n}) = 1.365$$

$$\mu_u := b^n = 4.25$$

$$k := \frac{-a}{b} = 10.476$$

Floc density $\rho_f := \frac{[\rho_s + (k - 1) \cdot \rho_l]}{k} = 1.153 \frac{\text{gm}}{\text{cm}^3}$

Floc diameter $D := \left[\frac{\left(18 \mu \cdot \mu_u \cdot \frac{\text{mm}}{\text{min}} \right)^5}{\text{g} \cdot (\rho_f - \rho_l)} \right] = 7.078 \times 10^{-6} \text{ m}$ ■

Appendix D

Apparatus



(a)



(b)

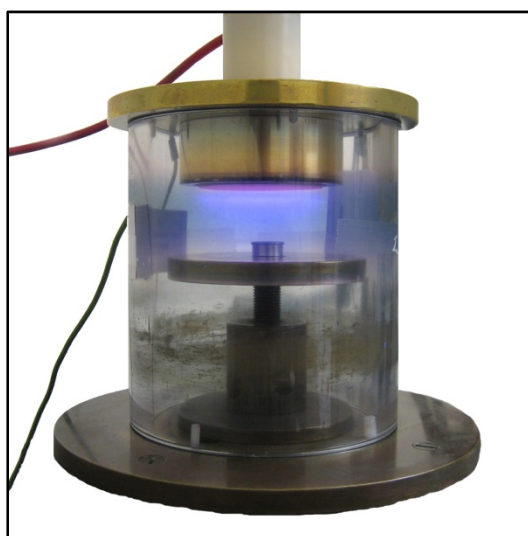
Figure D.1: Apparatus for viscosity measurement: (a) Brookfield LVDV-1 Prime Viscometer, and (b) Spindles #S61, #S62, #S63, and #S64



Figure D.2: Apparatus for liquid limit measurement: Humboldt penetrometer (model number: H-4236, Humboldt Mfg. Co., IL)



(a)



(b)



(c)

Figure D.3: Apparatus for SEM study: (a) SEM S-3500N (Hitachi Inc.), (b) gold sputter, and (c) SEM sampler

REFERENCES

- Ahmadi, S. J., Huang, Y. D., and Li, W. (2005), "Morphology and characterization of clay-reinforced EPDM nanocomposites", *Journal of Composite Materials*, 39(8), 745-754.
- Bakumov, V., Gueinzius, K., Hermann, C., Schwarz, M., and Kroke, E. (2007), "Polysilazane-derived antibacterial silver-ceramic nanocomposites", *Journal of the European Ceramic Society*, 27(10), 3287-3292.
- Barbour, S. L., and Yang, N. (1993), "Review of the Influence of Clay-Brine Interactions on the Geotechnical Properties of Ca-Montmorillonitic Clayey Soils from Western Canada", *Canadian Geotechnical Journal*, 30(6), 920-934.
- Barvenik, F. W. (1994), "Polyacrylamide characteristics related to soil applications", *Soil Science*, 158, 235-243.
- Ben-Hur, M., and Keren, R. (1997), "Polymer effects on water infiltration and soil aggregation", *Soil Science Society of America Journal*, 61(2), 565-570.
- Besra, L., Sengupta, D. K., Roy, S. K., and Ay, P. (2002), "Flocculation and dewatering of kaolin suspensions in the presence of polyacrylamide and surfactants", *International Journal of Mineral Processing*, 66(1-4), 203-232.
- Besra, L., Sengupta, D. K., Roy, S. K., and Ay, P. (2004), "Influence of polymer adsorption and conformation on flocculation and dewatering of kaolin suspension", *Separation and Purification Technology*, 37(3), 231-246.
- Bhatty, J. I., Dollimore, D., and Zahedi, A. H. (1978), "The aggregation of kaolinite suspensions in gum tragacanth solutions", *Transactions and journal of the British Ceramic Society* 77(4), 126-131.
- Bikales, N. (1973), Water-soluble polymers, Plenum Press, New York, pp.
- Brady, P. V., Cygan, R. T., and Nagy, K. L. (1996), "Molecular Controls on Kaolinite Surface Charge", *Journal of Colloid and Interface Science*, 183(2), 356-364.
- Braggs, B., Fornasiero, D., Ralston, J., and Smart, R. S. (1994), "The effect of surface modification by an organosilane on the electrochemical properties of kaolinite", *Clays and Clay Minerals*, 42, 123-136.
- Brandrup, J., and Immergut, E. H. (1989), Polymer handbook, 3rd, Wiley, New York, 1 v. (various pagings) pp.
- British Standard (1990), "Determination of Liquid Limit", 1377-90 Section 4.
- Carasso, M. L., Rowlands, W. N., and O'Brien, R. W. (1997), "The Effect of Neutral Polymer and Nonionic Surfactant Adsorption on the Electroacoustic Signals of Colloidal Silica", *Journal of Colloid and Interface Science*, 193(2), 200-214.
- Carty, W. M. "The colloidal nature of kaolinite." St. Louis, MO, United States, 31.
- Daniels, J. L., and Inyang, H. I. (2004), "Contaminant barrier material textural response to interaction with aqueous polymers", *Journal of Materials in Civil Engineering*, 16(2), 265-275.
- Daniels, J. L., Inyang, H. I., and Iskandar, I. K. (2003), "Durability of Boston Blue Clay in waste containment applications", *Journal of Materials in Civil Engineering*, 15(2), 144-152.
- Deng, Y., Dixon, J. B., White, G. N., Loeppert, R. H., and Juo, A. S. R. (2006), "Bonding between polyacrylamide and smectite", *Colloids and Surfaces A: Physicochemical and Engineering Aspects*, 281(1-3), 82-91.

- Dobias, B., Qiu, X., and Rybinski, W. v. (1999), Solid-liquid dispersions, Marcel Dekker, New York, vii, 562 p. pp.
- Ebnesajjad, S. (2006), Surface treatment of materials for adhesion bonding, William Andrew Pub., Norwich, NY, U.S.A., xvi, 260 p. pp.
- Fleer, G. J., Koopal, L. K., and Lyklema, J. (1972), "Polymer adsorption and its effect on the stability of hydrophobic colloids", *Colloid & Polymer Science*, 250(7), 689-702.
- Flegmann, A. W., Goodwin, J. W., and Ottewill, R. H. (1969), "RHEOLOGICAL STUDIES ON KAOLINITE SUSPENSIONS", (13), 31-45.
- Font, R., Garcia, P., and Rodriguez, M. (1999), "Sedimentation test of metal hydroxides: hydrodynamics and influence of pH", *Colloids and Surfaces A: Physicochemical and Engineering Aspects*, 157(1-3), 73-84.
- Galimberti, M., Lostritto, A., Spatola, A., and Guerra, G. (2007), "Clay delamination in hydrocarbon rubbers", *Chemistry of Materials*, 19(10), 2495-2499.
- Godard, K., and Richardson, J. F. (1969), "Correlation of data for minimum fluidising velocity and bed expansion in particularly fluidised systems", *Chemical Engineering Science*, 24(2), 363-367.
- Green, V. S., Stott, D. E., Norton, L. D., and Graveel, J. G. (2000), "Polyacrylamide molecular weight and charge effects on infiltration under simulated rainfall", *Soil Science Society of America Journal*, 64(5), 1786-1791.
- Grim, R. E. (1968), Clay Mineralogy, 2nd, New York, Mcgraw-hill [1968], 596 p. pp.
- Hogg, R. (1999), "Role of polymer adsorption kinetics in flocculation", *Colloids and Surfaces A: Physicochemical and Engineering Aspects*, 146(1-3), 253-263.
- Hunter, R. J. (1993), Introduction to Modern Colloid Science, 1st, Oxford University Press, Oxford ; New York, 338 p. pp.
- Hunter, R. J. (2001), Foundations of Colloid Science, 2nd, Oxford University Press, Oxford ; New York, 806 p. pp.
- Inagaki, Y., Kuromiya, M., Noguchi, T., and Watanabe, H. (1999), "Reclamation of waste polystyrene by sulfonation", *Langmuir*, 15(12), 4171-4175.
- Inyang, H. I., and Bae, S. (2005), "Polyacrylamide sorption opportunity on interlayer and external pore surfaces of contaminant barrier clays", *Chemosphere*, 58(1), 19-31.
- Irani, R. R., and Callis, C. F. (1963), Particle size: measurement, interpretation, and application, Wiley, New York,, 165 p. pp.
- Israelachvili, J. N. (1991), Intermolecular and surface forces, 2nd, Academic Press, London ; San Diego, xxi, 450 p. pp.
- Kaya, A., Oren, A. H., and Yukselen, Y. (2006), "Settling of kaolinite in different aqueous environment", *Marine Georesources and Geotechnology*, 24(3), 203-218.
- Laird, D. A. D. (1997), "Bonding between polyacrylamide and clay mineral surfaces", *Soil science*, 162(11), 826-832.
- Lee, L. T., Rahbari, R., Lecourtier, J., and Chauveteau, G. (1991), "Adsorption of Polyacrylamides on the Different Faces of Kaolinites", *Journal of Colloid and Interface Science*, 147(2).
- Letterman, R. D., and Pero, R. W. (1990), "Contaminants in polyelectrolytes used in water treatment", *Journal of American Water Works Association*, 82, 87-97.
- Ma, C., and Eggleton, R. A. (1999), "Cation exchange capacity of kaolinite", *Clays and Clay Minerals*, 47(2), 174-180.
- Mitchell, J. K. (1956), "The Fabric of Natural Clays and its Relation to Engineering Properties", *Highway Research Board Proceedings*, 35(35th Annual Meeting, Washington, D.C.), 693-713.
- Mitchell, J. K. (1993), Fundamentals of Soil Behavior, 2nd, John Wiley & Sons, New York, 437 pp.

- Mitchell, J. K., and Soga, K. (2005), Fundamentals of Soil Behavior, 3rd, John Wiley & Sons, 577 pp.
- MMP. (2003), "Virtual Museum of Minerals and Molecules", <<http://virtual-museum.soils.wisc.edu/displays.html>>. (Accessed Aug, 2007).
- Moore, C. A., and Mitchell, J. K. (1974), "ELECTROMAGNETIC FORCES AND SOIL STRENGTH", *Geotechnique*, 24(4), 627-640.
- Moore, R. (1991), "Chemical and mineralogical controls upon the residual strength of pure and natural clays", *Geotechnique*, 41(1), 35-47.
- Mpofu, P., Addai-Mensah, J., and Ralston, J. (2003), "Investigation of the effect of polymer structure type on flocculation, rheology and dewatering behaviour of kaolinite dispersions", *International Journal of Mineral Processing*, 71(1-4), 247-268.
- Murray, H. H. (1991), "Overview - Clay mineral applications", *Applied Clay Science*, 5, 379-395.
- Nadler, A., Perfect, E., and Kay, B. D. (1996), "Effect of polyacrylamide application on the stability of dry and wet aggregates", *Soil Science Society of America Journal*, 60, 555-561.
- Nasser, M. S., and James, A. E. (2006), "Settling and sediment bed behaviour of kaolinite in aqueous media", *Separation and Purification Technology*, 51, 10-17.
- Palomino, A. M. (2004), "Fabric Formation and Control in Fine-Grained Materials", Ph.D. dissertation, Georgia Institute of Technology, Atlanta, Georgia, 193p.
- Palomino, A. M., and Santamarina, J. C. (2005), "Fabric Map for Kaolinite: Effects of pH and Ionic Concentration on Behavior", *Clays and Clay Minerals*, 53(3), 209 - 222.
- Pefferkorn, E. (1999), "Polyacrylamide at solid/liquid interfaces", *Journal of Colloid and Interface Science*, 216, 197-220.
- Pefferkorn, E., Nabzar, L., and Varoqui, R. (1987), "POLYACRYLAMIDE Na-KAOLINITE INTERACTIONS: EFFECT OF ELECTROLYTE CONCENTRATION ON POLYMER ADSORPTION", *Colloid and Polymer Science*, 265(10), 889-896.
- Peng, F. F., and Di, P. (1994), "Effect of multivalent salts - calcium and aluminum on the flocculation of kaolin suspension with anionic polyacrylamide", *Journal of Colloid and Interface Science*, 164(1), 229-237.
- Pierre, A. C., and Ma, K. (1999), "DLVO Theory and Clay Aggregate Architectures Formed with $AlCl_3$ ", *Journal of the European Ceramic Society*, 19(8), 1615-1622.
- Pierre, A. C., Ma, K., and Barker, C. (1995), "Structure of kaolinite flocs formed in an aqueous medium", *Journal of Materials Science*, 30(8), 2176-2181.
- Rand, B., and Melton, I. E. (1977), "Particle Interactions in Aqueous Kaolinite Suspensions I. Effect of pH and Electrolyte Upon the Mode of Particle Interaction in Homoionic Sodium Kaolinite Suspensions", *Journal of Colloid and Interface Science*, 60(2), 308-320.
- Ravve, A. (2000), Principles of polymer chemistry, 2nd, Kluwer Academic/Plenum Publishers, New York, xv, 626 p. pp.
- Richardson, J. F., and Zaki, W. N. (1954), "Sedimentation and fluidisation -- 1", *Institution of Chemical Engineers -- Transactions*, 32(1), 35-52.
- Sadhu, S., and Bhowmick, A. K. (2004), "Preparation and Properties of Styrene-Butadiene Rubber Based Nanocomposites: The Influence of the Structural and Processing Parameters", *Journal of Applied Polymer Science*, 92(2), 698-709.
- Santamarina, J. C., Klein, K. A., and Fam, M. A. (2001), Soils and Waves : Particulate Materials Behavior, Characterization and Process Monitoring, J. Wiley & Sons, Chichester ; New York, 488 pp.
- Santamarina, J. C., Klein, K. A., Wang, Y. H., and Prencke, E. (2002), "Specific Surface: Determination and Relevance", *Canadian Geotechnical Journal*, 39(1), 233-241.
- Schroth, B. K., and Sposito, G. (1997), "Surface charge properties of kaolinite", *Clays and Clay Minerals*, 45(1), 85-91.

- Siffert, B., and Kim, K.-B. (1992), "Study of the surface ionization of kaolinite in water by zetametry - influence on the rheological properties of kaolinite suspension", *Applied Clay Science*, 6(5-6), 369-382.
- Sojka, R. E., Westermann, D. T., and Lentz, R. D. (1998), "Water and erosion management with multiple applications of polyacrylamide in furrow irrigation", *Soil Science Society of America Journal*, 62, 1672-1680.
- Sposito, G. (1984), The surface chemistry of soils, Oxford University Press, New York, xii, 234 p. pp.
- Sposito, G. (1989), The Chemistry of Soils, Oxford University Press, New York, 277 pp.
- Sposito, G. (1998), "On Points of Zero Charge", *Environmental Science & Technology*, 32(19), 2815-2819.
- Sridharan, A., and Prakash, K. (1999), "Mechanisms controlling the undrained shear strength behaviour of clays", *Canadian Geotechnical Journal*, 36(6), 1030-1038.
- Stumm, W. (1992), Chemistry of the solid-water interface : processes at the mineral-water and particle-water interface in natural systems, Wiley, New York, x, 428 p. pp.
- Stutzmann, T., and Siffert, B. (1977), "Contribution to the adsorption mechanism of acetamide and polyacrylamide onto clay", *Clays and Clay Minerals*, 25, 392-406.
- Sun, Q., and Deng, Y. "Polymer/nanoclay nanocomposites for paper barrier coating." Atlanta, GA, United States, 16.
- Tekin, N., Demirbas, O., and Alkan, M. (2005), "Adsorption of cationic polyacrylamide onto kaolinite", *Microporous and Mesoporous Materials*, 85(3), 340-350.
- Theng, B. K. G. (1979), Formation and Properties of Clay-Polymer Complexes, Amsterdam ; New York, 362 p. pp.
- Theng, B. K. G. (1982), "Clay-polymer interactions: summary and perspectives", *Clays and Clay Minerals*, 30(1), 1-10.
- Torchilin, V. P. (2006), Nanoparticulates as drug carriers, Imperial College Press, London, xxix, 724 p. pp.
- Vaia, R. A., Benson Tolle, T., Schmitt, G. F., Imeson, D., and Jones, R. J. (2001), "Nanoscience and nanotechnology: Materials revolution for the 21st century", *SAMPE Journal*, 37(6), 24-31.
- van Olphen, H. (1977), An Introduction to Clay Colloid Chemistry : For Clay Technologists, Geologists, and Soil Scientists, 2d, Wiley, New York, 318 pp.
- Van Oss, C. J. (2006), Interfacial forces in aqueous media, 2nd, CRC/Taylor & Francis, Boca Raton, 438 p. pp.
- Vu, Y. T., Mark, J. E., Pham, L. H., and Engelhardt, M. (2001), "Clay nanolayer reinforcement of cis-1,4-polyisoprene and epoxidized natural rubber", *Journal of Applied Polymer Science*, 82(6), 1391-1403.
- Wei, G. C. (2005), "Transparent ceramic lamp envelope materials", *Journal of Physics D: Applied Physics*, 38(17), 3057-3065.
- Whittingham, M. S., and Jacobson, A. E. (1982), Intercalation Chemistry, Academic Press, New York, pp.
- Wieland, E., and Stumm, W. (1992), "Dissolution Kinetics of Kaolinite in Acidic Aqueous Solutions at 25[deg]C", *Geochimica et Cosmochimica Acta*, 56(9), 3339-3355.
- Wierer, K. A., and Dobias, B. (1988), "EXCHANGE ENTHALPIES OF H** plus AND OH** minus ADSORPTION ON MINERALS WITH DIFFERENT CHARACTERS OF POTENTIAL-DETERMINING IONS", *Journal of Colloid and Interface Science*, 122(1), 171-177.
- Wroth, C. P., and Wood, D. M. (1978), "The Correlation of Index Properties with Some Basic Engineering Properties of Soils", *Canadian Geotechnical Journal*, 15(2), 137-145.

- Yu, J., Lei, T., Shainberg, I., Mamedov, A. I., and Levy, G. J. (2003), "Infiltration and erosion in soils treated with dry PAM and gypsum", *Soil Science Society of America Journal*, 67(2), 630-636.
- Yudin, V. E., Divoux, G. M., Otaigbe, J. U., and Svetlichnyi, V. M. (2005), "Synthesis and rheological properties of oligoimide/montmorillonite nanocomposites", *Polymer*, 46(24), 10866-10872.
- Zeng, Q. H., Yu, A. B., Lu, G. Q., and Paul, D. R. (2005), "Clay-based polymer nanocomposites: Research and commercial development", *Journal of Nanoscience and Nanotechnology*, 5(10), 1574-1592.
- Zhang, X. C., and Miller, W. P. (1996), "Polyacrylamide effect on infiltration and erosion in furrows", *Soil Science Society of America Journal*, 60, 866-872.
- Zhang, X. C., Miller, W. P., Nearing, M. A., and Norton, L. D. (1998), "Effects of surface treatment on surface sealing, runoff, and interrill erosion", *Transactions of the ASAE*, 41(4), 989-994.
- Zhou, Z., and Gunter, W. (1992), "The nature of the surface charge of kaolinite", *Clays and Clay Minerals*, 40(3), 365-368.
- Zhu, L., and Wool, R. P. (2006), "Nanoclay reinforced bio-based elastomers: Synthesis and characterization", *Polymer*, 47(24), 8106-8115.